INVESTIGATION OF GEOTECHNICAL AND HYDRAULIC ASPECTS OF LANDFILL DESIGN AND OPERATION

By

YOUNG MIN CHO

A DISSERTATION PRESENTED TO THE GRADUATE SCHOOL
OF THE UNIVERSITY OF FLORIDA IN PARTIAL FULFILLMENT
OF THE REQUIREMENTS FOR THE DEGREE OF
DOCTOR OF PHILOSOPHY

UNIVERSITY OF FLORIDA

2010

To my mother, father and brother

ACKNOWLEDGMENTS

I would like to thank my academic advisor and committee chairman, Professor Timothy Townsend, for sharing his precious knowledge and experience. I was very lucky to work with him. He gave me a wonderful experience to work on these valuable projects, and his tireless endeavors toward academic accomplishment inspired me. I remember his all efforts to train me as a researcher, engineer, and presenter. I would like to thank my other committee members, Professor Frank Townsend, Professor Michael Annable, and Professor David Bloomquist for their guidance in completing my graduate studies. Also, I am very thankful for all supports from people at the Polk County Waste Resource Management, Brooks Stayer, Allan Choate, Sharon Hymiller, Kimberly Byer, Matthew Dial, and David Huff. It was always delightful working with them. I thank John Schert of Florida Center of Solid and Hazardous Waste Management. Many of my works could not be done without his supports.

I would like to thank my friends, Dr. Jaehyun, Dr. Yongchul Jang, Dr. Hwidong Kim, Dr. Jaehac Ko, Dr. Brajesh Dubey, Dr. Dinesh Kumar, Dr. Pradeep Jain, Dr. Qiyong Xu, Sejin Yoon, Myunghee Woo, and Hwanchul Cho, for providing me with wonderful advice and support. I acknowledge the support from my friends, Dr. Ravi Kadambala, Edmund Azah, Shrawan Singh, Wang Yu, Sendhil Kumar, Stephanie Conner, Wesley Oehmig, Jose Antonio Yaquian Luna, and Karamjit Singh.

At last, I would like to thank my mom, dad, and brother for their love, support, and encouragement. I love you.

TABLE OF CONTENTS

LIST OF TABLES

LIST OF FIGURES

LIST OF ABBREVIATIONS

ASTM	American society for testing and materials
BMP	Bio-chemical methane potential
CPT	Cone penetration test
EPA	Environmental protection agency
FS	Full scale
HDPE	High-Density Polyethylene
LSDST	Large-scale direct shear test
MSW	Municipal solid waste
NGVD	represents U.S. National Geodetic Vertical Datum
NOAA	National Oceanic and Atmospheric Administration
SCADA	Supervisory control and data acquisition
SPT	Standard penetration test
SS	Settlement sensor
SSDST	Small-scale direct shear test
TPC	Total pressure cell
US	United States
VS	Volatile solid

Abstract of Dissertation Presented to the Graduate School
of the University of Florida in Partial Fulfillment of the
Requirements for the Degree of Doctor of Philosophy

INVESTIGATION OF GEOTECHNICAL AND HYDRAULIC ASPECTS OF LANDFILL DESIGN AND OPERATION

By

Young Min Cho

August 2010

Chair: Timothy G. Townsend
Major: Environmental Engineering Sciences

This study includes various topics related to landfill design and operation. The topics include evaluating the impact of pressurized liquid addition on the landfill pore pressure development, estimating the settlement of municipal solid waste and the landfill foundation due to waste placement, and evaluating the impact of food waste content on the internal friction angle of municipal solid waste.

Pressure transducers were installed around horizontal liquid addition lines with trenches filled with crushed glass, shredded tires, and excavated waste as bedding material. It was found that the added liquids were successfully transferred to the end of the shredded tire and crushed glass trenches without considerable head loss, but were not in the excavated waste trench. As the added liquids migrated outward from the trenches, pressure head dropped sharply near the trenches. This suggests that in the design of landfills with similar horizontal liquids addition systems, a slope stability analysis may need to consider pore pressure variation in waste as a function of horizontal distance. Using analytical models and in-situ pore pressure measurements, horizontal and vertical hydraulic conductivities were estimated to be in the ranges of

7.0×10^{-4} - 3.0×10^{-4} cm/sec and 1.0×10^{-5} - 1.9×10^{-5} cm/sec, respectively. Anisotropy values of horizontal to vertical hydraulic conductivities were estimated to be from 37 to 277.

Settlements of a bioreactor landfill subjected to surcharge were investigated using an in-situ settlement profiling technique. During the settlement profiling period, an average settlement rate was estimated to be 3.76 % per year which is 1.4 times greater than an average settlement rate prior to the waste placement (2.66% per year). Overall, relatively wide ranges of the values of compression properties (C_c', m_v, and c_v) were estimated: C_c' (0.1 – 1.7), m_v (3.0×10^{-4} – 7.3×10^{-3} m^2/kN), and c_v (0.89×10^{-2} to 1.44×10^{-2} cm^2/sec). Vertical hydraulic conductivities of the bioreacted waste were estimated to be in a range of 4.6×10^{-7} to 9.8×10^{-6} cm/sec.

To investigate the settlement behavior of the foundation of a landfill, total pressure cells and settlement sensors were installed under the bottom liner of a municipal solid waste landfill and monitored for 39 months. The readings of the total pressure cells near the toe of the landfill side slope averaged 1.3 times greater than the overburden pressure predictions calculated using the Boussinesq influence factor charts, the waste lift thickness, and the bulk unit weight, while overburden pressures beneath the central area were found to be over predicted (average 0.8 of measured to estimated overburden pressure ratio). Settlement predictions made using conventional one-dimensional settlement models (elastic theory and Terzaghi's consolidation model) did not provide reasonable settlement estimates of the foundation area beneath the landfill side slope toe. Settlement predictions of the area of the landfill central body were over predicted up to 2.6 cm, which might be overly conservative.

The impact of food waste content on the municipal solid waste friction angle was studied. Using reconstituted fresh MSW specimens with different food waste content (0, 40, 58, and 80%), 48 small-scale (100-mm-diameter) direct shear tests and 12 large-scale (430 mm×430 mm) direct shear tests were performed. A stress-controlled large-scale direct shear test device allowing approximately 170-mm sample horizontal displacement was designed and used. At both testing scales, the mobilized internal friction angle of MSW decreased considerably as food waste content increased. As food waste content increased from 0 to 40% and from 40 to 80%, the mobilized internal friction angles (estimated using the mobilized peak (ultimate) shear strengths of the small-scale direct shear tests) decreased from 39 to 31^0 and from 31 to 7^0, respectively, while those of large-scale tests decreased from 36 to 26^0 and from 26 to 15^0, respectively. Most friction angle measurements produced in this study fell within the range of those previously reported for MSW.

CHAPTER 1
INTRODUCTION

Background

While new municipal solid waste (MSW) disposal technologies have been developed over the last several decades, landfilling is still the preferred method in the United States. In 2005, approximately 245 million tons of MSW were generated from residents, businesses, and institutions and 54 percent of this was landfilled (US EPA 2007). Difficulties in siting new landfills have led designers and operators to develop new landfill operation technologies, stimulating decomposition of landfilled waste and thus enhanced airspace (waste disposal capacity) recovery. Subsurface pressurized liquid addition technologies (referred to as bioreactor landfill operation) were developed as part of such efforts. The benefits of bioreactor landfill operation are well documented by multiple researchers (Pohland 1975; Townsend 1995; Townsend et al., 1996; Reinhart 1996; Townsend and Miller 1998; Reinhart et al., 2002). Introducing liquid into a landfill enhances waste decomposition, and consequently, airspace can be recovered. In addition, stimulated waste stabilization reduces the required period for post-closure care of a landfill. Finally, the landfill leachate treatment cost can also be mitigated.

Problem Statement

The slope stability of a landfill is a major concern of designers and operators. Since liquids are added under pressure, understanding pore pressure variation in bioreactor landfills becomes especially important. That is, increased pore pressure due to pressurized liquids addition may decrease an effective normal stress and therefore the slope stability of those landfills. In spite of the importance of monitoring pore pressure inside a landfill, few in-situ measurement studies of the impact of pressurized

liquid addition on the pore pressure change have been conducted. In addition, the internal friction angle of waste is one of the most important parameters to decide the side slope angle of a landfill. In previous studies, a wide range of friction angles have been reported, most typically between 15 and 35˚, which may lead to practical difficulties in applying friction angles reported in literature for landfill design (Kavazanjian et al. 1995; Kavazanjian et al. 1999; Sadek et al. 2001; Machado et al. 2002; Mahler and Netto 2003; Harris et al. 2006; Gabr et al. 2007; Zhan et al. 2007; Zekkos et al. 2007; Kavazanjian 2008; Zekkos et al. 2008; Reddy et al. 2009).

Another geotechnical engineering factor of importance in landfill design and operation is landfill settlement. Researchers and landfill owners are usually interested in landfilled waste and landfill foundation settlement. Unexpected instances of both may result in damage to landfill infrastructure such as landfill gas or leachate collection systems. Because the failure of those systems may result in deleterious consequences (e.g., the contamination of soil and groundwater), it is one of the major concerns of landfill design and operation. The aforementioned settlements were commonly predicted using various equations of conventional soil mechanics such as elastic theory and Terzaghi's one-dimensional consolidation model (Sowers 1973; Powrie and Beaven 1999; Landva et al., 2000; Machado et al., 2002; Anderson et al., 2004; Durmusoglu et al., 2006). However, to the author's knowledge, no landfill foundation settlement measurement using an in-situ hydrostatic settlement sensor has been conducted to verify these models. Therefore, the reliability of such landfill foundation settlement predictions is in question. In addition, no study has been performed which investigates

the settlement of a landfill previously operated as a bioreactor due to additional waste placement (surcharge).

Research Objectives

This doctoral research explores a number of important aspects of landfill design and operation. By conducting field-scale experiments, mechanical and hydraulic properties of landfilled MSW were investigated. In addition, the variation of load and settlement of landfill foundation due to waste placement were monitored using in-situ instrumentation (total pressure cells and settlement sensors). Shear strength parameters (e.g., internal friction angle and apparent cohesion) of compacted MSW were estimated by conducting small- and large-scale direct shear tests.

The first objective was to provide in-situ measurements of pore pressure variation in waste due to liquids addition into horizontal trenches. Pore pressure was monitored by pressure transducers within the waste and the trenches surrounding the horizontal lines. As part of the in-situ data analysis for head loss in waste, hydraulic properties of landfilled waste (e.g., hydraulic conductivity and anisotropy) were estimated by comparing field data with analytical models (Townsend 1995).

The second objective was to present the settlement monitoring results of an MSW landfill due to additional waste placement. The settlement was measured using a settlement profiler. Assuming the settlement of the study landfill could be modeled as the consolidation settlement of soil, compression properties (e.g., coefficients of volume change, coefficients of consolidation, and modified primary compression indices) and hydraulic conductivities of waste were determined. The results are expected to provide better understanding of the settlement behavior of landfilled waste and basic inputs for landfill settlement prediction models.

The third objective was to present the monitoring results of load variation and settlement of the foundation of an operating municipal solid waste landfill using field instrumentation consisting of settlement sensors and total pressure cells. The in-situ settlement data (spanning 39 months) were compared with theoretical settlement estimates made using conventional one-dimensional settlement models (elastic settlement and Terzaghi's consolidation).

The fourth objective was to investigate the relationship between the internal friction angle of waste and food waste content. The food waste content in municipal solid waste varies geologically and seasonally, (2 – 70% by wet weight). This study is expected to provide guidelines for landfill designers to decide an internal friction angle of waste and thus a landfill side slope angle.

Research Approach

Objective 1. Evaluating the impact of pressurized leachate addition on the pore pressure in a bioreactor landfill

Approach. Two 110-m horizontal leachate addition lines were installed in excavated waste, crushed glass and shredded tire bedding media trenches (0.9 m × 0.9 m × 110 m). A total of eighty one vibrating wire pressure transducers (piezometers) were installed around the horizontal lines. The data was collected every 30 minutes during the operation of the leachate addition system. Liquids were added at a constant flow rate of 0.076 m^3/min. Liquids addition was continued until pressure reached a halting pressure designated by the bioreactor operation permit. The pore pressure variation in and near media trenches due to pressurized liquids addition were monitored.

Objective 2. Evaluating the impact of additional waste placement on the settlement of a landfill previously operated as a bioreactor landfill

Approach. The settlement was measured by employing five 46 m settlement profiling pipes with 10-cm diameter, which were installed on the top surface of a landfill previously operated as a bioreactor landfill. The initial locations and elevations of each pipe were surveyed in September 2008. Another waste lift was placed on top of the bioreacted waste layer from November to December 2008. Using a settlement profiler, settlement was monitored from December 2008 to March 2010. The relationship between landfill settlement and overburden pressure increase was investigated based on in-situ settlement measurements. In addition, compression parameters (e.g., modified primary compressibility index, coefficient of consolidation and coefficient of volume change) and hydraulic conductivity of the landfilled waste were estimated based on the field settlement data.

Objective 3. In-situ measurements of landfill foundation settlement and overburden pressure variation due to waste placement

Approach. Prior to waste placement, vibrating wire settlement sensors and total pressure cells were installed under the bottom liner of the study landfill in February 2006. The data from the instruments were collected periodically (every 2 to 4 weeks) before and during active waste placement. In-situ overburden pressure measurements during waste placement were compared with theoretical estimates. Based on standard penetration and cone penetration tests conducted before the landfill foundation construction, the theoretical settlements of the foundation as a function of vertical stress were calculated and compared with actual settlements.

Objective 4. Evaluating the impact of food waste content on the internal friction angle of MSW

Approach. Small-scale direct shear tests (SSDSTs) and large-scale direct shear tests (LSDSTs) were conducted on fresh synthetic MSW samples containing various amounts of food waste (0, 40, 58, and 80% by wet weight). To prepare a reproducible specimen, eight representative waste components were selected: food waste, paper, plastic, metal, wood, textile, glass, and ash. For SSDSTs, a typical soil direct shear test machine with a 10-cm-diameter and 5-cm-height shear box was used. For LSDSTs, a stress-controlled direct shear box testing device (430mm length × 430mm width) was constructed and used. The effective normal stresses used for SSDSTs were 48, 97, 145, 194, and 290 kPa, and those for the LSDSTs were 96, 192, and 287 kPa.

Outline of Dissertation

This dissertation is presented in six chapters. Chapter 1 presents introductory material, problem statement, objectives, and research approach. Chapters 2 through 5 provide the methodologies, results and discussion of each individual research topic. The results of evaluating the impact of pressurized leachate addition on the pore pressure in a bioreactor landfill are presented in Chapter 2. Chapter 3 presents the results of evaluating the impact of additional waste placement on the settlement of a landfill previously operated as a bioreactor landfill. Chapter 4 presents the results of investigating the impact of waste placement on the landfill foundation settlement. The impact of food waste content on the internal friction angle of MSW is presented in Chapter 5. Chapter 6 provides the comprehensive summary and conclusion of the entire research of this dissertation. Supplementary tables, figures, and example calculations to determine various parameters are provided in the appendices. Cited references are included at the end.

CHAPTER 2
IMPACT OF PRESSURIZED LIQUID ADDITION ON THE PORE PRESSURE IN A BIOREACTOR LANDFILL

Introduction

In recent decades, numerous efforts have been made to develop and improve techniques for liquids addition into waste as part of bioreactor landfill operations (Pohland 1975; Townsend 1995; Townsend et al., 1996; Reinhart 1996; Townsend and Miller 1998; Reinhart et al., 2002). Buried horizontal liquids addition lines consisting of perforated pipes bedded in a trench with porous media are one of the more common methods because of good moisture distribution and less odor and vector issues compared to surface systems. Hydraulic properties (e.g., hydraulic conductivity and anisotropy) of landfilled material are key parameters for the design of liquid distribution systems; in this chapter anisotropy is defined as the ratio of horizontal to vertical hydraulic conductivities. The design of horizontal liquids addition systems includes specification of spacing between trenches, bedding material, and operating constraints such as flow rate and pressure. The engineer's goal is to provide the landfill operator with a system that both provides needed moisture distribution in the target time period and prevents deleterious outcomes such as seeps and slope failure. While mathematical models to predict the movement of liquids added into a landfill have been developed and serve as helpful design tools (Townsend 1995; Reinhart and Townsend 1997; Al-Yousfi and Pohland 1998), a better understanding of actual field performance (e.g., moisture distribution and required pressure) is needed. Only limited field experiments, however, have been conducted (Townsend 1995; Jain 2005; Townsend et al. 2008).

This chapter reports the results of study at an operational landfill where liquids were added through horizontal lines, and the impact of the pressurized liquids addition on pore pressures in the waste surrounding the lines were examined. To monitor pore pressure variation, eighty one pressure transducers were installed within the waste and the trenches surrounding the horizontal lines. As part of the in-situ data analysis for head loss in waste, hydraulic conductivity and anisotropy of landfilled waste were roughly estimated by comparing field data with analytical models (Townsend 1995).

Material and Methods

Background

The study landfill site and liquids addition system described here has been the subject of other research. Larson (2007) conducted air addition tests using thirteen pressure transducers to determine the in-place vertical air permeability of landfilled waste overlain by 3 – 6 m of waste plus cover soil layer (January – March 2006). By comparing the field pore pressure measurements to a hydrogeologic analytical solution derived by Shan (1995) and revised by Shan and Javendel (1999), air permeability in the range of 2×10^{-13} to 8×10^{-13} m^2 was estimated. Larson (2007) reported that the corresponding vertical hydraulic conductivities were estimated to be 1.9×10^{-4} to 7.8×10^{-4} cm/sec.

Kumar (2009) studied the spatial variation of pore water pressure in waste as a result of pressurized liquid addition from July to October 2007. At a constant flow rate of 0.057 m^3/min, liquids were intermittently added through horizontal lines in bedding media trenches filled with shredded tires, crushed glass, or excavated waste. The current study is the follow-up study of Kumar (2009). This chapter includes the results and discussion of Kumar's 2009 study which is designated as Experiment 1. The

experiment conducted by the author is designated as Experiment 2. The main difference between Experiment 1 and Experiment 2 was liquids addition flow rate; a flow rate of 0.076 m^3/min was used for Experiment 2. In addition, during Experiment 2, liquids were added into the tire and glass trenches, not into the excavated waste trench.

Site Description and Experimental Preparation

Three horizontal liquids addition lines in trenches surrounded by bedding media were constructed on a 5,000 m^2 area of a municipal solid waste landfill in Florida. Figure 2-1 shows the plan and cross-sectional views of the study area; detailed plan and cross-sectional views are provided in Figures B-1 and B-2, respectively. The three trenches were excavated to dimensions of 0.9 m × 0.9 m × 110 m; the distance between the trenches was approximately 15 m. The trenches were back-filled to a height of 0.6 m with excavated waste, shredded tires, or crushed glass. A 110-m length of perforated 10-cm-diameter HDPE pipe was placed in each trench. Two 1-cm perforations were added at 0.6-m intervals along with the pipe; the pipe was placed with the perforations facing downward at an angle of 90º to each other. The remaining top 0.3 m of each trench was backfilled with the same bedding media.

Upon completion of waste filling (November 2007), the thickness of waste plus cover soil layers on top of the trenches was approximately 19 m. Experiment 1 was conducted from July to October in 2007, before the entire landfill capacity had been reached, but after the completion of waste placement over the horizontal lines. Experiment 2 was performed in April and May of 2010, approximately 30 months after the completion of the landfilling. Because no additional lift had been placed since Experiment 1, the thickness of the waste plus cover soil layers on top of the horizontal

trenches during Experiment 2 was assumed to be same as that during Experiment 1. The details of the experiments are explained in a later section.

A total of eighty one vibrating wire pressure transducers were installed surrounding the liquids addition lines for the in-situ measurement of pore pressure change due to pressurized liquids addition (Figure 2-1). To prevent damage, as recommended by Geokon, Inc. (vendor), each pressure transducer was inserted into a sand bag saturated with water. Also, the sand was chosen to quickly transmit the pressure developed in waste to the pressure transducer. The transducer wires were encased in PVC pipes filled with polyurethane expanding foam to prevent damage and preferential liquid flow. As shown in Figure 2-1, two layers of transducers were installed in a "V" formation around each pipe. This formation was selected to prevent disturbing the migration path of added liquids from the trenches to each transducer.

Pressure Transducers (Piezometer)

The pressure transducers (Model 4500S, Geokon, Inc.) were factory calibrated to a gauge pressure range of 0 to 345 kPa with a reported accuracy and resolution of ± 0.34 kPa and 8.6×10^{-2} kPa, respectively. The transducers were designed with thermistors to correct for the effects of temperature. The thermistors have a measurement range of -20˚C to 80˚C.

The transducer wires were connected to a data-logger (CR10X, Geokon, Inc.) placed on the side slope of the study landfill. The responses from all pressure transducers were recorded by the data-logger every 10 minutes for Experiment 1 and every 30 minutes for Experiment 2; the liquids addition data for the line in the excavated waste media trench were collected hourly. A laptop computer was used to download the raw frequency and temperature data from the data-logger (Figure B-3).

The raw data (Hz) of each pressure transducer was converted to pressure (kPa) using the calibration reports that were specific to each pressure transducer. The calibration equation for the pressure transducers was provided by the manufacturer as follow:

$$R = \frac{(Hz)^2}{1000} \quad (2\text{-}1)$$

$$P = G(R_0 - R_i) + K(T_i - T_0) \quad (2\text{-}2)$$

where R = reading (digits); (Hz) = raw data of a pressure transducer; P = pressure (kPa); G = calibration factor (kPa/digits); R_0 = initial reading (digits); R_i = reading at time i (digits); K = temperature correction factor (kPa/^{0}C); T_i = temperature at time i (^{0}C); T_0 = initial temperature (^{0}C). An example calculation is provided in Appendix D.

Bioreactor Operation

The bioreactor operation system at the study landfill was designed and built with a supervisory control and data acquisition (SCADA) system. Operation data such as liquids addition pressure, flow rate, added volume, and operation time were automatically recorded by the SCADA system. The bioreactor system was operated 3 to 7 hours a day depending on the field situation; due to various reasons (e.g., periodic SCADA system maintenance, breakage of a liquid distribution pipe, and cleaning leachate storage tanks), the bioreactor system was often stopped. In addition, the bioreactor operation permit limited the liquids addition pressure under a halting pressure in each horizontal line: 237 kPa for the excavated waste trench, 238 kPa for the shredded tire trench and 219 kPa for the crushed glass trench. These halting pressures were estimated by summing hydrostatic pressure (the average elevation of each

horizontal line which was initially placed × unit weight of water, 9.8 kN/m^3) and 34 kPa of liquids addition pressure (the limit set in the permit of the study bioreactor landfill).

This study consisted of two sets of liquids addition experiments; the details of the experiments are summarized in Table 2-1. In Experiment 1, liquids were added into all three lines at a constant flow rate of 0.057 m^3/min until liquids addition pressures reached the halting pressures. During this period, the results from fifty out of eighty one pressure transducers were found to be useful to monitor the pore pressure variation. The rest of the transducers produced unrealistic data (Kumar 2009). One possible explanation for this high failure rate could be harsh landfill conditions (e.g., sharp material and compaction efforts) which resulted in damage to the instruments. During Experiment 2 (conducted in 2010), the lines in the shredded tires and crushed glass trenches were operated at a constant flow rate of 0.076 m^3/min; no liquid was added through the line in the excavated waste trench. In the course of this experiment, twenty one out of eighty one pressure transducers were determined to be working properly.

Hydraulic Conductivity

Using the in-situ spatial pore pressure change data, vertical and horizontal hydraulic conductivities of the landfilled waste could be roughly estimated. Vertical hydraulic conductivities (K_y) were estimated using Equation 2-3, which was developed to determine the horizontal extent of saturated zone of a horizontal liquids addition line source (Townsend 1995); the derivation of Equation 2-3 is provided in Appendix E, and an example calculation of K_y using Equation 2-3 is presented in Appendix F.

$$K_y = \frac{q}{4x_{well}} \tag{2-3}$$

where q = constant linear flow rate (flow rate per unit length of line source, m^2/sec); X_{well} = horizontal maximum extent of saturated zone at the elevation of the horizontal liquids addition line source (m). X_{well} values were determined based on in-situ pore pressure variation monitoring results. A X_{well} value is a distance from the line source where practically no pressure is build-up; in this study, 5 kPa of pore pressure build-up was assumed to be practically negligible. Several assumptions need to be made to use Equation 2-3 (Townsend 1995). First, the medium is homogeneous and that axes of anisotropy of hydraulic conductivities are the principal axes of the system. Second, the primary driving forces for liquid transport are liquid addition pressure and gravity; capillary force within landfilled waste is negligible. Third, the trench can be treated as a horizontal line source. Fourth, there is no elevation difference between the center of a horizontal line source and a pressure transducer (no gravity influence). Fifth, the distance between the line source and the landfill bottom is infinite and liquid flow downward is not deterred.

With the same assumptions made for Equation 2-3, horizontal hydraulic conductivities could be roughly estimated using Equation 2-4 introduced by Bear (1979) and utilized by Townsend (1995).

$$S_{(R)} = \phi_{(R)} - \phi_{(r_w)} = \frac{q}{2\pi\sqrt{K_x K_y}} \ln\left(\frac{R}{r_w}\right) \qquad (2\text{-}4)$$

where $S_{(R)}$ = head drawdown (m); $\Phi_{(R)}$ = potential at a distance R (m); $\Phi_{(rw)}$ = potential in a horizontal trench (m); R = horizontal distance from a line source (m); r_w = effective well radius (m); K_x = horizontal hydraulic conductivity (m/sec). A $(K_xK_y)^{0.5}$ value was determined by finding a theoretical $S_{(R)}$-R curve closest to an actual $S_{(R)}$-R curve plotted based on the in-situ measurements; by varying $(K_xK_y)^{0.5}$ values while keeping other

parameters constant, theoretical $S_{(R)}$-R curves were developed and superimposed on an actual $S_{(R)}$-R curve. Note that Equation 2-4 was developed to determine head loss (or build-up) as a function of horizontal distance from a vertical recharging well (Bear 1979). An effective well radius (r_w) of 0.45 m (half of the trench width) was assumed; assuming r_w = 0.3 and 0.6 m, K_x values were also determined. Since a steady-state condition with respect to liquids addition pressure was not achieved during the study period, the highest pressure values within the trenches were used for Equation 2-4. In Appendix F, an example calculation of K_x using Equation 2-4 is provided.

Results and Discussion

Pore Pressure Change in Liquid Addition Bedding Media

Figures 2-2 and 2-3 present the responses of the pressure transducers in the crushed glass trench and the shredded tire trench for multiple days of intermittent liquids addition runs. G1/T1, G2/T2, and G3/T3 are at distances of 0, 50, and 110 m away from the entry of each perforated pipe in each trench. When leachate addition began, the transducers in the trenches responded in a relatively short amount of time (approximately 30 minutes) to the pressure developed by the leachate addition. The injected leachate was delivered to the end of the trenches without considerable head loss. Based on the observation, crushed glass and shredded tires are good options as trench bedding material in bioreactor landfill design. During Experiment 1, liquids addition through the excavated waste trench was attempted. Liquid addition pressure increased up to its halting pressure (237 kPa) in just one day. This might be explained by the low permeability of waste surrounding the line. In this study, 1.2×10^{-4} – 7.5×10^{-4} cm/sec and 8.2×10^{-6} – 2.1×10^{-5} cm/sec were estimated for horizontal and vertical hydraulic conductivities, respectively; the details of these hydraulic conductivity

estimates are discussed in a later section. No liquid addition occurred following that day as the pressure required for addition would have been higher than allowed in the bioreactor operation permit.

The times required for the trenches to be filled with added liquids were roughly estimated based on the data of temperature variation resulting from liquids addition. The hypothesis was that because the injected leachate had a much lower temperature (20-25^{0}C) than that of the waste in the study landfill (55-65^{0}C), the temperature at each thermistor started to drop when the injected leachate reached the thermistor; after leachate addition ceased, temperature gradually increased back to the surrounding temperature. Figure 2-4 shows the responses of the thermistors in the crushed glass trench during Experiment 2. Temperature variations at G2 and G3 were relatively small compared to G1 until day 6, corresponding to approximately 18 hours of cumulative liquids addition time; it was at this time that the temperature began to drop sharply as more added liquids arrived. Similarly, it was found the tire trench was filled in approximately 16 hours of cumulative liquids addition during both Experiment 1 and Experiment 2. Theoretical estimations at flow rates of 0.057 and 0.076 m^3/min suggested that approximately 3 - 8 additional hours liquids addition was needed for the saturation of the trench; assuming 0.5 of void ratio, void space volume = $0.5\times(0.9\times0.9\times110)$ m^3 = 44.6 m^3. These delays in the trench saturation might be because some of the liquid added was distributed into surrounding waste while liquids were still being intermittently added. During Experiment 1, approximately 35 hours (double the time needed in Experiment 2) was needed to fill the glass trench. The reason for this large difference is not clear; the experimental conditions (e.g., liquids

addition flow rates, the thickness of waste on top of the lines and hydraulic conductivities of the waste) during Experiment 1 and Experiment 2 were consistent.

Once liquids addition stopped, pore pressure built-up in the trenches began to dissipate as the added liquids migrated into the waste surrounding the trenches. In the case where liquids were added before the pore pressure built by previous additions dissipated, the pore pressure increased cumulatively. Because pore pressure in landfilled waste at a constant liquids addition flow rate increases cumulatively, higher addition pressure is required to inject the same amount liquid achieved from previous addition. Therefore, intermittent operation with proper resting (shut-off) time is recommended to bioreactor landfill operators.

Figure 2-5 shows the pore pressure changes in the trenches as a function of cumulative liquids addition time. During the study period, addition pressures (pore pressure in the trenches) seemed to approach steady-state at constant flow rates of 0.057 and 0.076 m^3/min. In a later section, the peak pressures of the last addition events were considered pseudo steady-state addition pressures to estimate hydraulic conductivities and anisotropy of landfilled waste.

Pore Pressure Changes within Landfilled Waste

Figure 2-6 shows examples of the responses of the transducers installed at certain horizontal distances away from each addition trench. The magnitude of pore pressure due to liquids addition decreased remarkably with distance away from the trench; the greatest pressure drop was observed near the trenches. For example, liquid added into the glass trench traveled through waste approximately 1.1 m, 30 kPa of pressure loss was measured (Figure 2-6-A). The pressure drop between the transducers at 1.1 m and 2.6 m was 3 kPa (Figure 2-6-a). Figure 2-6-A clearly shows the trend of the decrease in

pore pressure with increasing distance away from the crushed glass trench. However, the pore pressure responses detected by the transducers surrounding the shredded tire trench showed no trend (Figure 2-6-B). During liquids addition through the pipe in the excavated waste bedding media, no considerable pressure build-up was detected by the transducers in the waste surrounding the trench. Overall, high pressure zones due to liquids addition were only observed in close proximity to the crushed glass and the shredded tire trenches. Given that the spacing between horizontal trenches is much greater than the radius of the trenches, pressurized liquids addition should be much less of a slope stability concern compared to the case where pressures are assumed uniform throughout the waste.

To estimate vertical hydraulic conductivity (K_y) using Equation 2-3, one must first determine the horizontal extent of the saturated zone at the elevation of a horizontal trench (x_{well}). Values for x_{well} could be determined by examining pore pressure in the waste as it varied horizontally away from the trenches; these values are presented -in Table 2-2. For example, while pore pressure in the glass trench increased as high as 40 kPa during Experiment 1, only 5 kPa of pressure build-up was detected at a distance of 11.4 m. Based on this in-situ observation, x_{well} for the tire trench during Experiment 2 was determined as 11.4 m (Figure 2-7). In the same manner, x_{well} for the shredded tire trench was determined to be 21.3 m during Experiment 1. During Experiment 2, x_{well} was estimated at 23 m for the crushed glass trench; note that during Experiment 2 x_{well} for the shredded tire trench was not estimated because liquids were added only for 24 cumulative operation hours in which liquid addition pressure was not considered to reach steady or pseudo steady state.

Hydraulic Conductivity and Anisotropy

Using the x_{well} values determined in a previous section and Equation 2-3, K_y values of the landfilled waste surrounding the crushed glass and shredded tire trenches were estimated to be 1.0×10^{-5} and 1.9×10^{-5} cm/sec, respectively (Table 2-2). The K_y estimates of this study fell into a range of 3.0×10^{-6} to 1.5×10^{-2} cm/sec reported by other researchers (Townsend et al., 1995; Powrie and Beaven 1999; Durmusoglu et al., 2006). Note that the K_y values (1.9×10^{-4} – 7.8×10^{-4} cm/sec) estimated by Larson (2007) at the same landfill site are 10 to 78 times greater than those determined in this study. This difference might be attributed to the change in overburden stresses. The thicknesses of waste plus cover soils over the horizontal lines were 3 – 6 m when Larson (2007) conducted the study. Bleiker et al. (1995) and Powrie and Beaven (1999) indicated that hydraulic conductivity of landfilled waste decreased with increasing effective stress applied to the waste. Figure B-4 adapted from Bleiker et al. (1995) shows the variation of hydraulic conductivity with increasing effective stress. Assuming a bulk unit weight of 12 kN/m^3 and 19-m waste plus cover soil, an estimated load of 228 kPa was applied above the landfilled waste. At 228 kPa of effective stress, hydraulic conductivities fell into a range between 5.0×10^{-6} cm/sec and 1.5×10^{-5} cm/sec (Figure B-4); this range is close to that for K_y estimated in this study (1.0×10^{-5} – 1.9×10^{-5} cm/sec). Using the equation of K (m/sec) = $2.1(\sigma_v')^{-2.71}$ introduced by Powrie and Beaven (1999), a K_y value was estimated at approximately 8.6×10^{-5} cm/sec.

For each liquid addition experiment, theoretical pore pressure variation as a function of horizontal distance (R) from the center of the horizontal wells were estimated using Equation 2-4 and compared with in-situ measurements; an example plot is provided in Figure 2-7. Overall, a similar trend was observed from both the

mathematical model and the in-situ data; pore pressure decreases with increasing horizontal distance. This trend in the field data became more obvious as liquids addition was continued (Figure 2-7). By varying $(K_xK_y)^{0.5}$ values at a given flow rate and a given liquid addition pressure (pore pressure in trench), mathematical model plots close to in-situ measurements could be developed. As $(K_xK_y)^{0.5}$ value decreased, greater head drawdown was estimated at a given distance. In Experiment 1, the theoretical pore pressure drawdown curves were close to in-situ measurements where K_x values were 9.0×10^{-4} cm/sec and 2.5×10^{-3} cm/sec for the waste surrounding the crushed glass trench and the shredded tire trench, respectively. In Experiment 2, a K_x value of 2.5×10^{-3} cm/sec was estimated for the waste surrounding the crushed glass trench. Note that the K_x values were determined assuming r_w = 0.45 m (half of the trench width). It was found that the variation of K_x values with respect to r_w values (0.3 – 0.6 m) was not considerable (Table 2-2); the plots of the theoretical and actual head drawdown–distance curves for r_w = 0.3 m, 0.45 m, and 0.6 m are provided in Figures B-5 and B-6, respectively.

Using the estimated values of K_x and K_y, anisotropy (K_x/K_y) was estimated in the range of 37 to 277 (Table 2-2); this is much greater than anisotropy values (2 – 8) reported in literature (Landva et al., 1998; Hudson et al., 1999). This difference might be attributed to waste compaction efforts and waste composition. The anisotropy values estimated based on Experiment 2, conducted in 2010, were generally greater than the values estimated based on Experiment 1, conducted in 2007. There was no additional waste placement during the period between Experiment 1 and Experiment 2. Hence,

the greater anisotropy during Experiment 2 might be due to settlement of waste with decomposition, resulting in a horizontal flattening of the waste.

Summary and Conclusions

Pore pressure variation in a bioreactor landfill was monitored while adding liquids under pressure. Pore pressure transducers were installed in liquids-introducing bedding media trenches and in the surrounding waste. This study consisted of two sets of experiments; during Experiment 1 (2007) and Experiment 2 (2010), liquids were added intermittently up to 7 hours per day at constant flow rates of 0.057 m^3/min and 0.076 m^3/min, respectively.

Transducers in the bedding media trenches responded relatively quickly (30 min) to liquid addition pressure. Added liquids were successfully transferred to the end of the crushed glass and the shredded tire trenches. This was confirmed by monitoring temperature variation in the trenches; temperature inside the trenches dropped sharply once added liquids reached each monitoring point. Hence, the bedding media used here (crushed glass and shredded tires) represent good options for porous media for this type of liquids addition systems. Horizontal liquid distribution within landfilled waste was also studied by monitoring pore pressure variation. Pressure build-up close to the limit set in the study bioreactor landfill operation permit was only observed within the trenches. Pressure dropped sharply near the trenches and then gradually with distance away from the trenches. Thus, a slope stability analysis for bioreactor landfills equipped with this type of liquids addition systems should consider the rapid pressure loss in the waste with distance away from the injection source.

Using analytical models presented by Townsend (1995) and in-situ measurements, hydraulic conductivities of the landfilled waste surrounding the horizontal trenches were

estimated. Horizontal hydraulic conductivities were estimated in a range of 7.0×10^{-4} to 3.0×10^{-3} cm/sec, while estimated vertical hydraulic conductivities fell into a range of 1.0×10^{-5} to 1.9×10^{-5} cm/sec. Certain assumptions were made to estimate the hydraulic conductivities, but the estimated values fell within a range reported in literature. Thus, it is concluded that the analytical models introduced in this chapter can be used as simple, useful tools to estimate hydraulic conductivities of landfilled waste. Anisotropy values of horizontal to vertical hydraulic conductivities were estimated to be in the range of 37 to 277; the magnitude of this data range, higher than reported in literature, may be due to compaction efforts during waste placement.

Table 2-1. Bioreactor operation summary

	Trench bedding material	Operation duration (days)	Cumulative volume of leachate injected (m^3)	Addition flow rate (m^3/min)
Experiment 1 (2007)	Shredded tire	14	309	0.057
	Crushed glass	12	281	
	Excavated waste	1	24	
Experiment 2 (2010)	Shredded tire	6	106	0.076
	Crushed glass	11	214	
	Excavated waste	—	—	—

Table 2-2. Summary of estimated hydraulic conductivity and anisotropy values of landfilled waste

	Bedding material	x_{well} (m)	r_w (m)	K_x (cm/sec)	K_y (cm/sec)	Anisotropy (K_x/K_y)
Experiment 1 (2007) Q = 0.057 m^3/min	Crushed glass	11.4	0.30	1.04×10^{-3}	1.89×10^{-5}	55
			0.45	8.96×10^{-4}		47
			0.60	7.01×10^{-4}		37
	Shredded tires	21.3	0.30	2.80×10^{-3}	1.01×10^{-5}	277
			0.45	2.47×10^{-3}		245
			0.60	2.08×10^{-3}		206
Experiment 2 (2010) Q = 0.076 m^3/min	Crushed glass	23	0.30	3.04×10^{-3}	1.25×10^{-5}	243
			0.45	2.45×10^{-3}		195
			0.60	2.17×10^{-3}		174
	Shredded tires	—	—	—	—	—

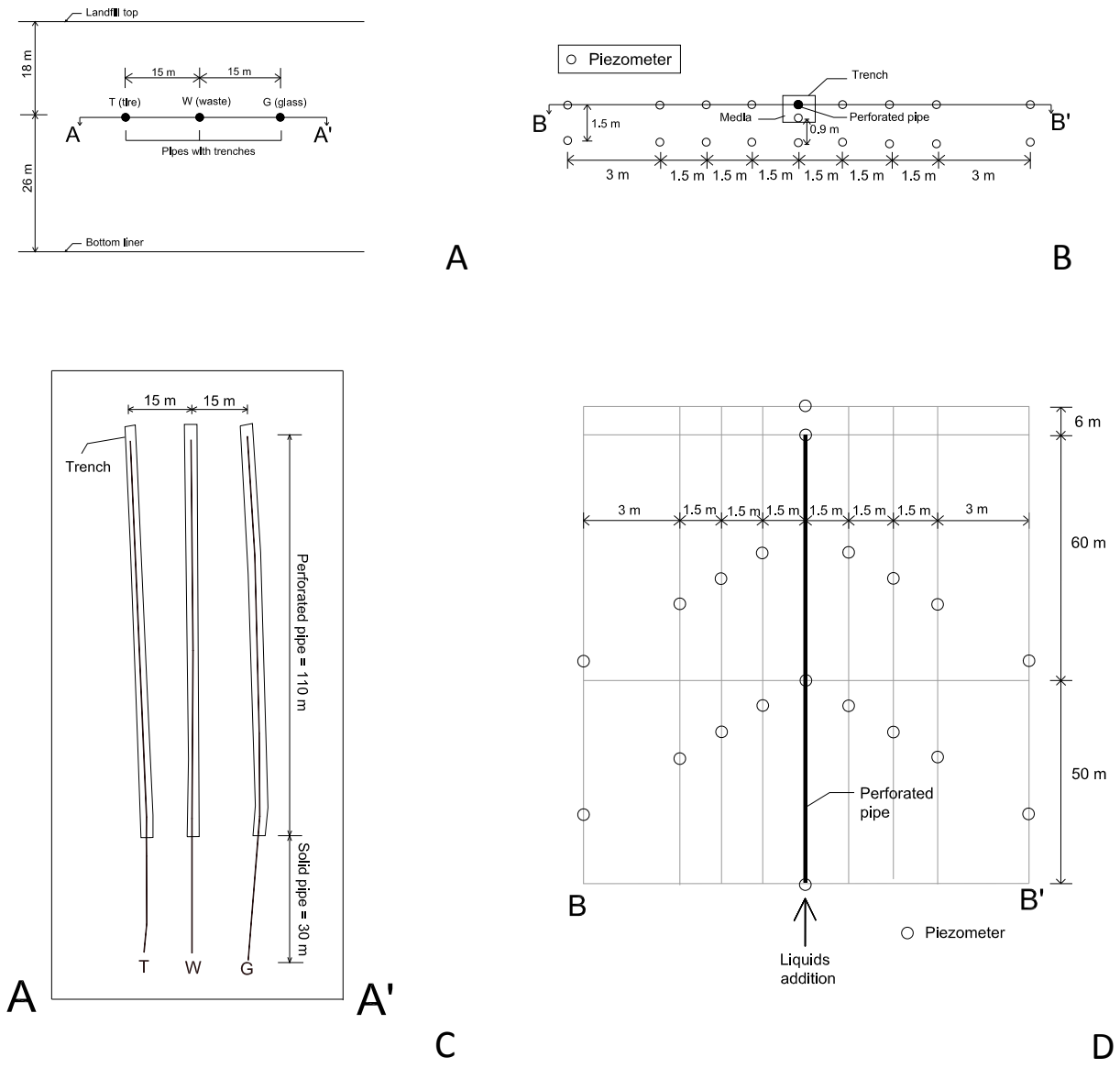

Figure 2-1. Schematic drawings of the cross-sectional and plan views of the study liquids addition system and piezometer distribution; the cross-sectional views of A) the horizontal liquids addition lines and trenches layout and B) the pressure transducers distribution surrounding each line and the plan views of C) the horizontal liquids addition lines and trenches layout and D) the pressure transducers distribution surrounding each line

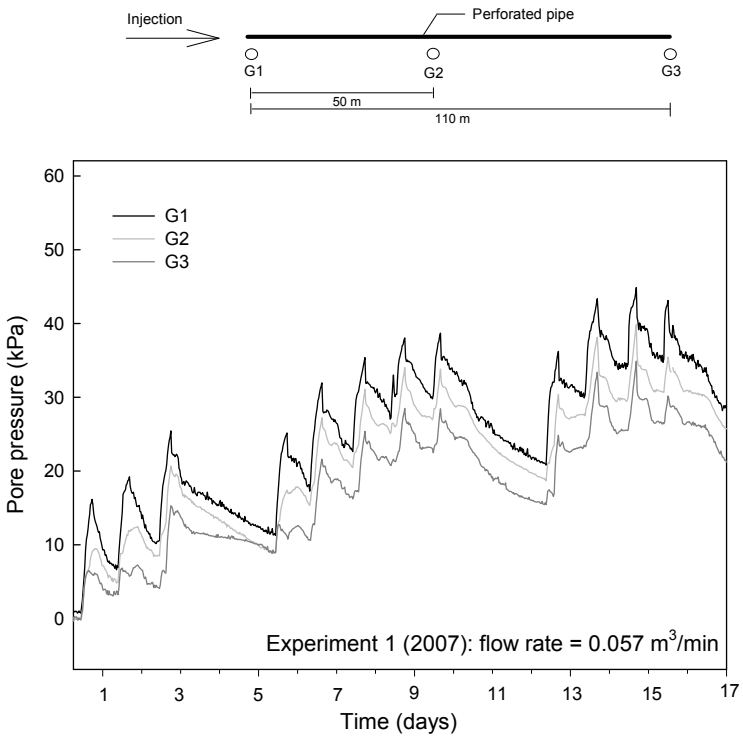

A

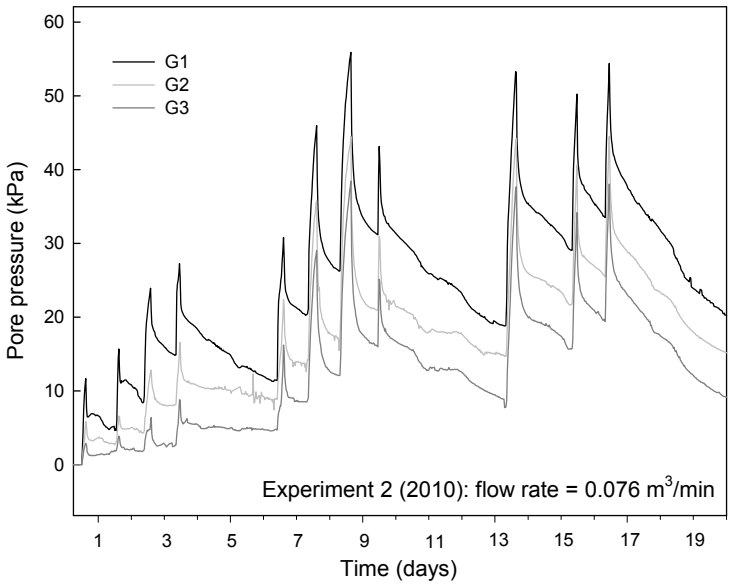

B

Figure 2-2. Pore pressure change in the crushed glass media trench due to liquids addition; G1, G2, and G3 are in the trench: A) Experiment 1 and B) Experiment 2.

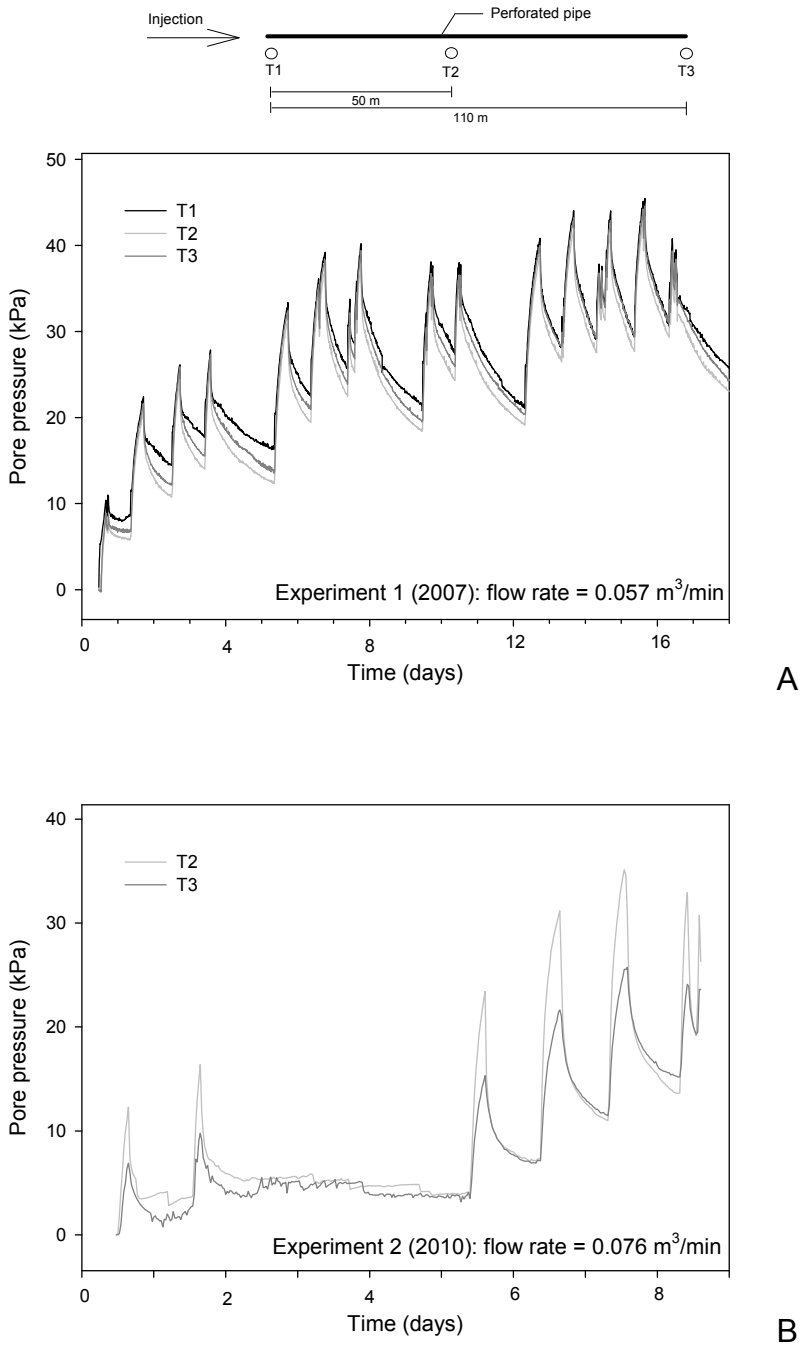

Figure 2-3. Pore pressure change in the shredded tire media trench due to liquids addition; T1, T2, and T3 are in the media trench: A) Experiment 1 and B) Experiment 2.

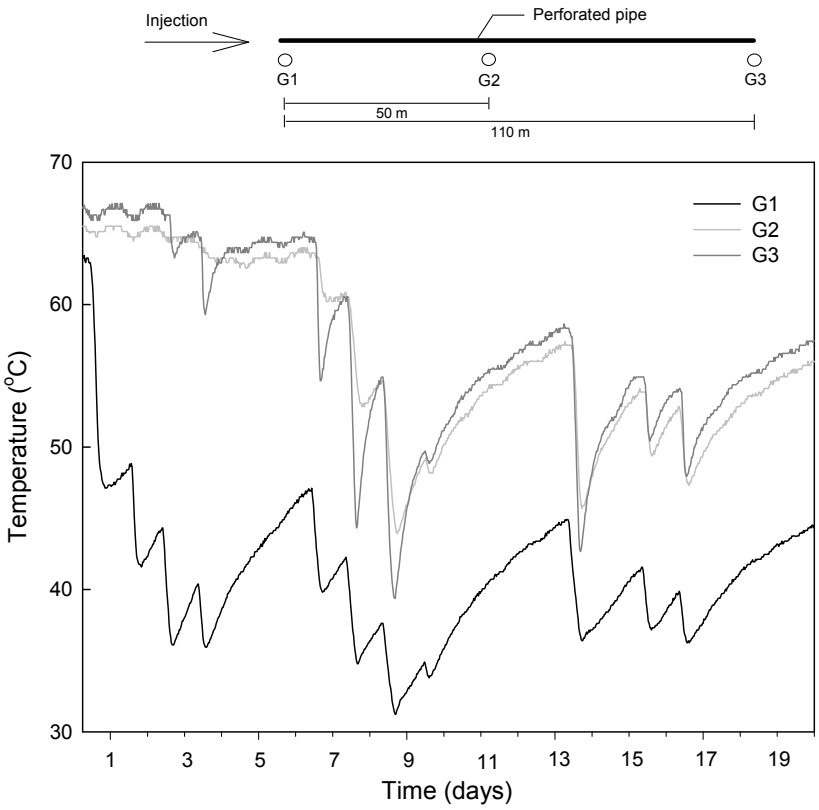

Figure 2-4. Temperature variation in the crushed glass media trench due to liquids addition; G1, G2, and G3 are in the trench. Data collected from Experiment 2 were used.

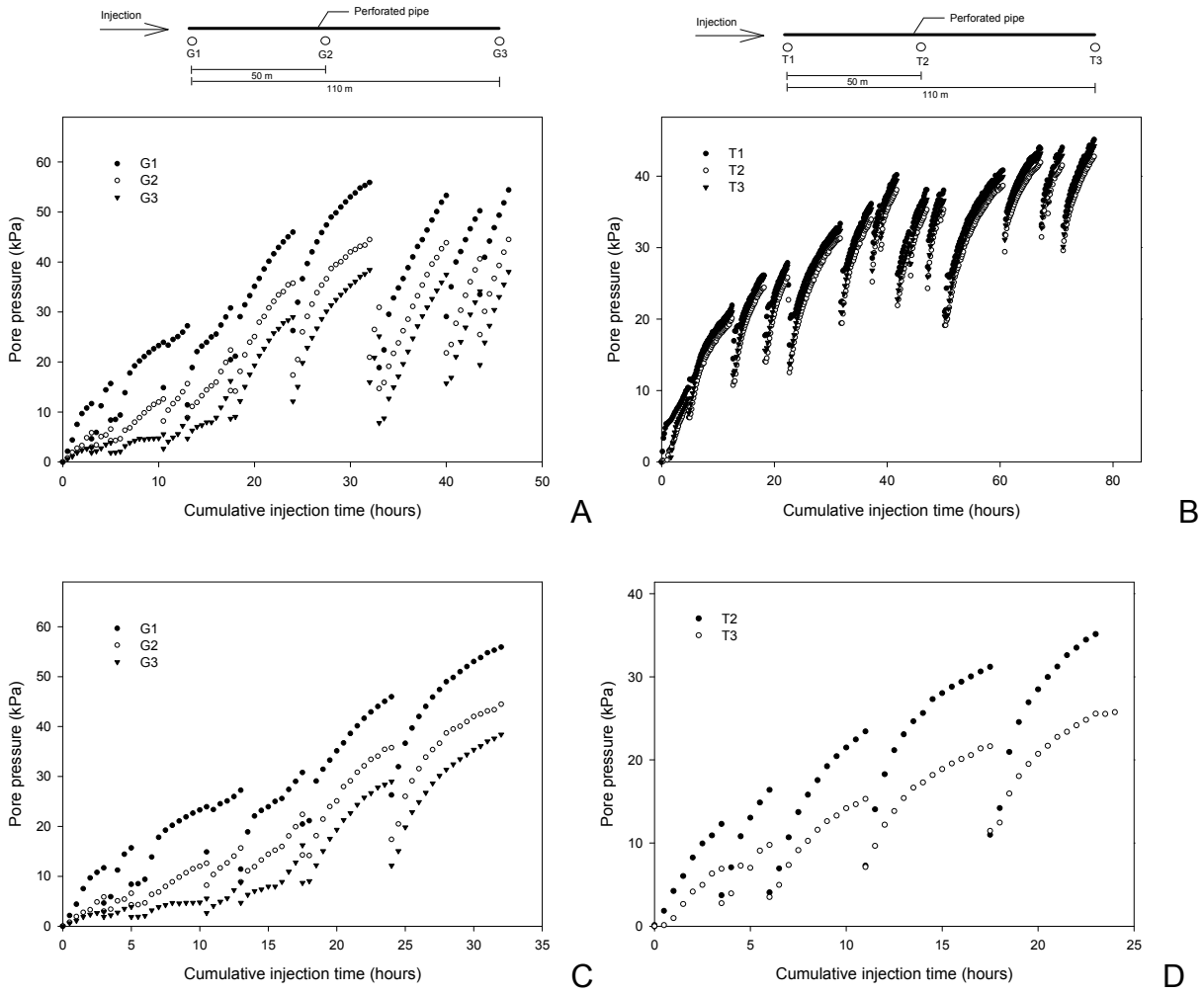

Figure 2-5. Pore pressure change as a function of cumulative liquids addition time: A) Experiment 1 (crushed glass trench), B) Experiment 1 (shredded tire trench), C) Experiment 2 (crushed glass trench), and D) Experiment 2 (shredded tire trench).

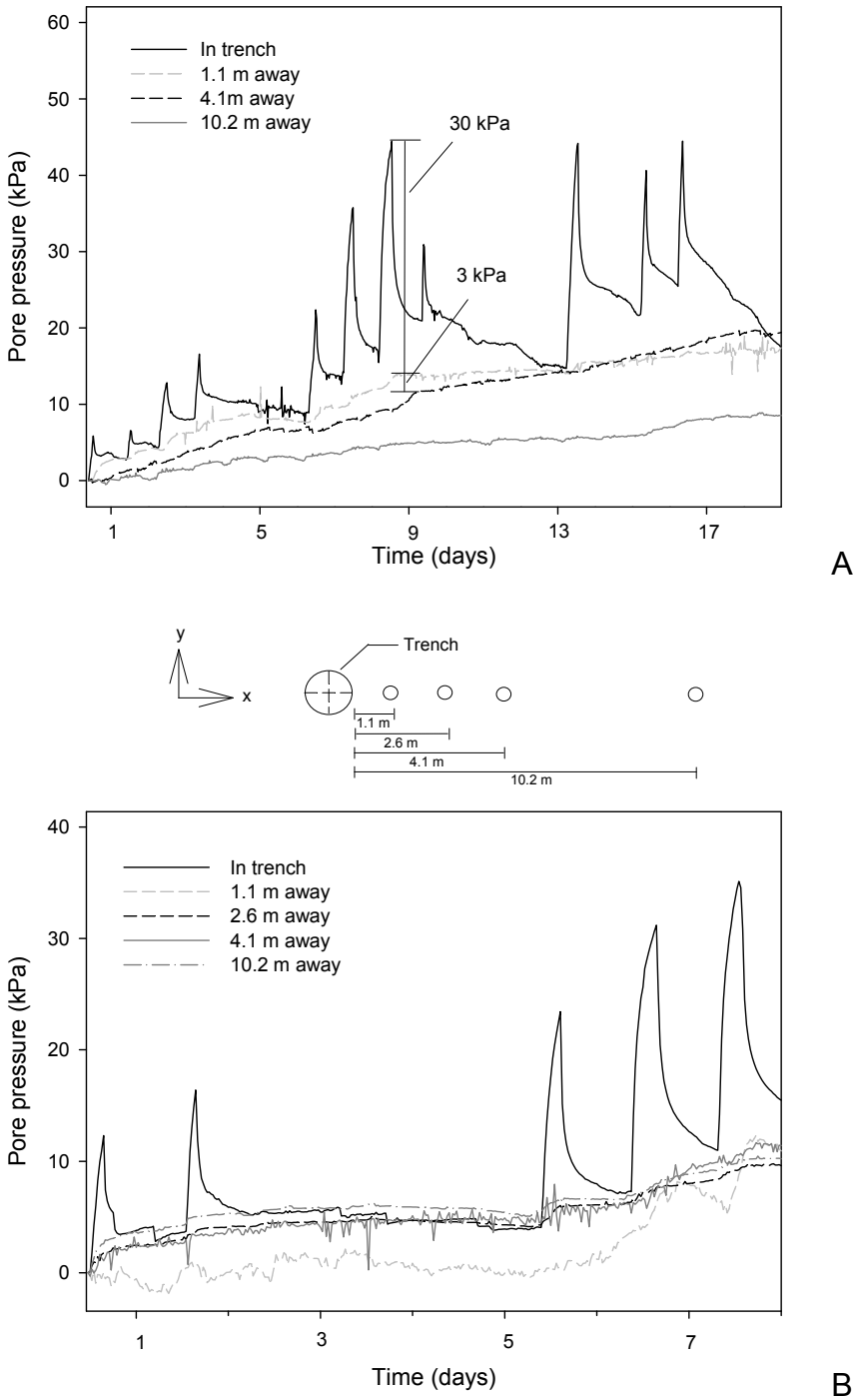

Figure 2-6. Example plots of pore pressure changes with distance away from the trenches with A) crushed glass and B) shredded tire bedding material; data collected during Experiment 2 (2010) were used.

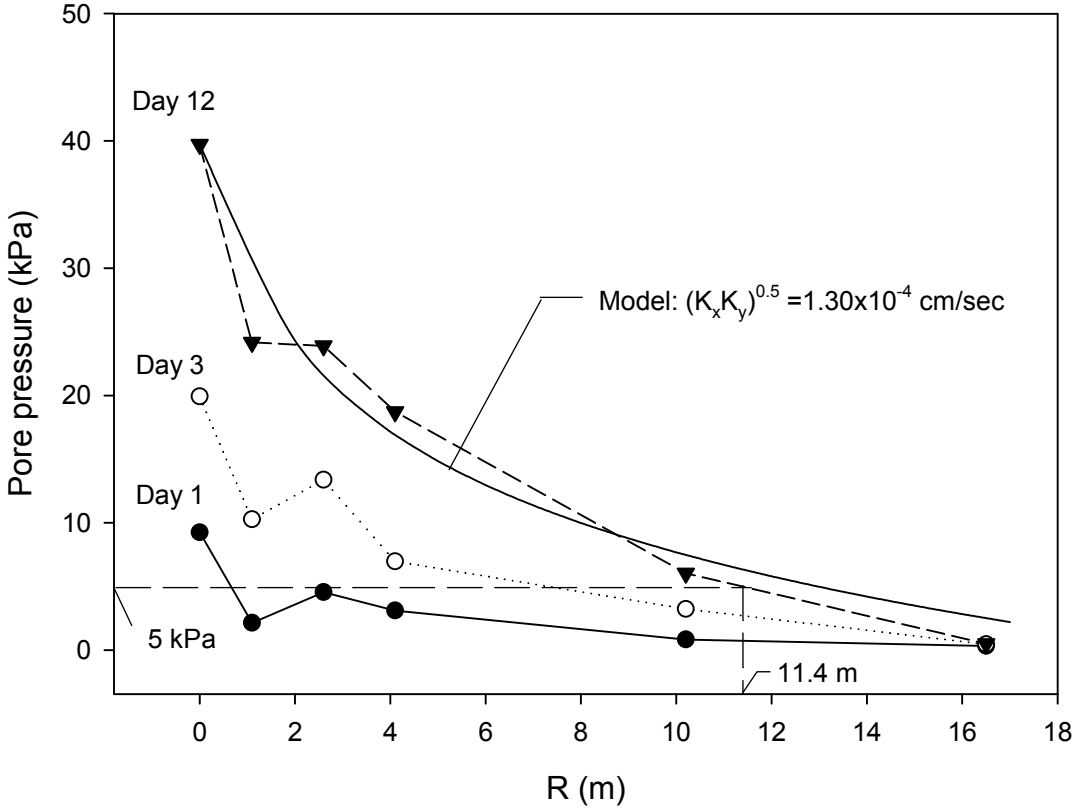

Figure 2-7. Comparison of pore pressure change as a function of a horizontal distance from the line source between the field data and theoretical estimates: the results of liquids addition into the crushed glass trench during Experiment 1.

CHAPTER 3
IN-SITU SETTLEMENT MEASUREMENTS OF A LANDFILL PREVIOUSLY OPERATED AS A BIOREACTOR SUBJECTED TO SURCHARGE

Introduction

The settlement of waste over time at a landfill results from a combination of mechanical and biological processes. Waste volume deforms in response to added stresses (e.g., new waste placement and other landfill infrastructure). Waste also settles as a result of mass loss accompanying biological decomposition. The settlement process is influenced by the presence of liquids and gases in the landfill and by long-term physical changes in the structure of waste components. While many attempts to estimate landfill waste settlement rely on classic soil consolidation models (Sowers 1973; Powrie and Beaven 1999; Landva et al., 2000; Machado et al., 2002; Anderson et al., 2004; Durmusoglu et al., 2006), it has become more widely recognized that multiple processes need to be considered in such estimates (Ling et al., 1998; El-Fadel and Khoury 2000; Liu et al., 2006; Oweis 2006; Elagroudy et al., 2007). Detailed monitoring of full-scale landfill settlement resulting from distinct processes will result in a better understanding of the phenomenon and the development and refinement of predictive tools.

This chapter reports the results of an experiment designed to measure waste settlement during one specific phase: mechanical settlement occurring in waste that is predominantly biologically degraded but still saturated or near saturated with moisture. In a previous study, waste settlement at a bioreactor landfill was found to be affected by the physical presence of moisture (Kadambala 2009). A follow-up study was conducted in which a load was placed on top of this area and the settlement was monitored. It is

hypothesized that this phase of settlement is similar to classic soil consolidation: as excess pore pressure resulting from the applied load dissipates, the soil skeleton (in this case, degraded waste) is consolidated, resulting in surface settlement. The main objective of this study is to present settlement monitoring results of a municipal solid waste landfill subjected to surcharge. The settlement of the waste layer under the surcharge was measured using a settlement profiling technique. In addition, coefficients of volume change, coefficients of consolidation, modified primary compression indices and hydraulic conductivities of waste were roughly estimated using the in-situ settlement measurements. The reported quantification of these parameters is expected to provide further understanding of the settlement behavior of bioreacted waste and fundamental inputs for landfill settlement prediction models.

Material and Methods

Bioreactor Landfill Operation and Characteristics

A4-hectare portion of the New River Regional Landfill (NRRL) in Florida, United States (Figure B-7) was chosen as the study site. MSW was accepted in this area from 1992 to 1998. Liquids addition was performed using vertical wells in an effort to promote waste stabilization (Jain 2005; Jain et al., 2005, 2006; Kadambala 2009) from June 2003 - April 2007. This liquids addition over 3.8 years delivered approximately 22.7×10^3 m^3 of liquid (primarily leachate from the same landfill, with some groundwater). A liquids volume of 400 to 1000 m^3 was added to each of 45 vertical well clusters. After this period, the liquids addition well field was decommissioned to allow for new waste placement.

The well field area was subject to several research experiments before, during and immediately following the period of liquids addition. Jain (2005) and Jain et al. (2005, 2006) estimated waste permeability using two different techniques: an air injection test and a borehole permeameter test. Kadambala (2009) examined the settlement of different waste layers using individual vertical well settlement measurements and concluded that the layers in the middle of the waste, where most of the liquids were added, settled the least. Given that biochemical methane potential measurements in these wetted areas indicated that biological decomposition was largely completed; Kadambala (2009) hypothesized that waste settlement was limited by the pressure of moisture in the waste matrix. The results of bio-chemical methane potential and moisture content analyses of the study landfill before and after the bioreactor operations are provided in Figure B-8. In addition, the settlement measurements (meters and %) with time during Kadambala's 2009 study are provided in Figure B-9.

Post Bioreactor Settlement Profiling

Settlement of the decommissioned bioreactor area was monitored using a settlement profiler; this technique employs hydrostatic pressure measurement between a pressure transducer and a liquid reservoir reference point. Prior to the placement of an additional layer of waste, five 46 m settlement profiling pipes (HDPE) with a diameter of 10 cm were placed on the top surface of the bioreactor area. Figure 3-1 shows a photograph of the settlement profiling pipes over the top surface of the study landfill prior to waste placement and the plan view of the layout of the settlement profiling pipes. The baseline elevations of the settlement profiling pipes were surveyed on September 26, 2008 by a local professional surveying company (Patrick B. Welch and Associates).

Settlement profiling was conducted six times: December 2008 (10 days after waste placement), May 2009 (152 days), June 2009 (175 days), August 2009 (266 days), December 2009 (380 days), and March 2010 (450 days). Each settlement profiling included temporary placement of the liquid reservoir at a reference station located at a higher elevation than the settlement profiling pipe. The elevation of the reference station from a benchmark was measured using a laser theodolite (Spectra Precision Gplus, Trimble); the method is explained in Appendix G. The benchmark was installed on the ground surface approximately 40 m away from the study landfill. The elevation of the benchmark was surveyed in December 2008 and it was assumed no elevation change occurred during the study period. The pressure transducer, liquid tube, and sensor cable tied to a series of 2.54-cm PVC pipes were slid into the settlement profiling pipe to a desired location. The vibrating wire settlement profiler used in this study (Model 4651, Geokon, Inc.) is equipped with a liquid tube connecting the transducer and the liquid reservoir filled with de-aired 55:45 (distilled water:commercial grade ethylene glycol) solution, specific gravity = 1.07. The profiler is also equipped with a vent line so that the transducer reading was not affected by barometric pressure variation. The settlement profiler had a gauge range of 7 meters with a reported accuracy and sensitivity of ± 7 mm and 1.75 mm, respectively. The readings from the settlement profiler were collected using a vibrating wire data recorder (Durham Geo Slope Indicator). The vibrating wire frequency detection range of the recorder was from 450 to 6000 Hz. The resolution and accuracy of the recorder were 0.01% full-scale and ± 0.02% of Hz reading, respectively.

The elevation of a desired location in a settlement profiling pipe was estimated using the following equations provided by the manufacturer.

$$R = \frac{(Hz)^2}{1000} \tag{3-1}$$

$$E = E_{ref} - G(R_o - R_c) \tag{3-2}$$

where R = reading (digits); (Hz) = raw data of a pressure transducer; E = elevation of the sensor (m); E_{ref} = elevation of the reference station (m); R_o = reading at the reference station (digits); R_c = reading at a target location (digits); G = calibration constant (meter per digits). An example settlement calculation using Equations 3-1 and 3-2 is provided in Appendix H.

Compression Properties and Hydraulic Conductivity Estimation

With the hypothesis that the settlement behavior of high-moisture content landfilled waste is similar to consolidation settlement, the hydraulic conductivity and compression properties of the landfilled waste were roughly derived using the soil mechanics approach utilized by multiple researchers (Sowers 1973; Morris and Woods 1990; Fassett et al., 1994; Landva et al., 2000; Durmusoglu et al., 2006).

The modified compression indices (C_c') were calculated using the following equation.

$$C_c' = -\frac{\Delta H}{H_i} \frac{1}{\log\left(\sigma_f / \sigma_i\right)} \tag{3-3}$$

where ΔH = change in elevation during the primary consolidation period (m); H_i= initial height of a bioreacted waste layer (m); σ_i, σ_f = initial and final stress applied to the midpoint of the bioreacted waste layer, 0.5 H_i, (kPa). It was assumed that the primary

consolidation of the underlain (bioreacted) waste layer ended in June 2008 based on an inflection point of the thickness of waste – time curve, and a difference in strain ($\Delta H/H_i$) at each settlement monitoring location during the period was used to determine the modified primary compression indices (C_c'). The increases in overburden pressures were estimated by multiplying a thickness of waste newly placed by a bulk unit weight; a bulk unit weight of the new waste layer was assumed to be 12 kN/m^3 based on the bulk unit weight estimates in Chapter 4. An example calculation of C_c' is provided in Appendix I.

Coefficients of volume change (m_v) were estimated with an assumption that the change in waste volume occurred vertically (no lateral volume change).

$$m_v = -\frac{\Delta H}{H_i}\frac{1}{\Delta \sigma'} \tag{3-4}$$

where $\Delta\sigma$' = pressure increment at $0.5H_i$ (kPa). Note that the same assumptions made for the C_c' estimation were used for m_v determination. An example calculation of m_v is provided in Appendix I.

To estimate the coefficient of consolidation (c_v), the logarithm of time fitting method developed by Casagrande (1940) was used.

$$c_v = \frac{(T_v)_{50}\, d^2}{t_{50}} = \frac{0.197 d^2}{t_{50}} \tag{3-5}$$

where $(T_v)_{50}$ = time factor corresponding to 50 % ultimate consolidation (-); $d = \frac{H_i + H_f}{4}$ = average drainage path for the pressure increment (m); H_i, H_f = initial and final thicknesses of the underlain waste layer (m); t_{50} = time to 50% ultimate consolidation

(minute). An example calculation can be found in Appendix I. The plots of the logarithm of time-fitting model used to estimate c_v are also provided in Figures B-14 to B-16.

Vertical hydraulic conductivity (K_y) of media could then be estimated using m_v and c_v values.

$$c_v = \frac{K_y}{m_v \gamma_w} \tag{3-6}$$

$$K_y = c_v m_v \gamma_w \tag{3-7}$$

where γ_w = unit weight of water (9.8 kN/m^3). It was assumed that the horizontal movement of moisture was confined by cover soil, and thus the hydraulic conductivities estimated using Equation 3-7 are vertical hydraulic conductivities (K_y). An example of K calculation using Equation 3-7 can be found in Appendix I.

Results and Discussion

Settlement and Bioreactor operation

At the study site, topographic surveying was conducted to evaluate the impact of liquids addition on the settlement of the bioreactor landfill from June 2003 to October 2007, by Kadambala (2009). In addition, topographic surveying was performed by the author in September 2008 to measure initial elevations of settlement monitoring points prior to additional waste placement.

Average settlement estimations (meter or %) in this time period are plotted as a function of time in Figure 3-4. Overall, three stages of settlement patterns were observed during this period: Stage 1 (August 2002 – October 2004), Stage 2 (October 2004 – April 2006), and Stage 3 (April 2007 – September 2008). The stages were distinguished based on the inflection points of the settlement (%) – time curve and a

settlement rate (% per year) for each stage was estimated by linear regression (Figure 3-4).

During Stage 1, a settlement rate of 1.15 % per year was estimated, which fell into a typical settlement rate range of conventional dry tomb landfills: 1.0 – 2.9 % per year (Edil et al., 1990; Sanchez-Aliciturri et al., 1995; El-Fadel et al., 1999; Yuen et al., 1999; Benson et al., 2007). As liquid was added, the study bioreactor landfill underwent accelerated waste decomposition and settlement; average settlement rate in Stage 2 was estimated to be approximately 5.1 % per year. In literature, settlement rates of bioreactor landfills including aerobic and anaerobic operation systems were reported in the range of 1.6% to 10.0% (Yuen et al., 1999; El-Fadel et al., 1999; Benson et al., 2007; US EPA 2007). In Stage 3, the landfill settlement rate decreased to approximately 1.7 % per year. This attenuation in settlement may be explained by the fact that a considerable amount of organic material in the waste was degraded during Stage 2. Average BMP values decreased from 0.22 to 0.11 L $CH_{4(g)}$ per gram VS during the bioreactor operation period (Figure B-8).

Settlement due to Surcharge

Initial settlement profiling was conducted 10 days after additional waste placement in December 2008. Settlement data were collected from eighty monitoring points and analyzed; settlement (%) data are compiled in Tables A-3 to A-7. The results showed extremely high settlement values; approximately 3.7 m of settlement were measured at a point where the thicknesses of waste layers above and below the pipe were 5.2 and 17.4 m, respectively. This was found to be unreasonable based on the results of subsequent settlement profilings. Figure 3-5 shows an example plot of the settlement

profiling results of Pipe 3; settlement measurements collected on Day 10 are much greater than those collected on Day 152. These false readings on Day 10 were attributed to air-bubbles in the liquid; air-bubbles interfered with hydrostatic pressure transmission to a pressure transducer. Since the readings of the first profiling were found to be false after comparing with the next profiling conducted 3 months after the first profiling, no attempt to re-measure the first readings could be made.

During the first 152 days after waste placement, an average of 0.49 % of settlement was measured, which was greater than settlement occurred for the next 298 days (an average of 0.43%). Figure 3-6-A shows an example plot of settlement measurements over time at settlement monitoring locations in Pipe 1. Near the entry of Pipe 1 above which only 0 – 0.3 m of waste plus cover soils were placed, less settlement occurred than other monitoring locations above which 0.3 – 8.5 m of waste plus cover soils were placed. However, no clear relationship between the thickness of waste plus cover soils (or overburden pressure) and settlement was found from the data collected from Pipe 1. The data collected from Pipe 3 and Pipe 4 showed that settlement generally increased with increasing thickness of waste plus cover soils. The Pipe 4 data, for example, is presented in Figure 3-6-B; the Pipe 3 data is provided in Figure B-11.

After waste placement, the bioreacted waste layers settled at an average settlement rate of 3.75 % per year (Figure 3-4), which is approximately 1.4 times greater than an average settlement rate (2.66 % per year) prior to the waste placement. It was hypothesized that the accelerated settlement of the profiling period could be attributed to the consolidation settlement of the bioreacted waste layer subject to surcharge. As

the trapped moisture was expelled due to surcharge, the waste layer might undergo consolidation settlement. Kadambala (2009) pointed out that a considerable amount of moisture was trapped in the middle and bottom layers as a result of liquids addition; the average moisture contents of middle and bottom layers were 46% with standard deviations of ± 4.3% and 44 % with standard deviations of ± 4.6%, respectively (Figure B-8). Figure 3-7 shows the monthly variation in leachate generation. Before the additional waste placement, average monthly leachate generation volume was approximately 200 m^3 (January 2007 – June 2008). Note that after removing the top geomembrane cover of the bioreactor, the leachate generation increased sharply due to rain water inflow into the leachate collection system of the landfill (July – October 2008). Additional waste layer was placed on top of the bioreacted waste layer in the period of November to December 2008. The leachate generation amount started to increase from February 2009 (approximately 2 months after the waste placement) and peaked at approximately 1100 m^3 in May 2009. Since the top surface of the additional waste lifts was planted after the additional waste placement, rain water inflow into the leachate collection system was considered to be negligible in this period. The delay in leachate generation increase after the waste placement was likely attributed to the low permeability of landfilled waste.

Compression Properties and Hydraulic Conductivity of Landfilled MSW

Based on the in-situ settlement measurements, hydraulic conductivities (K) and compression properties (C_c', m_v, and C_v) of MSW landfilled in the study landfill were roughly estimated and compared with the values reported in literature (Sowers 1973; Oweis et al., 1990; Shank 1993; Townsend et al., 1995; Landva et al., 1998; Powrie and

Beaven 1999; Landva et al., 2000; Machado et al., 2002; Anderson et al., 2004; Durmusoglu et al., 2006; Jain 2005; Jain 2006). The values of the parameters were determined using Equations 3-3 through 3-8 and were compiled In Table 3-1. The details of the estimation method used in this chapter and an example calculation were provided in Appendix I.

Figure 3-8 shows the histograms of C_c', m_v, c_v, and K of the bioreacted waste determined in this study; estimated compression properties and K values are compiled in Tables A-8 to A-12. A relatively wide range of C_c' values (0.1 – 1.7) were estimated in this study while approximately 75% of the estimated C_c' values fell into a range of 0.1 – 0.5, close to the values (0.1 - 0.41) reported in literature (Sowers 1973; Landva et al., 2000; Machado et al., 2002; Anderson et al., 2004; Durmusoglu et al., 2006). The relatively large C_c' values (0.5 – 1.7) estimated might be due to the compression of waste structure weakened by waste decomposition. The m_v values estimated in this study are most frequently found in a range of 2.9×10^{-4} – 2.3×10^{-3} m^2/kN which fell into the range of 2.5×10^{-4} – 5×10^{-3} m^2/kN reported in literature (Powrie and Beaven 1999; Landva et al., 2000; Durmusoglu et al., 2006); the compression properties in the literature are provided in Table A-1. Overall, the m_v values had a tendency to decrease with increasing load while the coefficient of consolidation showed no clear correlation to load change. Figure 3-8-C shows the histogram of the c_v values estimated using Equation 3-6. The c_v values were estimated to be in a range of 0.89×10^{-2} to 1.44×10^{-2} cm^2/sec which are smaller than the range of c_v values (5.62×10^{-2} – 5.12 cm^2/sec) reported by Durmusoglu et al. (2006). Durmusoglu et al. (2006) pointed out that the lower values of c_v are typically attributed to good compaction. Note that not all data sets

collected from each settlement monitoring location could be used to estimate a c_v because some of them were found to be inappropriate to develop a semi-log plot of a time-consolidation curve including a primary-secondary consolidation inflection point. The K_y values of 4.6×10^{-7} to 9.8×10^{-6} cm/sec could be estimated using the estimated values of m_v and c_v and found to be overall lower than those reported in literature, 3×10^{-6} – 1.5×10^{-2} cm/sec (Townsend et al., 1995; Landva et al., 1998; Powrie and Beaven 1999; Jain 2005; Durmusoglu et al., 2006; Larson 2007); the K values in the literature are provided in Table A-1 In addition, the K values were low compared to those estimated at the same study landfill (5.4×10^{-6} – 6.1×10^{-5} cm/sec) by Jain (2005). The decrease in hydraulic conductivity of the landfilled waste might be due to the increase in overburden pressure. Bleiker et al. (1995) and Powrie and Beaven (1999) pointed out that hydraulic conductivity of landfilled waste decreases as overburden pressure applied to the waste increases (Figure B-4).

Summary and Conclusions

Settlement patterns of a landfill site subjected to surcharge were investigated using an in-situ settlement profiling technique. Prior to additional waste placement, five HDPE pipes with a 10-cm diameter were placed over the study landfill cells and equipped with 45 vertical liquids addition well clusters. This landfill had been previously operated as a bioreactor. The thicknesses of the waste layers above and below the pipes varied from 0 to 6 m and 13 to 20 m, respectively. Settlement profiling was conducted six times after the waste placement. However, the settlement profiler used in this study often generated false readings due to air-bubbles in the liquid employed by the profiler; this was corrected by exchanging the faulty liquid with de-aired solution. It is

recommended that liquid in the profiler be examined to determine the presence of air-bubbles prior to use.

During the settlement profiling period, average settlement rate was estimated to be 3.76 % per year; this is 1.4 times greater than the average settlement rate prior to the waste placement (2.66% per year). It was hypothesized that the settlement mechanisms of the landfilled waste due to surcharge might be similar to the consolidation settlement of saturated clay, so the amount of leachate generation would increase as the moisture trapped in waste matrix was expelled due to the surcharge. This hypothesis was verified by monitoring leachate generation; average monthly leachate generation was found to increase from approximately 200 m^3 to 1100 m^3 approximately 5 months after the waste placement. In addition, Kadambala (2009) reported that the moisture content of the middle waste layer of the study landfill was increased to an average of 40% due to liquids addition. This increase in moisture content and resulting pore pressure build-up hindered settlement.

Using the settlement profiling data, compression properties (C_c', m_v, and c_v) were estimated. The estimated ranges of C_c' (0.1 – 0.5) and m_v (2.9×10^{-4} – 2.3×10^{-3} m^2/kN) values most frequently found in this study were consistent with ranges reported in literature. Wide overall ranges of C_c' and m_v values were estimated; however, these wide ranges could be attributed to the heterogeneous nature of MSW. The estimated c_v values fell into a relatively narrow range (0.89×10^{-2} to 1.44×10^{-2} cm^2/sec); this range was lower than values reported in literature. These low c_v values might be due to accelerated settlement during the bioreactor operation period. Vertical hydraulic conductivities of the bioreacted waste were estimated to be in the range of 4.6×10^{-7} to

9.8×10^{-6} cm/sec; this is lower than estimated vertical hydraulic conductivities at the same study landfill (5.4×10^{-6} – 6.1×10^{-5} cm/sec) by Jain (2005). The decrease in hydraulic conductivity of the landfilled waste may be attributable to the increase in overburden pressure.

Table 3-1. Summary of the compression properties and hydraulic conductivities (K) of waste in the study landfill

Pipe ID-Distance from pipe entry	Cc'	c_v (cm^2/sec)	m_v (m^2/kN)	K (cm/sec)
P1-10 m	0.97	0.012	4.63×10^{-3}	5.62×10^{-6}
P1-13 m	1.43	0.014	6.48×10^{-3}	9.12×10^{-6}
P1-16 m	1.64	0.014	7.10×10^{-3}	9.84×10^{-6}
P1-19 m	1.02	0.011	4.24×10^{-3}	4.60×10^{-6}
P1-22 m	0.72	0.011	2.91×10^{-3}	3.08×10^{-6}
P1-25 m	0.28	0.012	1.09×10^{-3}	1.32×10^{-6}
P1-31 m	0.16	0.012	5.46×10^{-4}	6.29×10^{-7}
P1-34 m	0.12	0.012	4.02×10^{-4}	4.88×10^{-7}
P1-37 m	0.11	0.014	3.40×10^{-4}	4.59×10^{-7}
P2-6 m	1.03	0.009	4.69×10^{-3}	4.08×10^{-6}
P2-9 m	1.00	0.010	4.38×10^{-3}	4.18×10^{-6}
P2-12 m	0.45	0.010	1.88×10^{-3}	1.81×10^{-6}
P2-15 m	0.47	0.012	1.88×10^{-3}	2.24×10^{-6}
P2-27 m	0.23	0.012	8.03×10^{-4}	9.56×10^{-7}
P5-14m	0.75	0.013	3.48×10^{-3}	4.52×10^{-6}
P5-23m	0.65	0.012	2.95×10^{-3}	3.45×10^{-6}
P5-35m	0.42	0.013	1.84×10^{-3}	2.40×10^{-6}

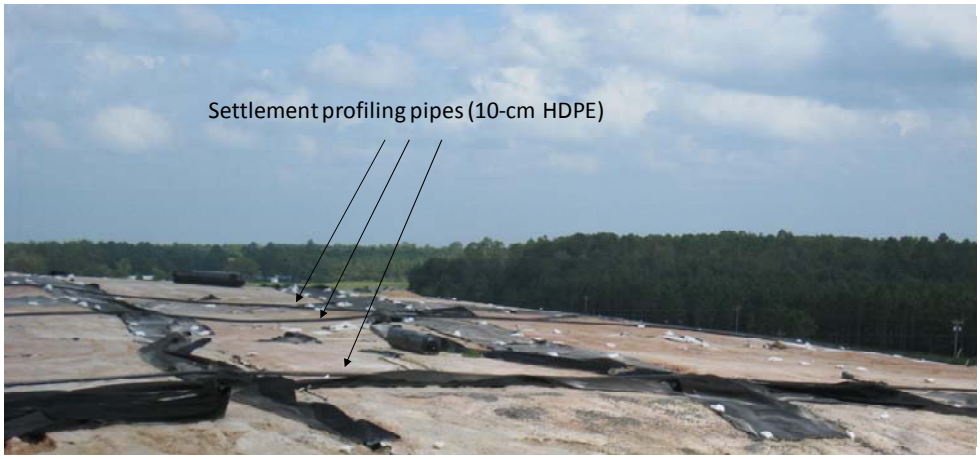

A

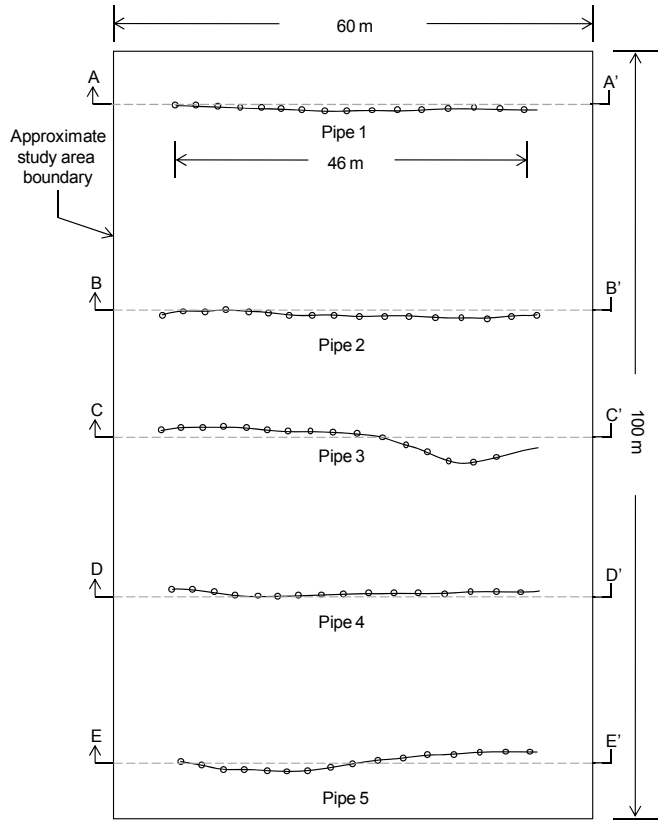

B

Figure 3-1. Installation of settlement profiling pipes: A) photograph of settlement profiling pipes on the study landfill cells (only three of five settlement profiling pipes installed were shown in this photograph) and B) plan view of locations of the profiling pipes and settlement monitoring. Each symbol ○ represents a settlement measurement location.

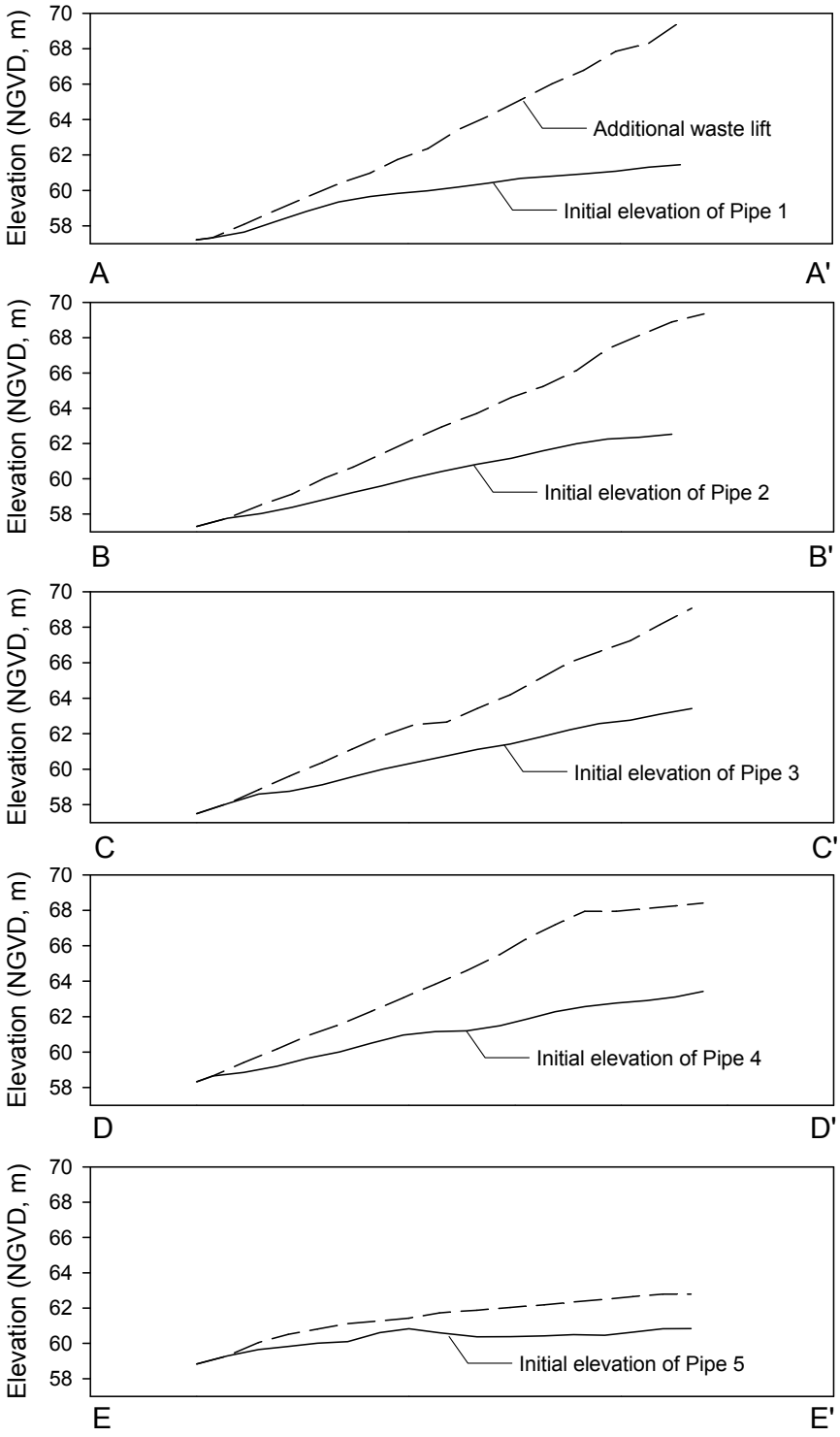

Figure 3-2. Cross-sectional views of existing and additional waste lifts; A-A' through E-E' correspond to those in Figure 3-1; NGVD represents U.S. National Geodetic Vertical Datum.

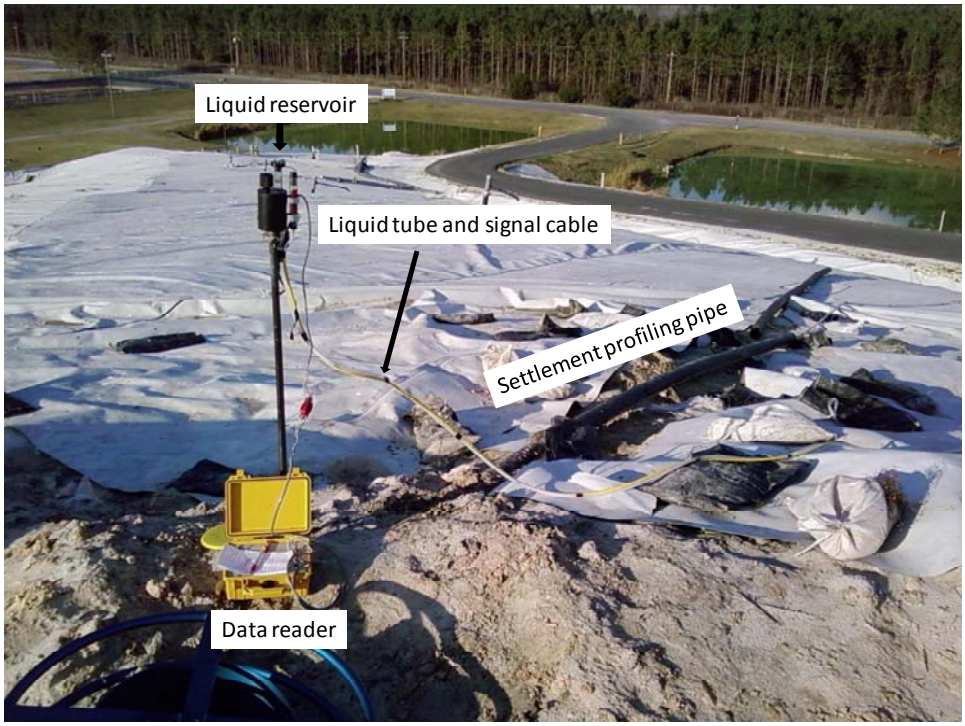

A

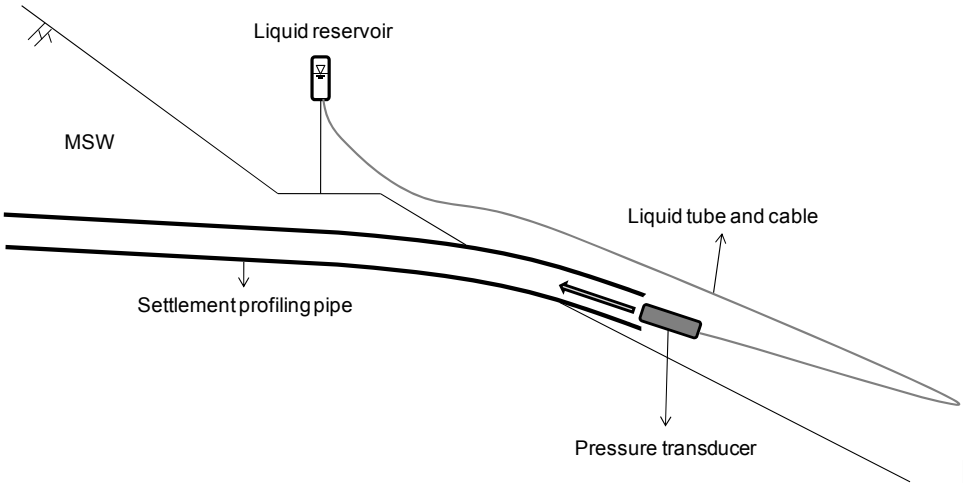

B

Figure 3-3. Schematic drawing of settlement profiling

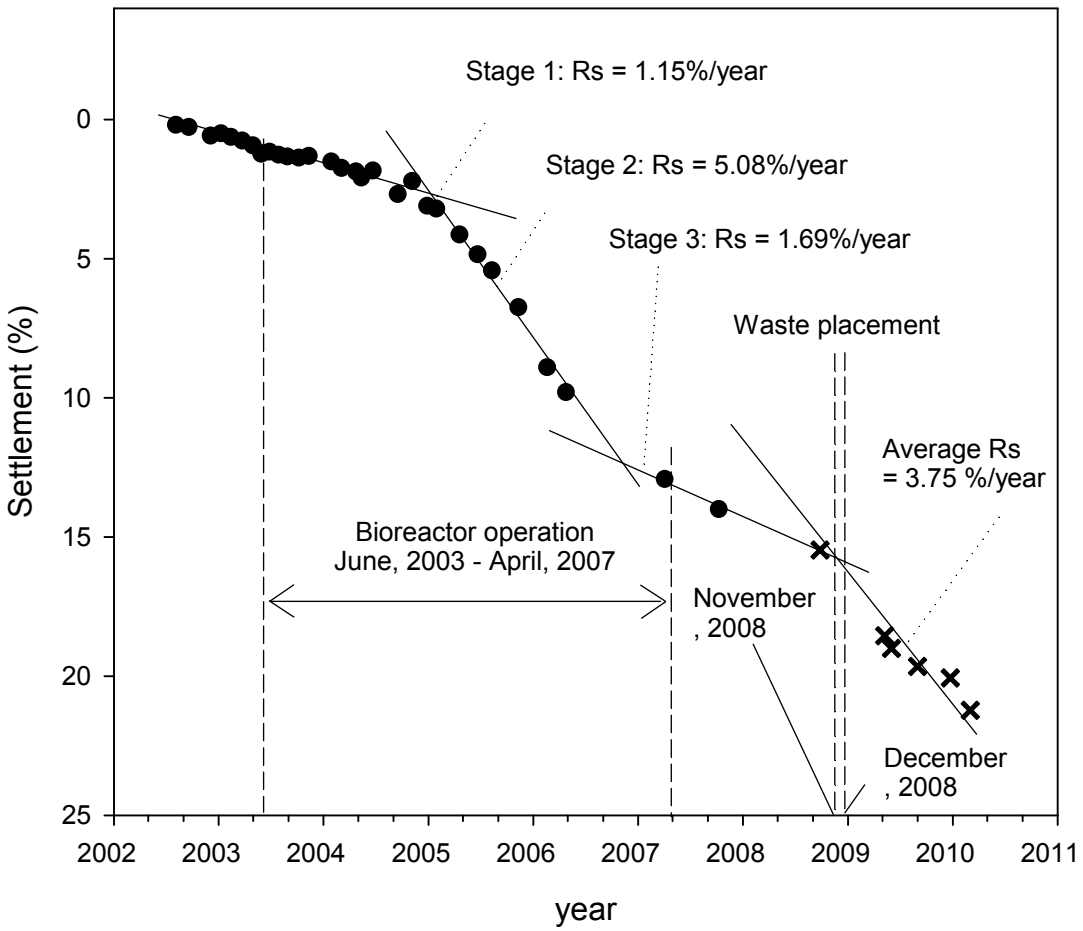

Figure 3-4. Change in the settlement rate (Rs, %/year) of the study landfill due to bioreactor operation and subjected to surcharge; the data points plotted are average settlement (%) values.

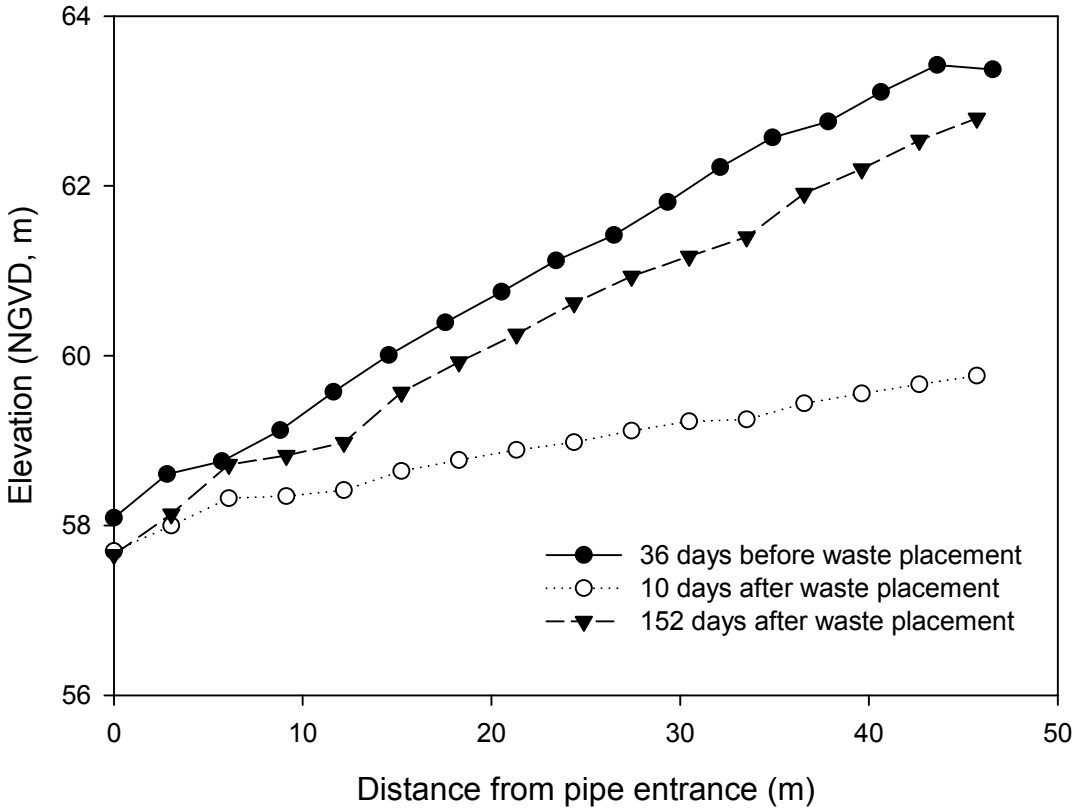

Figure 3-5. Example plot of false settlement readings recorded during the first settlement profiling (data from Pipe 3); NGVD represents U.S. National Geodetic Vertical Datum.

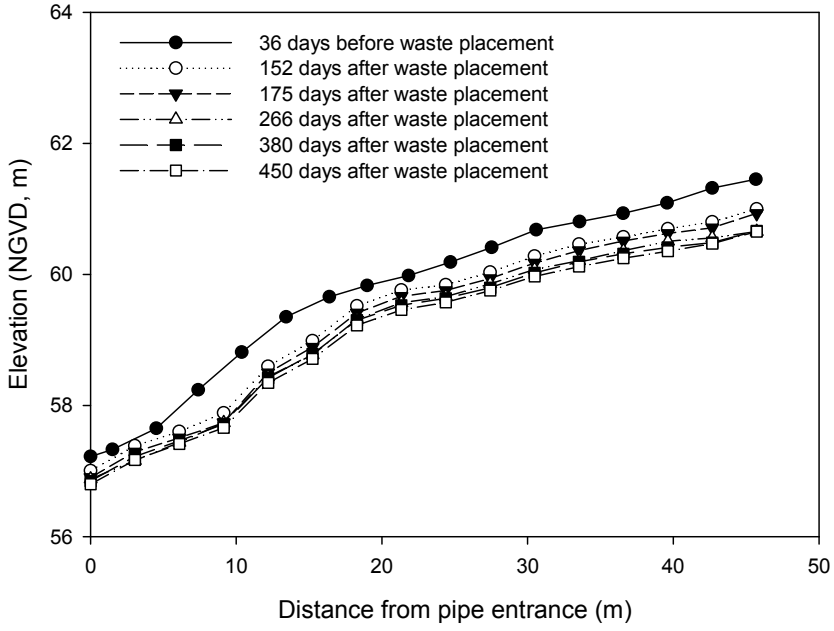

A

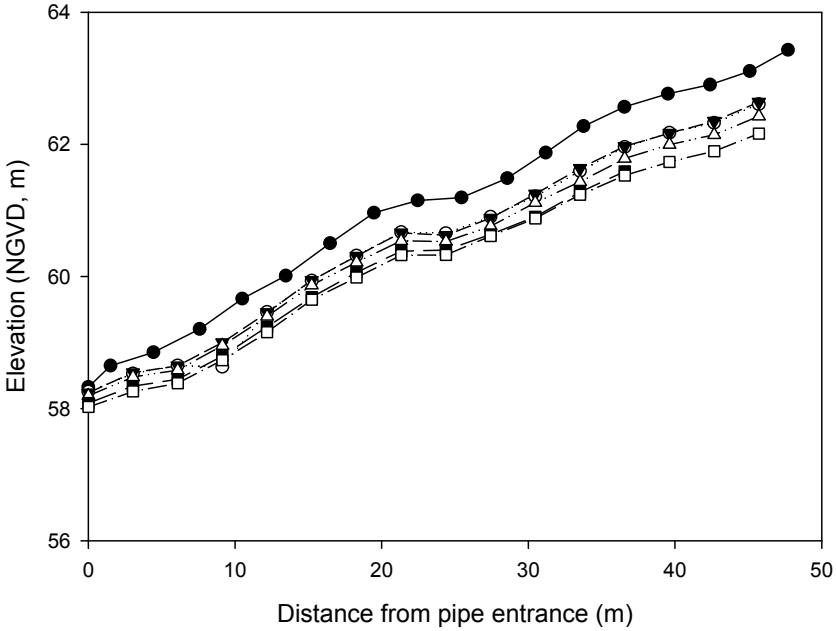

B

Figure 3-6. Example plots of settlement over time at each settlement measurement location in settlement profiling pipes: A) data from Pipe 1 and B) data from Pipe 4. NGVD represents U.S. National Geodetic Vertical Datum.

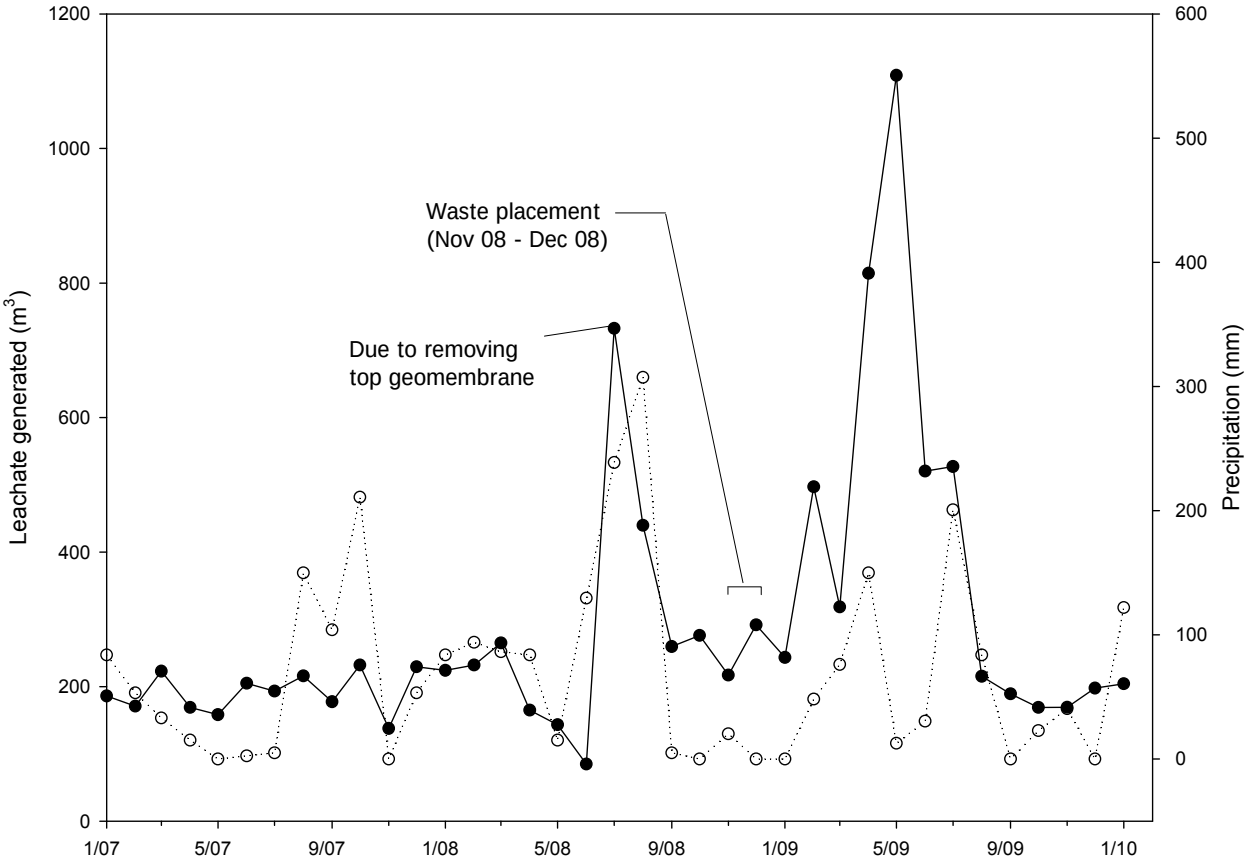

Figure 3-7. Monthly leachate generation of the study landfill and precipitation; the precipitation data collected at the Raiford State Prison Station, Florida, were used (National Oceanic and Atmospheric Administration, www.noaa.gov).

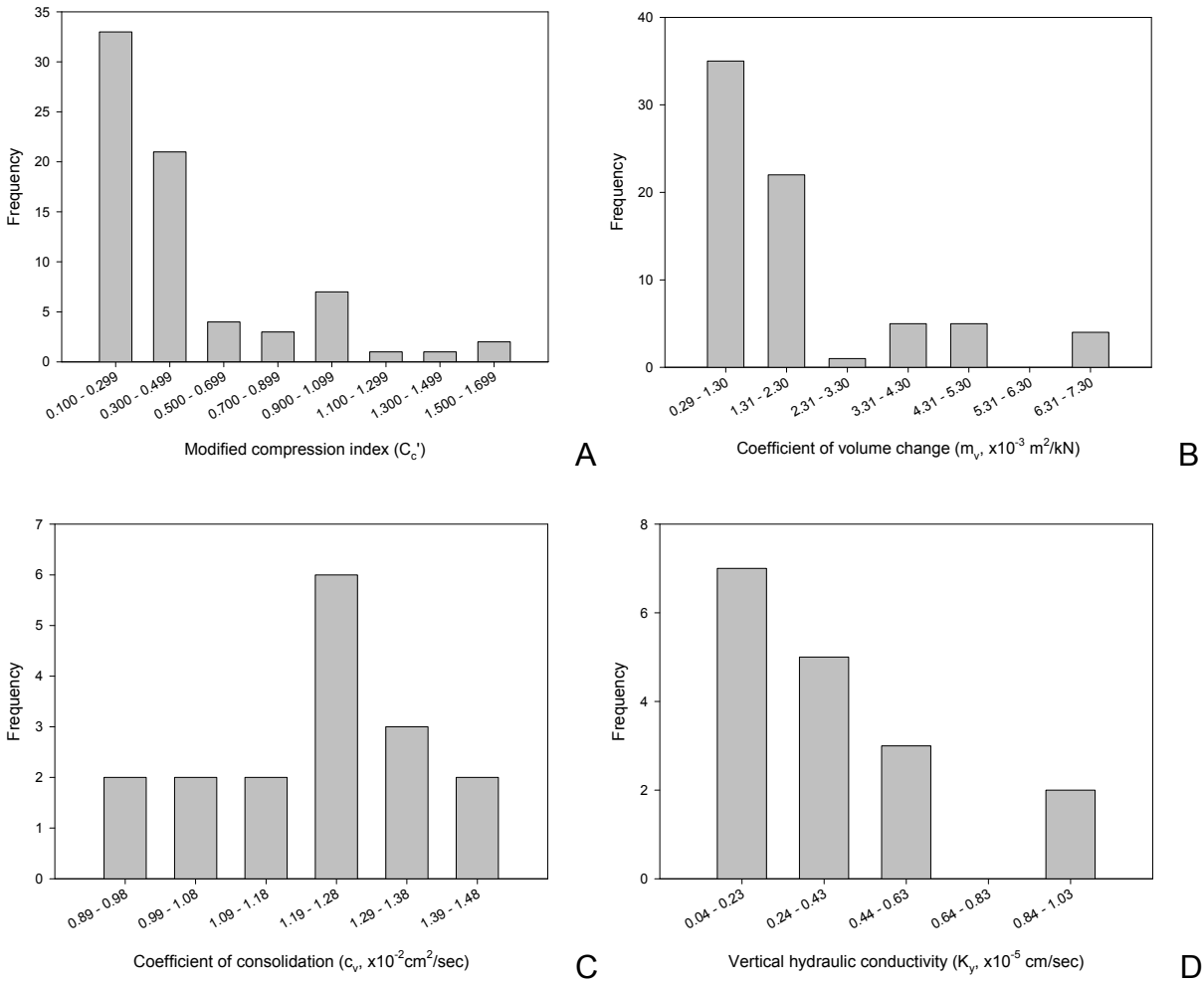

Figure 3-8. Histograms of the properties of landfilled waste: A) modified compression index, B) coefficient of volume change, C) coefficient of consolidation, and D) vertical hydraulic conductivity

CHAPTER 4
IN-SITU MEASUREMENTS OF LANDFILL FOUNDATION SETTLEMENT AND OVERBURDEN PRESSURE

Introduction

Predicting the settlement of a landfill foundation is a critical design consideration. Landfill bottom liners are graded to promote gravity drainage of leachate; unexpected excessive settlement could result in leachate collection system failure by altering the grade. A fundamental input necessary for the prediction of landfill foundation settlement is the overburden pressure produced from the waste, cover soil, and other landfill infrastructure. Overburden pressure estimates can be used with soil characterization data (e.g., stress-strain modulus) to estimate foundation soil settlement at distinct points at the base of the landfill. While overburden pressure estimates and subsequent settlement calculations are common in landfill design, actual measurements of these parameters is uncommon.

The main objective of this study was to measure load and settlement patterns of the foundation of an operating MSW landfill in the early stages of construction. The method of measurement was in-situ settlement sensors and total pressure cells. Prior to bottom geomembrane installation, sixteen settlement sensors and sixteen total pressure cells were installed and monitored underneath the liner of the landfill for 39 months (before and during waste placement). To the author's knowledge, this study was the first attempt to monitor landfill foundation settlement behavior using in-situ sensors. The in-situ settlement data were compared with theoretical settlement estimations normally calculated during the design phase of landfill construction. This chapter was intended to

provide insight into actual landfill foundation settlement behavior, which is very important to ensure the integrity of landfill structure.

Material and Methods

Site Description

This study was performed on a lined landfill unit (designated herein as "the landfill") of the Polk County North Central Landfill located in Florida, US. The landfill began accepting waste in October 2007, accepting approximately 2000 tons of MSW per day during the course of this study. The planned landfill capacity upon completion of waste filling is 6.1million m^3, with a 23-hectare area and a height of 55.6 m. Figure 4-1 shows the schematic of the plan and cross-sectional views of the study landfill consisting of two subcells bisected by a center berm. Detailed topographic drawing of the study site is provided in Figure B-20. The landfill is equipped with a double-liner system consisting of a geosynthetic clay liner and a 0.76-cm drainage net sandwiched by two 1.5-mm HDPE geomembrane (textured) overlain by 0.6-m sand drainage layer ($K = 1.0\times10^{-3}$ cm/sec).

Standard penetration tests (SPTs) and cone penetration tests (CPTs) to 16.7 m below the ground surface were performed by design engineers prior to bottom liner construction. Figures B-18 and B-19 shows the locations of SPTs and CPTs. Table A-13 presents a soil profile schematic under the center berm based on the results of the SPTs and CPTs performed near the center berm (overburden pressure and settlement monitoring area); a considerable amount of clayey soils, as well as silty and sandy soils, are present in this area. The groundwater table is approximately between 3 and 4 m below the bottom liner.

Instrumentation and Data Collection

Prior to bottom liner installation, eight pairs of settlement sensors (SS) and eight pairs of total pressure cells (TPC) were placed along the center berm (March 2006). At each monitoring location, a pair of TPCs were placed above a pair of SSs (Figure 4-1). To prevent damage, SSs were inserted in a 10-cm HDPE pipe. The instrument wires were connected to a data station at the east end of the center berm (Figure 4-2). Designations A through H and in Figure 4-2 (A) indicate the instrument locations; duplicates (A' through H') were installed approximately 0.6 m apart.

The SSs used in this study (Model 4650, Geokon, Inc., New Hampshire) are designed to measure the relative settlement between two points: a reference point (the data-logger) and a target point. The settlement results reported in this chapter were measured assuming that the reference point did not settle or upheave during the monitoring period. The SSs (pressure transducer) measure the hydrostatic pressure in the unit of hertz (frequency) caused by the height of liquid column difference between the sensor and the liquid reservoir placed at a reference station (data-logger). The liquid in the tube was a de-aired 55:45 (distilled water : commercial grade ethylene glycol) solution with a specific gravity of 1.07. Liquid tubes, vent lines, and signal cables were run from the data-logger to each settlement monitoring location, approximately at distances of 30, 61, 122, 183, 244, 305, 366, 427 m from the data-logger. Two types of vibrating wire SSs were used in this study. Half of the SSs were equipped with air-vent tubes (labeled A through H), and the others were not (labeled A' through H'). The vent line was used to avoid the barometric pressure impact on SS readings. Atmospheric pressure at the barometer monitoring point may be different from that at the point of the

settlement sensor, which may lead to misinterpreted data. From a maintenance standpoint, non-vented SSs are beneficial because blockages in the vent lines due to pinching, dirt, or moisture can cause false readings. However, the accuracy of a vented SS is better because they do not require barometric pressure correction. The SSs were factory calibrated to a gauge range of 7 meters with a reported resolution and accuracy of 1.75 mm and ± 7 mm, respectively. Additionally, each SS was equipped with a thermistor for the thermal impact correction of SS readings. Temperature in a range between -20 and 80 ^{0}C could be measured with ±1^{0}C accuracy.

The TPCs used (Model 4810, Geokon, Inc., New Hampshire) were designed to measure the total stresses in soil or the pressure of soil on structures. They are constructed from two stainless steel plates (diameter of 230 mm and thickness of 6 mm) welded together around the periphery; the narrow space between them is filled with de-aired oil which is connected by a liquid tube to a pressure transducer. The oil pressure is converted to an electrical signal (frequency) which is transmitted through a signal cable to the data station. The TPCs were factory calibrated to a gauge range of 2 MPa with a reported resolution and accuracy of 0.5 kPa and± 2 kPa, respectively. The TPC was equipped with a thermistor capable of detecting temperature in a range of -20 to 80ºC.

The outputs of the instruments were collected every two to four weeks from March 2007 through June 2010. Over the study period, no particular maintenance issues originated from the TPCs. In the early course of the study, severe data fluctuations were observed from fourteen SSs due to air-bubble accumulation in the liquid; this problem was corrected by exchanging the solution with new de-aired liquid. The readings from

the TPCs and SSs were collected using a vibrating wire data recorder (DURHAM GEO SLOPE INDICATOR, Washington). The data recorder can detect vibrating wire frequency in the range of 450 to 6000 Hz and has a resolution of 0.01% FS (full-scale), and an accuracy of ± 0.02% of Hz. In addition, thermistor readings in resistance (ohm) were automatically converted into the unit of Celsius degree in a range between -20 and 120 ºC with ±1ºC accuracy and recorded.

Unit Conversion of Instrument Readings

Readings from each TPC and SS have a unit of frequency and thus were converted to the proper units of kPa and cm, respectively. Unit conversion and calibration equations for the SSs are as follows:

$$R = \frac{(Hz)^2}{1000} \tag{4-1}$$

$$E = G\,(R_o - R_i) + \Delta E_{res} + K(T_i - T_0) + \{B_0 - B_i\} \tag{4-2}$$

where R = reading (digits); (Hz) = raw data from settlement sensor; E = elevation of the sensor (cm); ΔE_{res} = any change of the liquid level inside the reservoir sight glass (cm); R_o = initial sensor reading (digits); R_i = reading at time i (digits); G = calibration constant provided by the manufacturer (cm/digits); T_i = temperature at time i (^{0}C); T_0 = initial temperature (^{0}C); K = temperature correction factor (cm/^{0}C) provided by the manufacturer; $\{B_0 - B_i\}$ = barometric pressure correction for non-vented SSs (cm H_2O). An example calculation is provided in Appendix J.

Unit conversion and calibration equations for the TPCs were as follows:

$$R = \frac{(Hz)^2}{1000} \tag{4-3}$$

$$P = G(R_0-R_i) + (B_0-B_i) - K(P) \quad (4\text{-}4)$$

where R = reading (digits); (Hz) = raw data from pressure transducer; P = pressure (kPa); G = calibration factor provided by the manufacturer (kPa/digits); R_0 = initial reading (digits); R_i = reading at time i (digits); B_0 = initial barometric pressure (kPa); B_i = barometric pressure at time i (kPa); K(P) = thermal impact correction equation derived from a best-fit regression of P versus (T_0-T_i) data; T_i = temperature at time i (^{0}C); T_0 = initial temperature (^{0}C). An example calculation is provided in Appendix K.

Bulk Unit Weight and Overburden Pressure Estimation

To determine the bulk unit weight, landfill volume estimation is necessary; this was obtained from the site's survey record. Table 4-1 provides the estimation of volume, mass placed, and bulk unit weight of the landfill site on each surveying day. The cumulative weight of waste plus cover soil deposited each surveying day was calculated assuming 18% of the apparent volume of the study landfill unit was comprised of cover soil with a unit weight of 25.5 kN/m^3. The methodology to estimate a bulk unit weight was explained in Appendix C. Bulk unit weight of the site varied in a range of 11.3 – 12.2 kN/m^3, and averaged 11.8 kN/m^3.

A theoretical overburden pressure at each monitoring location was estimated with two methods. First, overburden pressure was estimated by multiplying bulk unit weight by an apparent thickness of waste plus cover soil on top of a TPC (Equation 4-5). Second, using Boussinesq influence factor charts, the stress distribution beneath a side slope of the landfill was evaluated (Equation 4-6).

$$\Delta\sigma_v = H\cdot\gamma_B \quad (4\text{-}5)$$

$$\Delta\sigma_v = \sum I_\sigma\cdot H\cdot\gamma_B \quad (4\text{-}6)$$

where $\Delta\sigma_v$ = overburden pressure (kPa); H = apparent thickness of waste plus cover soil (m); γ_B = bulk unit weight (kN/m^3); I_σ = influence factor from Boussinesq charts.

Settlement Prediction

In this study, one-dimensional (vertical) elastic and primary consolidation settlements of approximately 16.7 m of the subsurface soil layers were estimated using the following equations:

$$S_t = S_e + S_c \tag{4-7}$$

$$S_e = \sum_i^n H_{0i} \frac{\Delta\bar{\sigma}_{vi}}{M_i} \tag{4-8}$$

$$S_c = \sum_{i=1}^{n} C_{ci} \frac{H_{0i}}{1+e_{0i}} \log \frac{\bar{\sigma}_{v,0i} + \Delta\bar{\sigma}_{vi}}{\bar{\sigma}_{v,0i}} \tag{4-9}$$

where S_t = total settlement (m); S_e = elastic settlement (m); S_c = primary consolidation settlement (m); H_{oi} = thickness of soil layer i (m); $\Delta\bar{\sigma}_{vi}$ = overburden stress increase caused by the waste placement at midpoint of soil layer i; M_i = constrained modulus of soil layer i (MPa); C_{ci} = primary compression index; e_{oi} = initial void ratio of soil layer i; $\bar{\sigma}_{oi}$ = initial overburden stress at the center of soil layer i. An average value of overburden pressure measurements on each day was used as input of $\Delta\sigma_v$. Typical ranges of other engineering parameters were not measured and assumed as follow: C_c = 0.1 for clay (Budhu 2000), e_o = 1.4 for clay (Das 1990), and $C_c/(1+e_o)$ = 0.002 for sand or silty sand (Coduto 2004).

Various equations introduced in Bowles (1996) were used to estimate the stress-strain (Young's) modulus E of each soil layer with the CPT(N) and SPT(N) as follow.

E(kPa) = 500(N + 15) for sand (normally consolidated) (4-10)

E(kPa) = 40000 + 1050N for sand (over consolidated) (4-11)

E(kPa) = 250(N + 15) for sand (saturated) (4-12)

E(kPa) = 320(N + 15) for clayey sand (4-13)

E(kPa) = 600(N + 6) + 2000 for gravelly sand, N>15 (4-14)

Constrained moduli M were correlated with

$$M = \frac{E(1-\nu)}{(1+\nu)(1-2\nu)} \quad (4\text{-}15)$$

where ν = Poisson's ratio; Poission's ratio of 0.3 was assumed (Budhu 2000). Constrained moduli of each soil layer were compiled in Tables A-14 to A-16. An example settlement estimation is presented in Appendix L.

Results and Discussion

Overburden Pressure Change with Waste Placement

All TPCs were determined to respond immediately to stress change during the study period. However, the thermal correction factors provided by the manufacturer were too small to account for the actual TPC output fluctuation from daily or seasonal temperature change. Figure 4-3 shows an example plot of the overburden pressure and temperature changes of TPC-H over time; each overburden pressure data point in the plot was estimated without including any thermal correction factor. The greatest magnitude of overburden pressure output fluctuation observed was approximately 11 kPa which was beyond the accuracy of TPCs used in this study (2 kPa). The trend of overburden pressure variation over time was very similar with respect to temperature; this trend was consistently observed from other TPCs. Daigle and Zhao (2003) pointed out that thermal correction factors of a TPC for increasing temperature was different for

decreasing temperature and should be estimated as a function of overburden pressure. For example, new thermal correction equations for TPC-G were derived by best-fit regression of overburden pressure versus temperature differences (Figure 4-4). The TPC-G' readings corrected using thermal impact correction equations were relatively steady compared to those not corrected (Figure 4-5).

The TPCs used in this study were found to be reliable. Overall, the differences between field pressure measurements and theoretical pressure predictions were relatively small. Figure 4-6-A shows example plots of theoretical overburden pressures estimated using Equation 4-6 and in-situ overburden pressure measurements at the monitoring locations H and H'. The step-wise increment of the measured overburden pressure indicates three layers of waste were placed during the monitoring period. TPC-H' initially generated slightly greater pressure outputs than did TPC-H, but this trend reversed, beginning in January 2009. This may be due to the change in stress distribution resulting from waste placement. Sowers (1973) pointed out that landfilled waste materials subjected to surcharge (or compaction efforts) would be distorted, bent, and reoriented.

TPC duplicates at locations A and G generated markedly different pressure measurements. However, given the heterogeneity of landfilled materials, this is not surprising. Uneven stress distribution (arching effect) among the interstitial matrix of solid waste might increase or decrease TPC readings. Spangler and Handy (1982) pointed out that in a soil matrix, positive and negative arching can effectively decrease and increase stress readings, respectively. For example, the outputs of TPC-G and -G' approximately 38 kPa difference consistently since waste placement began (Figure 4-6-

B). Another explanation for this extreme variability could be malfunctioning of the TPCs. However, the TPCs were tested and installed carefully to ensure proper operation. In addition, the outputs of the TPCs were steady. Thus, the discrepancy between TPC-G and –G' might not be due to malfunctioning. Overburden pressure measurements of TPC duplicates at each monitoring point (A to H) were presented in Figures B-16 to B-22.

In-situ overburden pressure measurements were compared with theoretical pressure predictions calculated using Equation 4-5; the pressure measurements were collected on dates closest to the topographic surveying dates (September 25, 2009 and May 20, 2010); topographic drawings of those days are presented in Figures B-22 and B-23, respectively. Overall, the pressure predictions of the monitoring points under the toe of the side slope were underestimated while those under the central area of the landfill body were overestimated. Figure 4-7 shows example plots of estimated and measured overburden pressures at each monitoring location; data collected in September 2009, were used. The variation of predicted overburden pressure had a very similar trend to that of measured overburden pressures. Overall, as the thickness of waste plus cover soil increased, the in-situ overburden pressure measurements also increased. The overburden pressure values measured near the edge of the side slope toe tended to be greater than theoretical pressure values estimated using Equation 4-5, but smaller than the pressure values estimated using Equation 4-6. This may be because vertical stress from the central area of the waste body was also applied to the bottom of the side slope. Beneath the central area of the landfill the measured pressure values tended to be smaller than predicted pressure values, which might be due to the

arching effect as explained earlier. Figure 4-8 presents the change in the ratio of measured to estimated pressures as a function of waste thickness. Under the toe, the field measurements were 1.7 - 6.4 times greater than estimated pressures. Using the Boussinesq influence factor charts, overburden pressures under the toe was re-estimated and the ratios of measured to estimated pressures found to fall into a range of 0.4 – 3.5. Conversely, the ratios at the locations under the central area of the landfill body were in a range of 0.5 to 1.1 with an average value of 0.8; in short, overburden pressures under the central area were over predicted. A similar trend that near the side slope overburden pressures were under predicted while over predicted under the central area was observed for another MSW landfill located in Florida, U.S. (Jason et al., unpublished internal report).

Landfill Foundation Settlement

To investigate the relationship between overburden pressure and foundation settlement, settlement was measured by means of in-situ instrumentation consisting of eight pairs of SSs. As mentioned in the methods section, during the early course of the monitoring period, it was found that the readings of fourteen out of sixteen SSs fluctuated mainly due to air-bubbles in liquid; ten of them were corrected by replacing the liquid with de-aired solution, the remaining four could not be corrected and may have malfunctioned for different reasons such as pinching of the vent lines. At least one SS at each monitoring location was used for the analysis of this study; the duplicates at A, B, C, and G worked properly. Because of the delays in the liquid replacement process, some SSs (C, C', D, E, F, and G') began to work properly several weeks after TPCs initially responded to waste placement. No considerable amount of overburden

pressure increase was observed during the period. It was thus assumed that no considerable settlement occurred in the period; the vertical movements of the foundation after each SS began to work properly were reported in this study.

Overall, the outputs of the SSs showed that the landfill foundation settled gradually with increasing overburden pressure (waste placement); immediate (elastic) settlement was not discernable based on the collected data. Figure 4-9 shows example plots of overburden pressure variation and settlement of the foundation at the monitoring point C. With an average 6.5 kPa of overburden pressure increase during the early course of the waste placement, the foundation settled gradually up to 3.8 cm. As overburden pressure increased to approximately 45 kPa between October 2009 and March 2010, approximately 1.2 cm of additional settlement was recorded. Similarly, from other SSs, more settlement was observed during the placement of the first waste lift than during the placement of subsequent lifts.

Figure 4-10 shows average in-situ settlements and overburden pressures measured on September 25, 2009 and May 20, 2010. On September 25, 2009, the monitoring points A, B, C, and D were located beneath the toe of the side slope of the waste lifts while E, F, G, and H were beneath the bottom of the central area of the landfill (Figure B-22). Even though consistent overburden pressure (approximately 10 kPa) was applied to the bottom of the side slope toe (A through D), the settlement behaviors varied greatly by location (0.6 - 6.6 cm). No relationship between overburden pressure and settlement was found from the data collected at A through D. Under the central area of waste body (E through H) settlement generally increased as overburden pressure increased. On May 20, 2010, all SSs were located under the bottom of the

central area of the landfill body (Figure B-23). The field data at this time showed a general trend that more settlement occurred with increasing overburden pressure. Note that at locations E, F, and H the average settlements measured on May 20, 2010 were smaller than those measured on September 25, 2009, indicating upward vertical movement of the foundation during the period. Similar upward vertical movement of the foundation (up to 4.2 cm) was consistently observed from other SSs while overburden pressure remained stable or increased. This magnitude of this vertical movement was beyond the accuracy of the SS (0.7 cm) and might be due to the swelling or shrinkage of clay in the subsurface soils with changes in the groundwater table elevation or temperature (Aschieri and Uliana 1984; Abuel-Naga et al., 2006; Whelan et al., 2005; McCarthy 2007).

Comparison of Settlement between Prediction and In-situ Measurements

Settlement predictions of the landfill foundation were made using one-dimensional elastic and consolidation settlement models (Equation 4-5 and Equation 4-6). The settlement predictions were presented in Figure 4-11 along with actual average settlements measured at each monitoring location on September 25, 2009 and May 20, 2010.

Settlements were predicted in three scenarios. In Scenario 1, elastic settlement was estimated using various stress-strain modulus equations which were considered to be most appropriate to the soil types and conditions present (Bowles 1996); example calculations for the soils beneath location A is provided in Appendix L. Figure 4-11-A shows that the settlements beneath the side slope toe (A, B, and C) were under predicted while those beneath the central landfill body (F, G, and H) were over

predicted. In Scenario 1, the one-dimensional settlement models provided reasonable settlement estimates for the locations under the central area; the difference between actual settlements and predictions were in a range of 1.0 to 2.1 cm. On the other hand, the settlement behavior beneath the side slope was found unpredictable with the one-dimensional settlement models used in this study. In Scenario 2, assuming that the soils were over-consolidated, the settlement predictions were calculated and found to be closest to actual settlements at locations D, F, G, and H; differences in the range of 0.01 to 7.0 mm between prediction and in-situ measurements were estimated. For Scenario 3, the stress-strain modulus equation for saturated sand (Equation 4-12) was applied for all types of soils. It was found that this scenario provided excessively over predicted settlement estimates at locations D through H.

Using the same three scenarios, settlements were predicted in and compared with the in-situ measurements on May 20, 2010 when all SSs were located under the central area of the landfill body. Most of the in-situ settlements on May 20, 2010 fall in the middle of ranges of settlement estimates using various stress-strain equations and those estimated with the assumption that soils were overconsolidated. Settlement estimates using a stress-strain equation for saturated sand were found to be overly conservative; the predictions were up to 2.3 times greater than actual settlements.

Summary and Conclusions

To investigate the settlement behavior of a landfill foundation, total pressure cells and settlement sensors were installed under the bottom of a municipal solid waste landfill in Florida, United States, and monitored from March 2007 to June 2010. During the study period, all sixteen total pressure cells and twelve of the sixteen settlement

sensors were determined to work properly; the remaining four settlement sensors transmitted unreasonable readings (i.e., data collected fluctuated without showing any trend and reason).

The readings of the total pressure cells near the toe of the landfill side slope averaged 3 times greater than the overburden pressure values estimated by multiplying the thickness of waste and cover soils above each pressure cell by bulk unit weight (11.8 kN/m^3); the readings averaged 1.3 times greater than those estimated using Boussinesq influence factor charts. Overburden pressure estimates beneath the central area were found to be over predicted: the measured to estimated overburden pressure ratio averaged 0.8. Settlement readings measured under the toe of the side slope showed no relationship between overburden pressure and settlement while settlement under the central area was found to generally increase with increasing overburden pressure.

Settlement predictions were made using conventional one-dimensional settlement models: elastic theory and Terzaghi's consolidation model. Constrained moduli for elastic settlement predictions were estimated using SPT(N), CPT(N), and various stress-strain (Young's) modulus equations from Bowles (1996). Overall, it was found that the one-dimensional settlement models may not provide reasonable settlement estimates of the area beneath the landfill side slope. In addition, settlement predictions of the area of the landfill central body were over predicted up to 2.6 cm which might be overly conservative; note that at one monitoring point settlement was under predicted by approximately 2.7 cm.

Table 4-1. Bulk unit weight change of the study landfill unit with waste placement

Day	Volume (m^3)	Mass ($\times 10^3$ kg)	Bulk unit weight (kN/m^3)
4/11/2008	431,284	523,414	11.9
9/25/2008	853,341	980,094	11.3
9/29/2009	1,433,771	1,781,424	12.2
-	-	Average	11.8

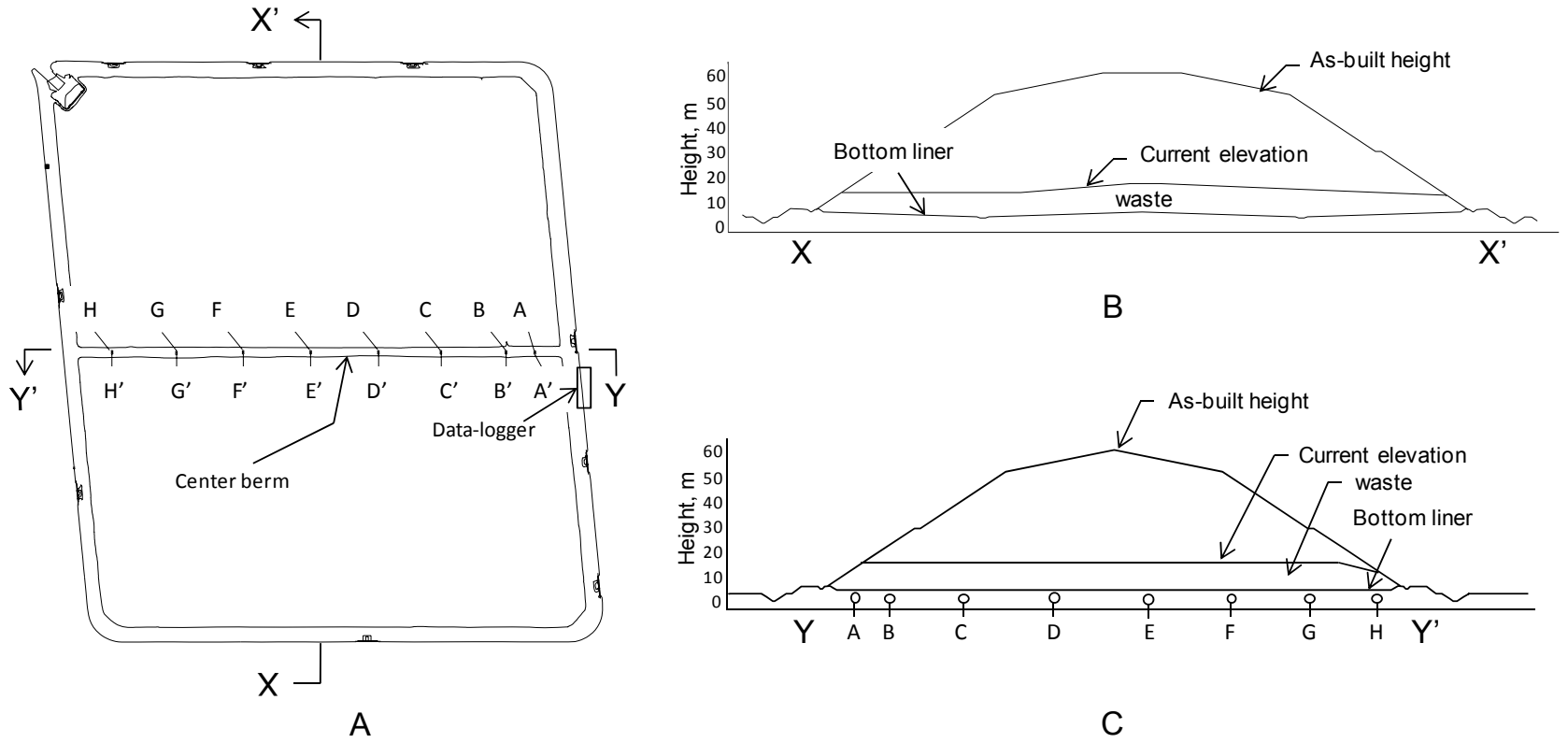

Figure 4-1. Distribution of instruments: A) plan view and B) X-X' and C) Y-Y' cross-sectional views; A through H in (A) and (C) represent a location of each pairs of instruments (TPC and SS) and A' through H' represent locations of corresponding duplicate instruments.

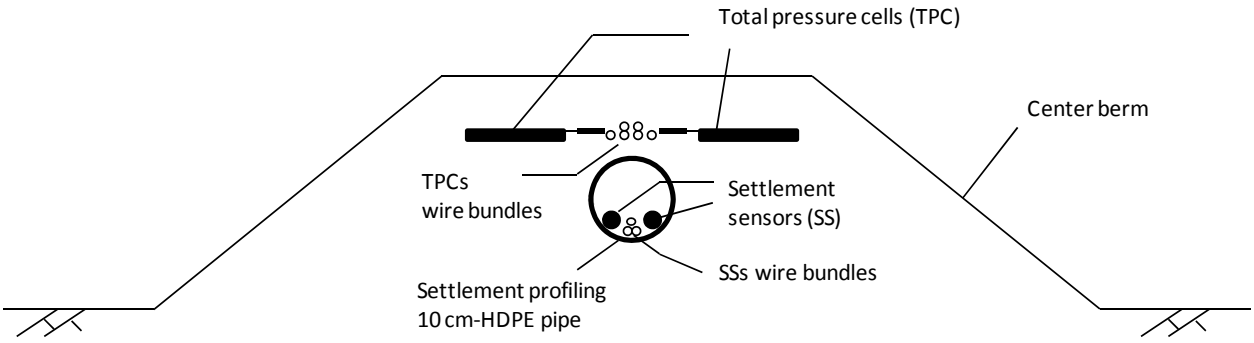

Figure 4-2. Schematic cross-sectional view of the instruments setting in the center berm of the study landfill

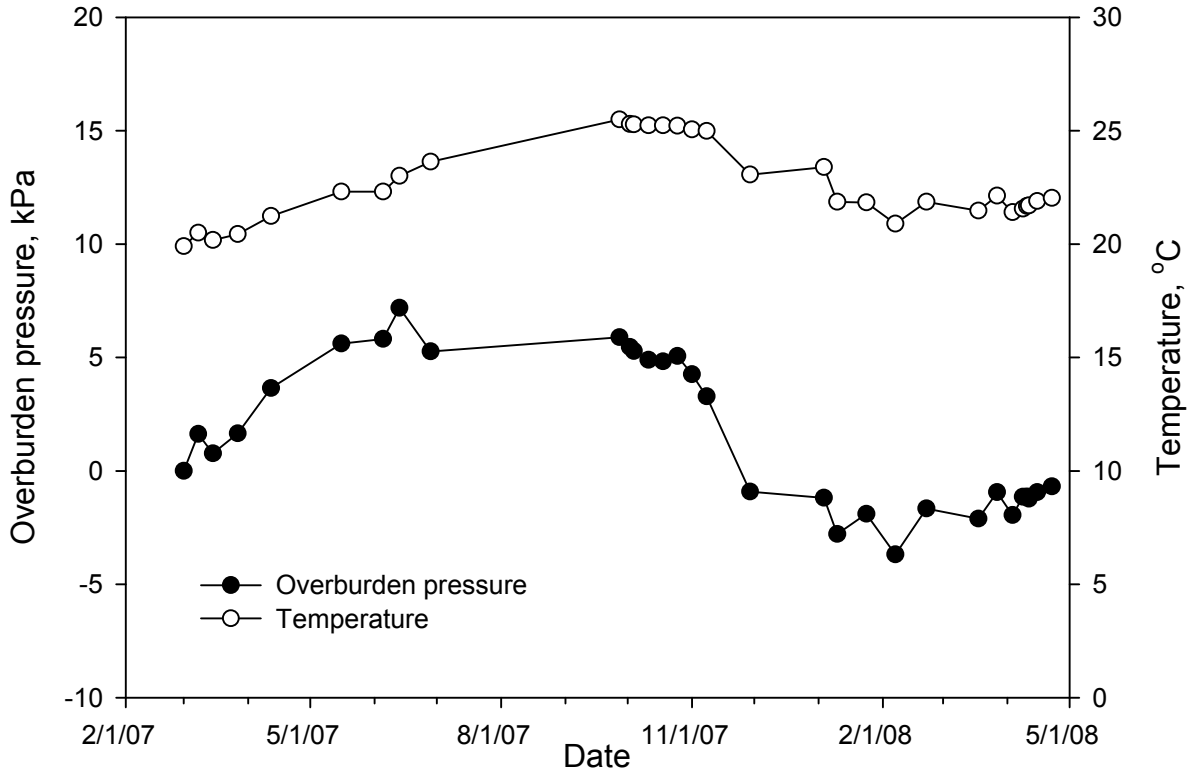

Figure 4-3. Seasonal overburden pressure and temperature variation prior to placing waste; each overburden pressure data point was estimated using conversion factors provided by the manufacturer.

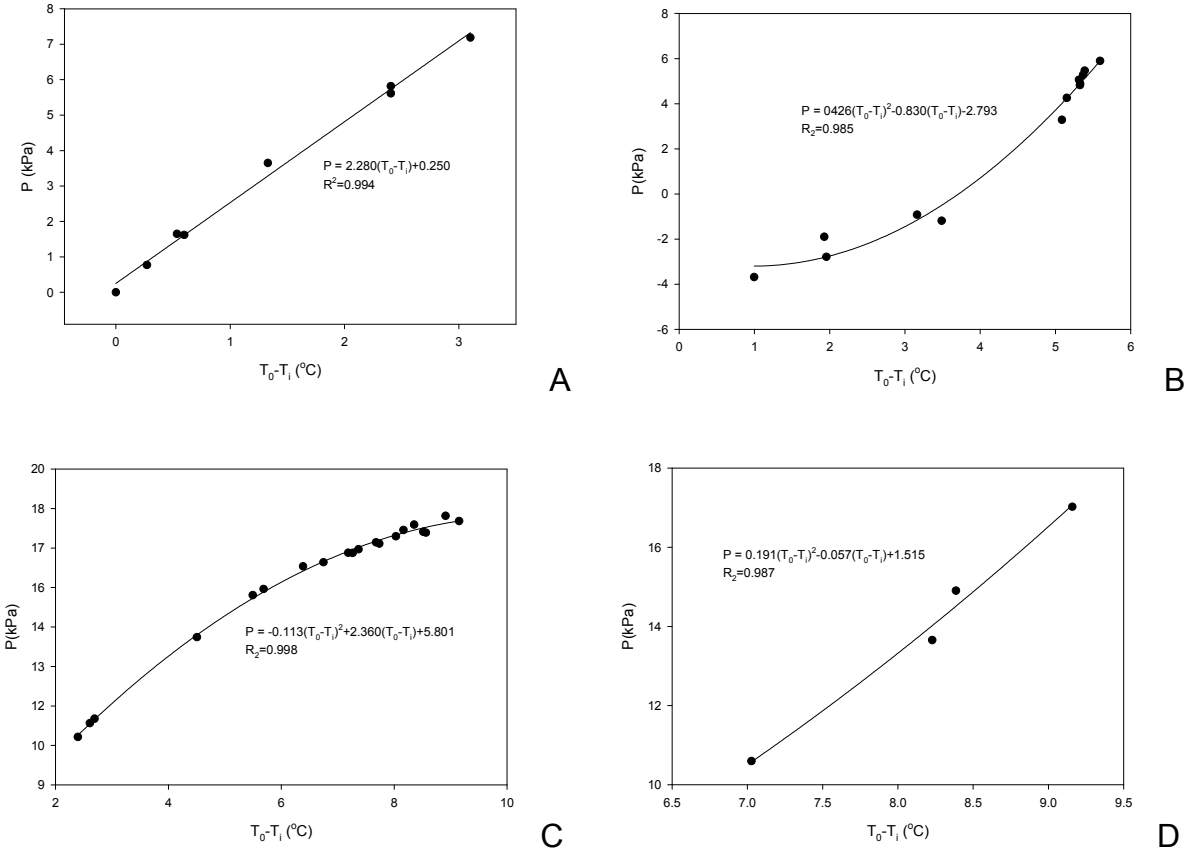

Figure 4-4. Examples of best-fit regressions of overburden pressure (P) versus temperature variation (T_0-T_i) to estimate thermal correction factors: A) winter to summer and B) summer to winter at an average overburden pressure of 0 kPa: C) winter to summer and D) summer to winter at an overburden pressure of 15.5 kPa

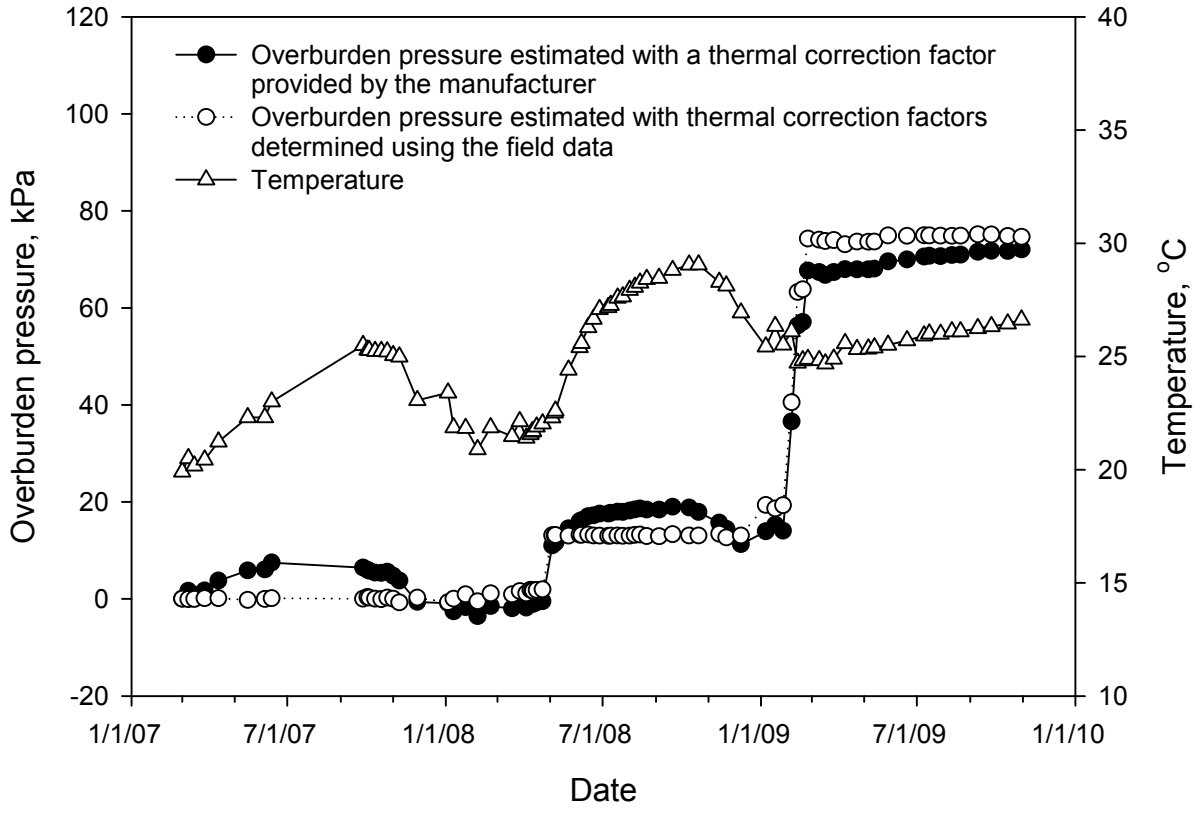

Figure 4-5. Impact of a thermal correction factor on estimating overburden pressure: overburden pressure over time estimated using thermal correction factors provided by the manufacturer and estimated based on the field data (from TPC-G')

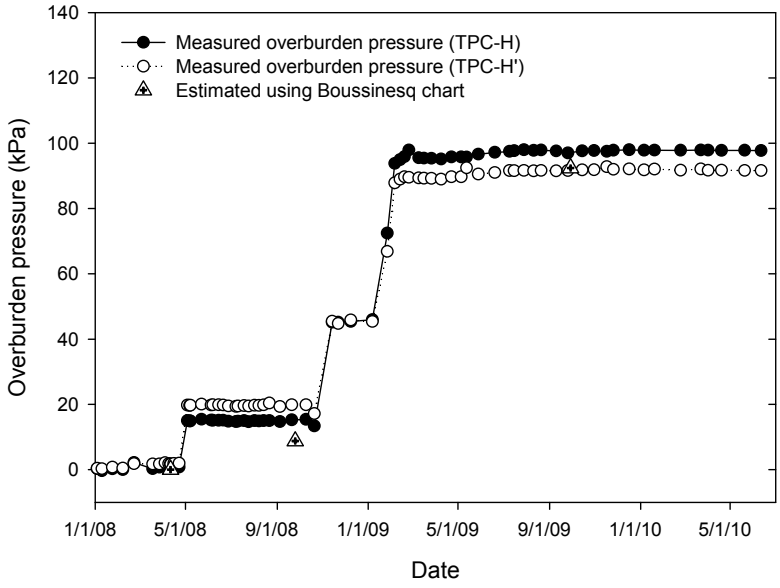

A

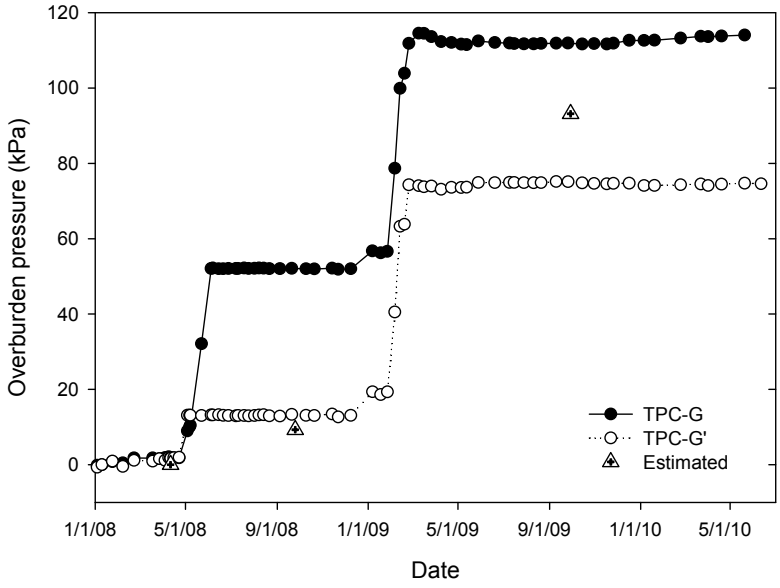

B

Figure 4-6. Example of overburden pressure change with waste placement: (predicted overburden pressure) = (bulk unit weight) × (thickness of waste plus cover soil) ×(Influence factor from Boussinesq chart); the data used were collected from A) TPC-H and –H' and B) TPC-G and -G'.

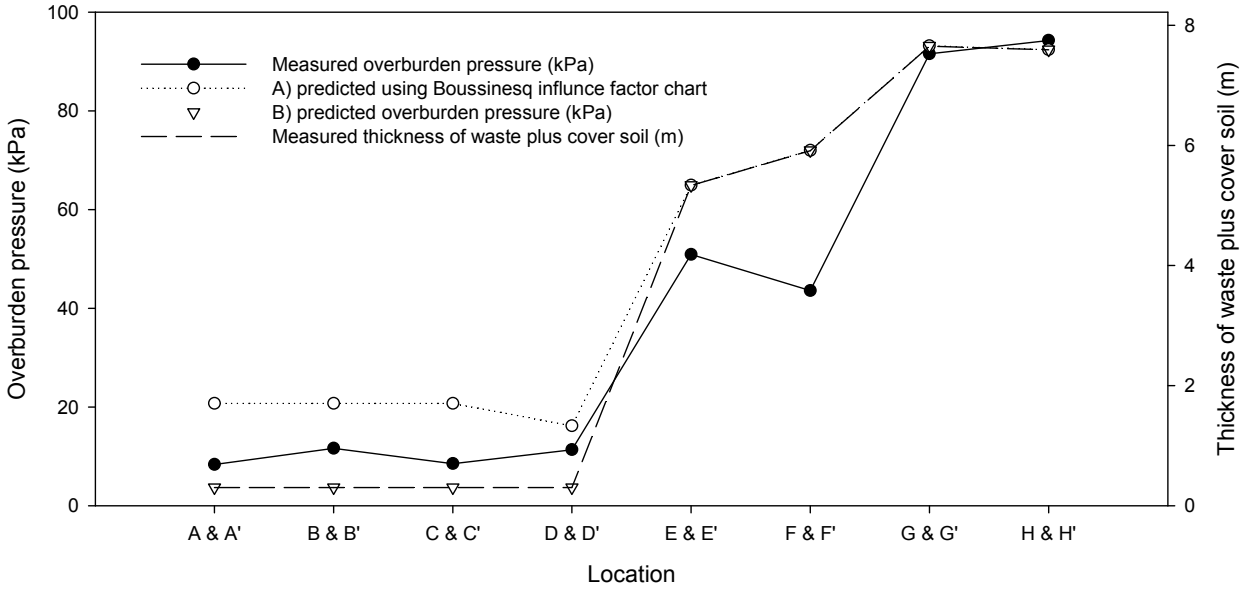

Figure 4-7. Comparisons of overburden pressures between measured and predicted at each monitoring location using topographic survey data and bulk unit weight estimation on September 29, 2009; A) overburden pressures were predicted using Boussinesq influence factor charts; B) (predicted overburden pressure) = (bulk unit weight) × (thickness of waste plus cover soil on top of each pressure cell).

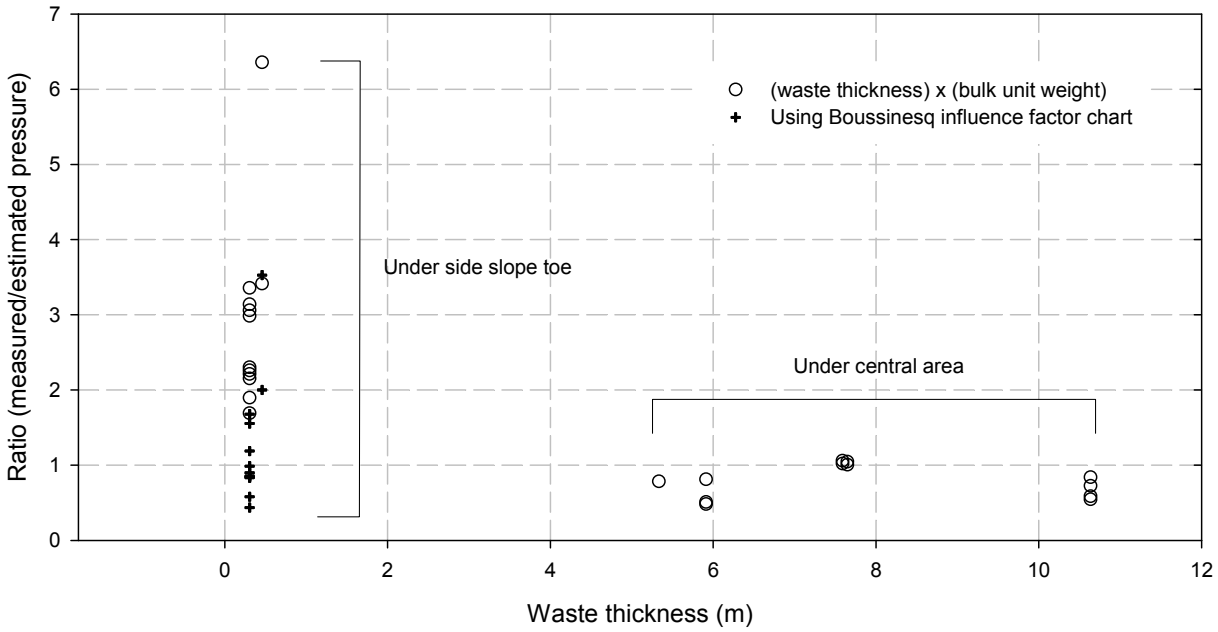

Figure 4-8. Changes in the ratio of measured to estimated overburden pressure as a function of waste thickness; each ratio was estimated using each surveying date.

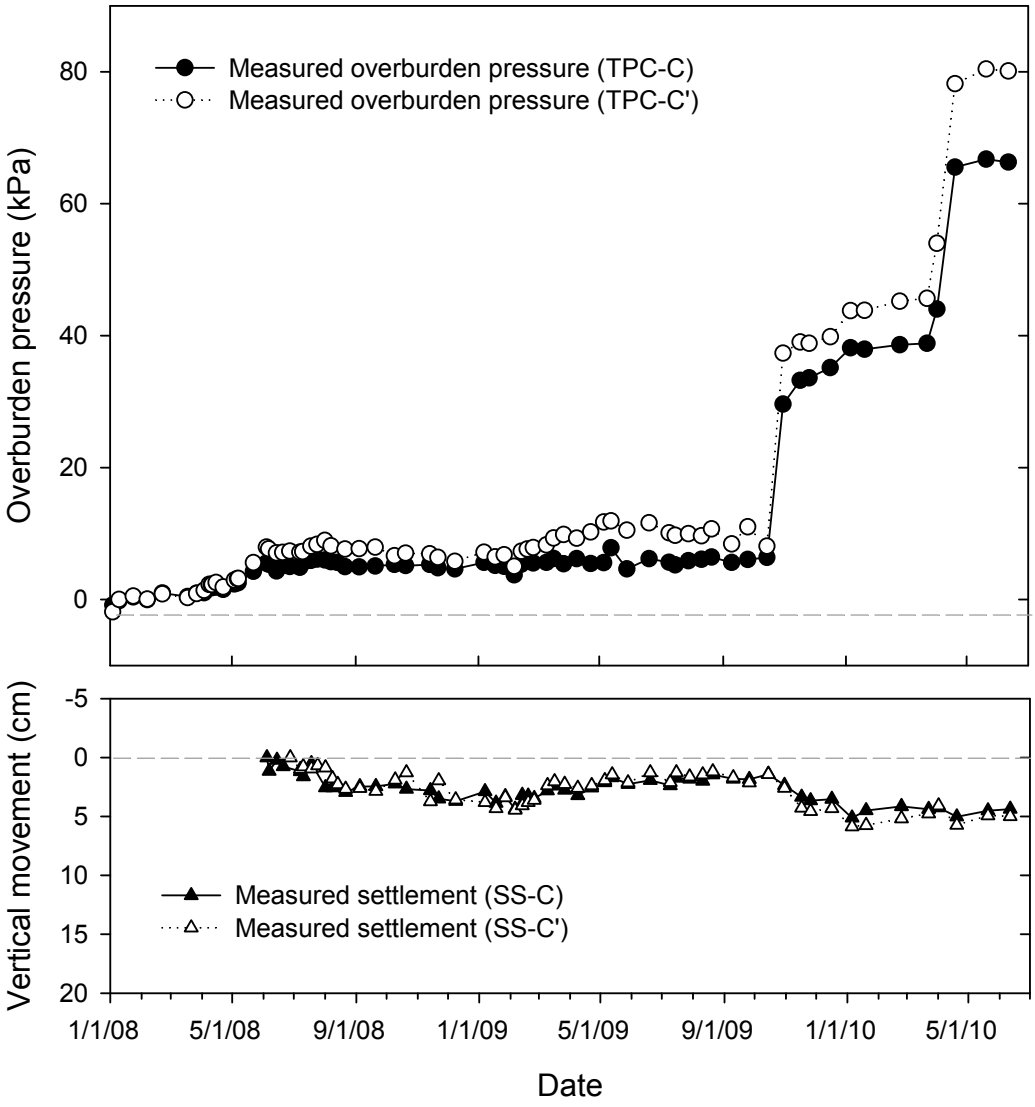

Figure 4-9. Settlement of the landfill foundation and overburden pressure changes at location C over time: the positive vertical movement indicates settlement.

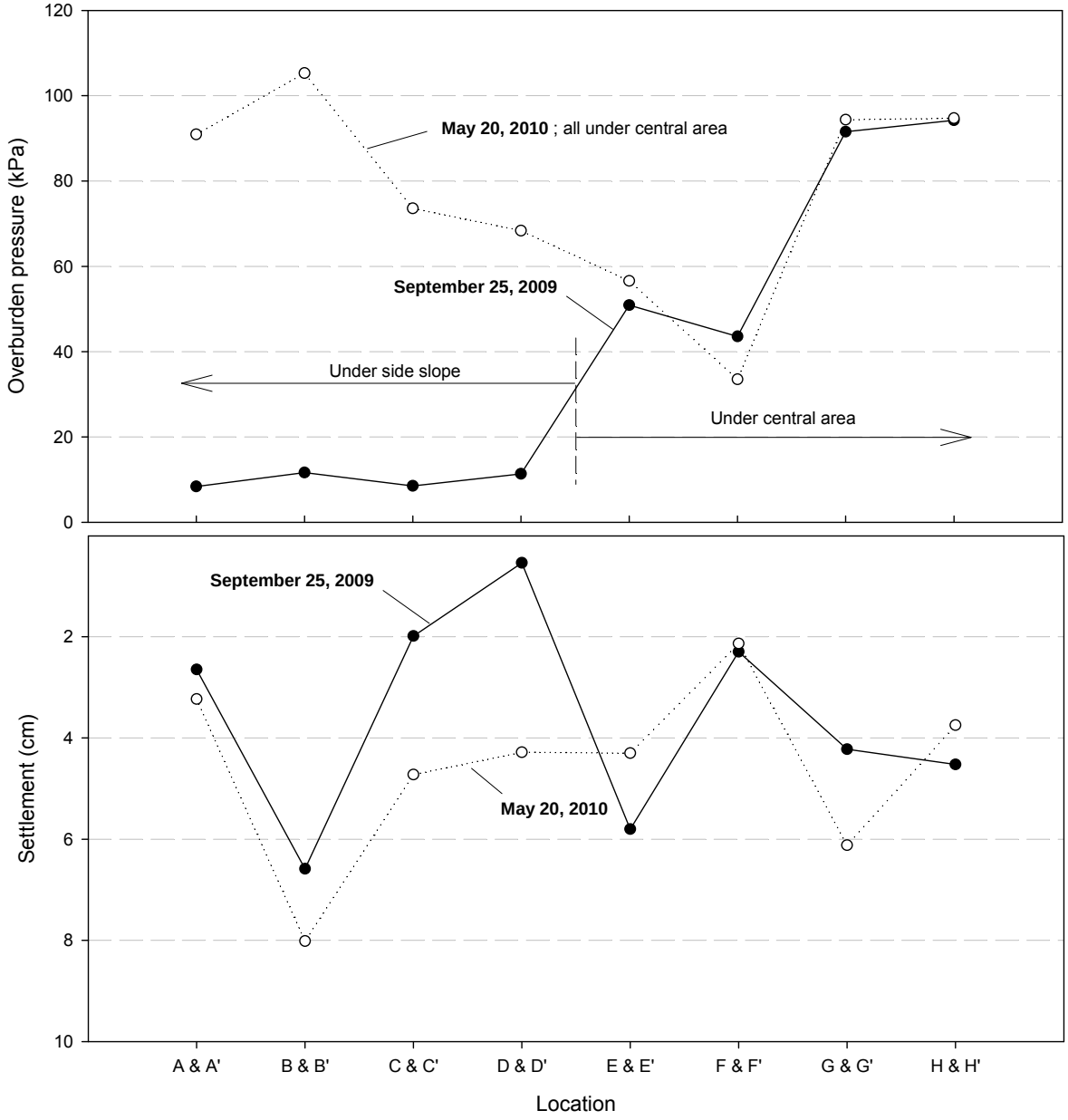

Figure 4-10. Overburden pressure and settlement measurements at each monitoring location; each data point indicates an average value of duplicate outputs or a value of one settlement sensor where a duplicate sensor was malfunctioning (D, E, F, and H).

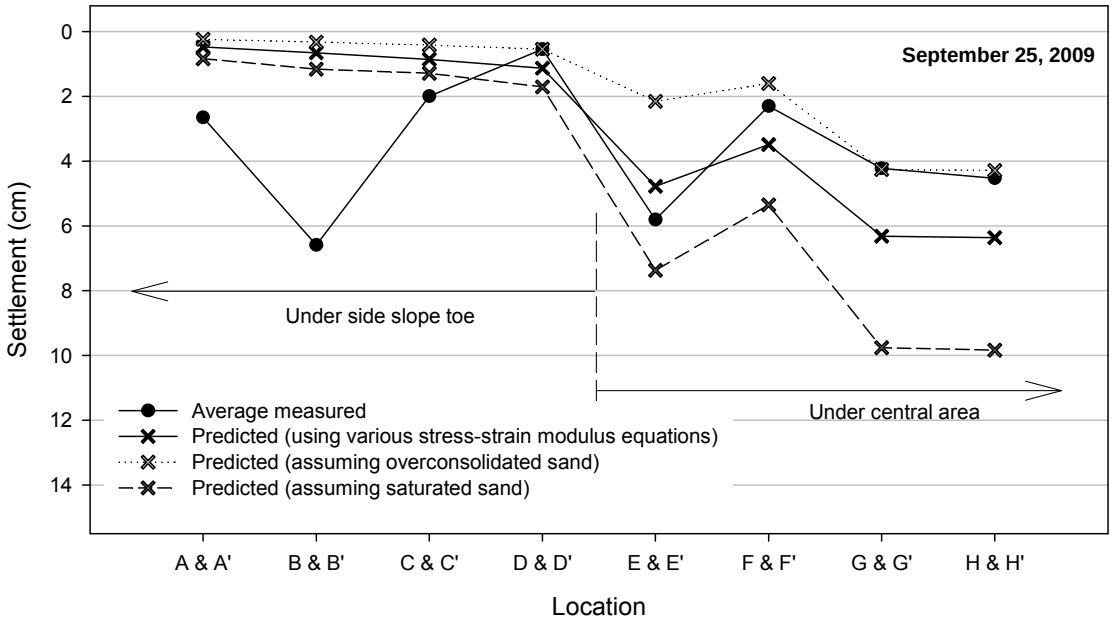

A

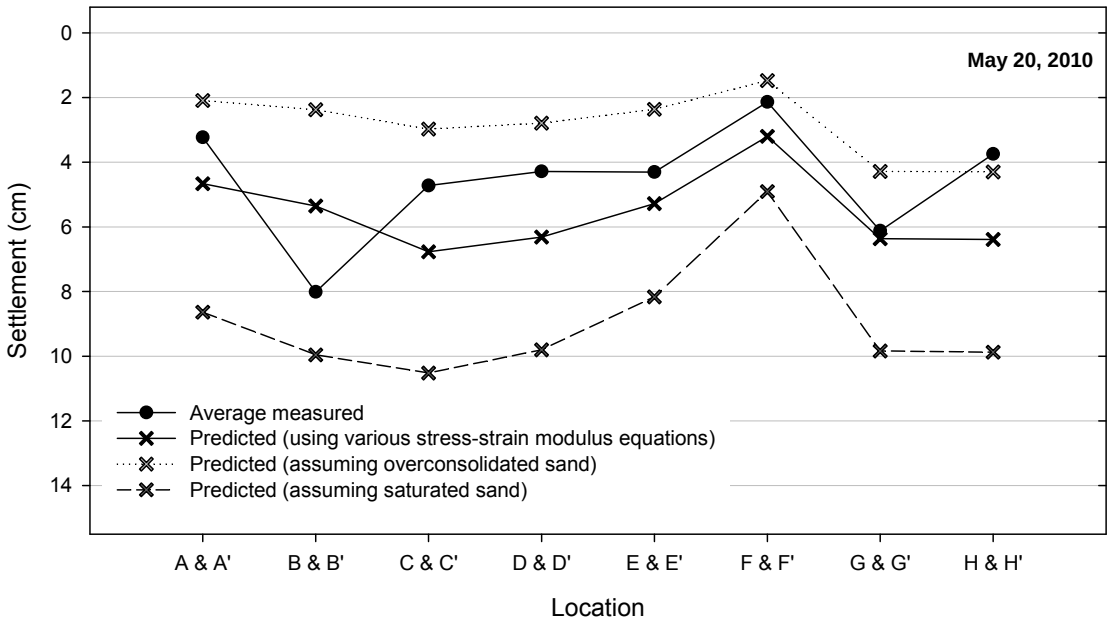

B

Figure 4-11. Comparisons of measured settlement with predicted settlement: data used were collected on A) September 25, 2009, and B) May 20, 2010.

CHAPTER 5
IMPACT OF FOOD WASTE CONTENT ON THE INTERNAL FRICTION ANGLE OF MUNICIPAL SOLID WASTE

Introduction

A major element in modern sanitary landfill design is a slope stability evaluation of the proposed landfill configuration and specified materials. In addition to assessing slope stability associated with the interfaces of different soil, geosynthetic, and waste layers, the internal stability of the disposed waste itself requires evaluation. Slope stability evaluation of compacted municipal solid waste (MSW) requires estimating waste mechanical properties, with much importance placed on the internal angle of friction. Research investigating appropriate MSW internal friction angles has been reported, with most values reported in the range of 15 to 35º (Kavazanjian et al. 1995; Kavazanjian et al. 1999; Sadek et al. 2001; Machado et al. 2002; Mahler and Netto 2003; Harris et al. 2006; Gabr et al. 2007; Zhan et al. 2007; Zekkos et al. 2007; Kavazanjian 2008; Zekkos et al. 2008; Reddy et al. 2009). The wide range is attributed to the heterogeneous composition of waste samples and difficulties associated with the testing procedures. Geotechnical characterization of MSW for internal friction angle is inherently more difficult than testing for soil, as MSW is heterogeneous in material composition, size, and mechanical properties. Considering the importance of internal friction angle as an input in the landfill design process, additional research to assess the impacts of waste composition and friction angle testing protocols is warranted.

The composition of MSW varies with geographical, cultural, and seasonal differences. Food waste content, for example, can vary dramatically among countries. The food waste content of U.S. MSW is approximately 12.5% on a wet-weight basis (USEPA, 2005), while that of China has been reported as up to 73% (The World Bank,

1999; Wang and Nie, 2001). This difference results from dissimilar material consumption practices, packaging, waste management practices, and socio-economic conditions. In some cases the composition of landfilled MSW varies due to region-specific policies and regulations. The Korean regulatory agency, for example, currently bans non-processed food waste from being disposed of in an MSW landfill (Ministry of Environment of Republic of Korea, 2006).

This study investigated the relationship between the MSW internal friction angle and food waste content. While it is expected that increasing food waste content will decrease the MSW internal friction angle, the magnitude of this relationship has not been measured. In addition to the value of such data to landfill design engineers assessing slope stability, friction angle data are also useful when evaluating mechanical MSW compaction efficiencies. Most of the previously reported data referenced earlier were determined for waste from western countries. As other parts of the world with different waste compositions begin to utilize large engineered sanitary landfills, it is important to better understand how different waste compositions (e.g., high food waste contents) might impact waste compaction and geotechnical stability.

The impact of food waste content on friction angle was investigated by conducting direct shear strength tests on synthetic MSW at a wide range of food waste contents (0 to 80% by wet weight). In addition to tests using a standard small-scale laboratory direct shear device designed for characterizing soil, a large-scale shear device was constructed and used. Given the wide range of results previously reported for MSW internal angle of friction as a whole, the results are intended to provide a clearer picture on the impact waste composition on this important design parameter.

Methods and Material

MSW Specimen Preparation

In this study, synthetic MSW specimens were created to represent waste characteristics expected upon initial landfill disposal (prior to the onset of biodegradation). Eight representative components were selected: food waste, paper, plastic, metal, wood, textile, glass, and ash. MSW composition data from mainland China was used to represent waste with a high initial food waste content; composition data from nine Chinese cities (as presented by Wang and Nie (2001)) were averaged, for a resulting food waste content of 58%. Three additional target MSW specimen compositions were selected by altering the food waste content (0, 40, and 80% by wet weight) while maintaining a constant ratio among other components (Table 5-1). The corresponding specimen weights for the 0, 40, 58, and 80% food waste conditions were 100, 180, 200, and 210 g for the small-scale direct shear tests (SSDSTs) and 25, 49, 55, and 60 kg for the large-scale direct shear tests (LSDSTs). Specimen weight increased with a larger food waste content as result of food waste's greater density compared to other waste components.

The target sizes, methods of size reduction, and average moisture contents for the different waste components are summarized in Table 5-2. Food waste was collected from a local restaurant specializing in Chinese food. The food waste consisted primarily of discarded cooked foods (meats, rice, noodles, and vegetables), cooking oil, and discarded uncooked vegetables and fruits; bones and shells were removed prior to use. The food waste was collected periodically throughout the project as needed, and a visual observation was used to ascertain that the general characteristics remained the same throughout. For all SSDSTs, a total of 5 kg of food waste was pulped and

homogenized using a food grinder (High-Speed Blender Mixing System, Magic Bullet Express, California, US). For the LSDSTs, 20 to 50 kg of food waste was used for each test, and size reduction was not performed (bones and shells were removed). The paper component consisted of 50% office paper and 50% newspaper by wet weight. Plastics used for the LSDSTs consisted of 50% plastic bottles and 50% film plastic by wet weight (only plastic bottles were used for the SSDSTs because of limitations in size-reducing the film plastic to a uniform size). Aluminum beverage cans served as the metal waste component for both tests. Chipped wood mulch of appropriate sizes for both tests was collected from a local waste transfer station. Discarded clothes were used for the textiles. Crushed glass bottles were used for the LSDSTs without sieving, while crushed and sieved (No. 4) glass was used for the SSDSTs. Coal ash from a local coal-fueled power plant (Gainesville Regional Utilities, FL US) served as the ash source.

For SSDST specimens, all waste components were mixed by hand. For LSDST specimens, mixing was accomplished in four batches to promote a more homogenous composition throughout the large shear device. Waste mixtures representing 25% of the target weight of each test were mixed individually using shovels in a stainless steel pan, and these mixtures were placed and compacted in the large-scale shear box until the target weight was reached.

The moisture content (wet weigh basis) of each component and specimen was determined by drying the specimens at 110°C (ASTM D2216-98). The average moisture content of each waste component and specimen is presented in Tables 5-2 and -3, respectively; the average moisture content of each component was used to estimate the initial moisture content of each specimen before consolidation.

Direct Shear Test

Direct shear tests were conducted using two separate devices; one device was at a scale normally used for characterizing soils and another was fabricated to allow larger samples to be characterized. For the SSDSTs, a Direct/Residual shear machine (Humboldt HM-2700, Humboldt Manufacturing Company, Illinois, U.S.) with a 10-cm-diameter and 5-cm-height shear box was used. The maximum displacement level is approximately 18% of the shear box diameter (1.8 cm of horizontal displacement). The SSDST apparatus is designed for a displacement-controlled test, and a horizontal displacement rate of 0.076 cm/min was used. The SSDSTs were performed in conformance with the ASTM standard method for soils under consolidated drained conditions (D 3080-04). For the LSDSTs, a stress-controlled direct shear box was designed as shown in Figure 5-1 (Stewart & Associates Manufacturing Corporation, Gainesville, Florida, U.S.); the photograph of the LSDST device is presented in Figure B-31. For normal stress and shear stress applications, hydraulic jacks equipped with hand pumps (SIMPLEX® P42 and P82, Broadview, Illinois, U.S.) and pressure gauges (GD1 SIMPLEX®, Broadview, Illinois) were used. The large-scale shear box includes an upper fixed shear box (43-cm length $\times$ 43-cm width $\times$ 46-cm height) and a movable lower shear box (43-cm length $\times$ 43-cm width $\times$ 16-cm height). The maximum displacement level of the large-scale device is approximately 40% of the shear box length (17 cm of horizontal displacement).

Each direct shear test was initiated by placing and compacting a well-mixed MSW specimen into the shear test box. The normal stresses applied for the SSDSTs were 48, 97, 145, 194, and 290 kPa, and those for the LSDSTs were 96, 192, and 287 kPa. Because all tests were performed under drained conditions, the applied normal stresses

were treated as the effective normal stresses. Specimens of both scales were consolidated under each effective normal stress for 4 to 30 hours until vertical deformation rates were less than 0.5% per hour for the LSDSTs and 2% per hour for the SSDSTs. For the LSDSTs, the normal stress was continuously monitored and adjusted during the consolidation of an MSW specimen. Densities of the specimens for the LSDSTs after consolidation and before shearing are provided in Table 5-3. Dry density was calculated by subtracting the moisture weight from the total weight of a specimen. Density was not monitored for SSDST specimens.

Data Analysis

Two data interpretation methods were used to estimate shear-strength parameters (internal friction angle and cohesion). First, the internal friction angles of both scales of tests were estimated using peak (ultimate) shear strength values produced in the available displacement of each shear testing device: 1.8 cm (18% displacement level) for SSDSTs and 17.2 cm (40% displacement level) for LSDSTs. The Mohr-Coulomb failure criterion expressed as Equation 5-1 was used to calculate the shear strength parameters. To develop a Mohr-Coulomb failure criterion envelope for each set of SSDST and LSDST data, a best-fit linear regression was conducted. For all 20 SSDSTs, duplicate tests were conducted at each normal stress and food waste content, and in some cases, triplicate tests were performed (in cases where the difference in shear strength values of the duplicates was larger than normal). All of the replicate data points for each set of SSDSTs were used for the best-fit linear regressions. Because of the scale, replication was not conducted for the LSDSTs. Although the internal friction angle is the focus of this study, the cohesion values were also calculated and are reported briefly later.

$$\tau' = c' + \sigma' \tan(\Phi') \quad (5\text{-}1)$$

Where τ' = (Effective) shear stress (kPa); c' = (Effective apparent) cohesion (kPa); σ' = (Effective) normal stress (kPa); Φ' = (Effective, or drained) angle of internal friction (degree).

In the second data interpretation method, the mobilized shear strength, cohesion and internal friction angle at various displacement levels were calculated to investigate the relationship between displacement level and mobilized shear-strength parameters. Based on the stress-displacement response data, mobilized internal friction angles of MSW were estimated at 5 (5%), 10 (10%), 15 (15%), and 18 mm (18%) of horizontal displacement for the SSDSTs and 22 (5%), 43 (10%), 65 (15%), 86 (20%), 108 (25%), and 129 mm (30%) of horizontal displacement for the LSDSTs. To remain consistent, the horizontal displacement level will be presented as both a magnitude (mm) and percentage in the remainder of the paper.

Results and Discussion

Stress-Displacement Response with Different Food Waste Contents

The stress-displacement response plots of SSDSTs showed relatively well-defined peak (ultimate) shear strengths at all tested food waste contents; stress-displacement curves are presented in Figures B-32 to B-39. Twenty eight out of 48 SSDSTs showed the fully mobilized, well-defined peak shear strength. In the remaining 20 SSDSTs, the stress-displacement response curves were close to their peak shear strengths at the maximum displacement of 18 mm (18%). For these tests the maximum shear strength values at a displacement of 18 mm (18%) were considered as the peak shear strength and those were used to develop Mohr-Coulomb failure criteria envelopes later. Figure 5-2 presents examples of each type of stress-displacement response of the SSDSTs.

Stress-displacement response plots of the 40 and 80% food waste specimens show shear stresses that approach their peak shear strengths, while the 0 and 58% food waste specimens were fully mobilized at 14 mm (14%) and 10 mm (10%) of displacement, respectively. These stress-displacement response plots are similar to typical stress-displacement responses of direct shear tests on a loose-soil sample (Budhu, 2000; McCarthy, 2007).

All LSDST stress-displacement response plots resulted in well-defined mobilized peak shear strength. Figure 5-3 shows examples of stress-displacement response plots produced from LSDSTs with 0, 40, 58, and 80% food waste contents under a stress of 192 kPa. Nine out of 12 LSDSTs showed peak shear strengths that were mobilized between 86 mm (20%) and 129 mm (30%) of displacement, while the rest were mobilized at approximately 65 mm (15%) of displacement. This suggests that a displacement of 129 mm (30%) is enough to mobilize a peak shear strength using the wastes and apparatus tested.

The peak shear strength of most of the SSDSTs was mobilized at smaller displacement levels (%) than the LSDSTs. One possibility is that the large sizes of fibrous materials used for the LSDSTs induced stronger reinforcement effect and required greater displacement level of LSDST specimens to mobilize their peak shear strengths. Reinforcement effect by fibrous materials is discussed more in a later section of the paper.

Unlike the results of this study, which consistently show the relatively well-defined peak shear strengths, other research has reported various types of displacement-stress responses (Harris et al. 2006; Gabr et al. 2007; Reddy et al. 2008). For example, in their

small-scale (100-mm-diameter-by-50-mm-thickness) direct shear tests Gabr et al. (2007) reported a particular type of stress-displacement response plot that had an initial peak followed by a residual and then a continuous increase in shear stress with displacement. The stress-displacement response difference between this study and other studies may be attributed to factors such as the composition, size, and preparation method of the waste components. Stress-strain response curves of triaxial shear tests on MSW in the literature show even upward curvilinear curves (Machado et al. 2002; Zekkos et al. 2007; Zhan et al. 2008). Sadek et al. (2001) pointed out that the shear strength of MSW might be mobilized at smaller displacement levels in a direct shear test than in a triaxial shear test. This is because the failure surface of a direct shear test is pre-determined during the sample preparation; most fibrous material is placed parallel to the failure surface.

The mobilized peak shear strength under a given normal stress increased as food waste content decreased. For example, with the SSDST and under a stress of 290 kPa, the mobilized peak shear strength decreased from 245 to 39 kPa as the food waste content increased from 0 to 80 %. This trend was consistently observed during all tests on both scales. As the ratio of food to other components became more dominant, shear strength decreased but the extent of this decrease declined as normal stress decreased. For example, in the SSDSTs the difference in the mobilized peak shear strength between 0 and 80% food waste specimens under an effective normal stress of 48 kPa was only 20 kPa, while that under a stress of 290 kPa was 206 kPa.

Change in Mobilized Internal Friction Angle with Food Waste Content

Figure 5-4 presents Mohr-Coulomb criteria envelopes plotted using the mobilized peak shear strength values produced from (a) SSDSTs and (b) LSDSTs. The linear

regressions showed a range of R squared values from 0.81 to 0.99 for SSDSTs and from 0.94 to 0.99 for LSDSTs. In both scales, the Mohr-Coulomb failure criteria envelopes showed that mobilized internal friction angles increased with decreasing food waste content, but the magnitude of the increase varied in different food waste content or with scales of testing. The mobilized internal friction angles of SSDSTs decreased from 39 to 31^{o} by increasing food waste content from 0 to 40% while the angles decreased more dramatically from 31 to 7° with an increase in the food waste content from 40 to 80%. The mobilized internal friction angles of LSDSTs decreased from 36 to 26^{o} by increasing the food waste content from 0 to 40%. There was no considerable change in internal friction angle as food waste content increased from 40 to 58%. However, the mobilized internal friction angles dropped from 24 to 15° as food waste content increased from 58 to 80% in LSDSTs. Overall, the extent of decrease in the internal friction angle with increasing food waste content of SSDSTs was greater than that of LSDSTs. One possible explanation is that the large size of the fibrous materials (metal, plastics, wood, and textile) used for the LSDSTs compared to the SSDSTs causes more additional shear resistance. Zekkos et al. (2007 and 2008) indicated that the increase in shear strength is attributed to the reinforcement effect of large fibrous material (> 20 mm). These results suggest that the food waste content has a greater impact on friction angle for processed waste (size-reduced) compared to non-processed waste. Because the food waste for the SSDSTs was pulped, the contribution of the food waste as a fibrous (reinforcement) material might be reduced. Film plastic was not used as a part of plastic waste component for the SSDSTs. This might induce slightly different shear behavior of the SSDSTs and LSDSTs.

The values of the mobilized internal friction angle and the mobilized cohesion at different displacement levels with different food waste contents are presented in Table 5-4. At each displacement level of both scales (except at the 15% displacement level of LSDSTs), the internal friction angle decreased with increasing food waste content. As shown in Table 5-4, when the displacement level increased from 5 to 10%, the mobilized internal friction angles of all tests (except LSDSTs with the specimens of 80% of food waste content) increased. However, at the other displacement levels, no correlation between the mobilized internal friction angle and the displacement level was found. This differs from the results from Zhan et al. (2008) who reported that the internal friction angle increased with strain based on the results of triaxial tests on MSW. Cohesion values overall increased with increasing displacement level except LSDSTs with 80% food waste content. The greatest cohesion among the tested conditions occurred at the 58% food waste content in SSDSTs and at the 40% food waste content in the LSDSTs.

Comparison of Internal Friction Angles with Previous studies

In Figure 5-6, the internal friction angle and the cohesion of the current study were compared to those from previous studies (Kavazanjian et al. 1999; Sadek et al. 2001; Machado et al. 2002; Harris et al. 2006; Zhan et al. 2008; Reddy et al. 2009). Reported internal friction angles ranged from 14 to 39° and cohesion ranged from 0 to 70 kPa as shown in Figure 5-6. The wide range of value can be attributed to differences in the test methods for shear strength employed, waste composition and processing, and age or level of decomposition of the waste samples. Again, this illustrates the need additional research to better understand the factors that impact waste shear strength parameters and how possible future changes to the waste stream might impact these parameters.

Internal friction angle values of 20 to 40º are often considered as a typical range for MSW from western countries where the waste is more dominated by packaging materials and discarded domestic goods, and less by food waste. The design engineer would use an internal friction angle estimate as an input for a landfill design. Thus a natural question that would come up in the design of a landfill with a much larger food waste content, such as might be currently encountered in some parts of China, is whether typical friction angle values used for the design of a landfill in the U.S. would be appropriate or not. The results here suggest that food waste contents greater than typically seen in western countries would still have an internal angle of friction within the typical range, but that at very high food waste contents, friction angle does decrease to levels lower than expected for wastes with lower food contents. The results of testing at both scales suggest that at a food waste content up to 40%, the friction angle falls within a typical range, with contents up to 60% close the lower end of typical ranges for design. The data here provide the design engineer with some guidance for better selecting input parameters for engineering applications. Clearly large food waste contents do impact friction angle and thus must be factored in the design of landfills containing this type of waste. As previously mentioned, the food waste content in some regions has been reported as high as 70% (The World Bank, 1999; Wang and Nie, 2001).

Summary and Conclusions

The impacts of changing food waste content on the mobilized internal friction angle of MSW were investigated by conducting direct shear tests with small-scale and large-scale direct-shear testing devices. The stress-displacement response plots of SSDSTs showed relatively well-defined peak (ultimate) shear strengths in all tested

food waste content. In 28 out of 48 SSDSTs and all 12 LSDSTs, well-defined peak shear strengths were observed. The shear stress approached the peak shear strength in the remaining 20 SSDSTs. In both scales of tests, the mobilized peak shear strength increased with a decrease in food waste content under a given normal stress. Also, decreasing food waste content resulted in increasing the internal friction angles. A greater decrease in the internal friction angle with increasing food waste content was observed in SSDSTs than in LSDSTs, which is likely a result of the greater sizes of the waste components in the LSDSTs which cause additional shear resistance (reinforcement effect). As food waste content increased from 0 to 80%, the mobilized internal friction angles decreased from 39 to 7° in SSDSTs and from 36 to 15° in LSDSTs. Internal frictions angles at food waste contents up to 40% for the SSDSTs and 58% for the LSDSTs were measured in the range of typical magnitudes reported in the literature; larger food waste contents resulted in below typical angles. In most of the tests, the mobilized internal friction angle increased with increasing horizontal displacement level from 5% to 10%, but displacement level increases beyond this were not found to change the internal friction angle estimate. These results suggest that the impact of high food waste content on the internal friction angle of MSW should be considered when designing for landfill slope stability.

Table 5-1. Composition of MSW specimens for LSDSTs and LSDSTs

Component	Content (%) by wet weight			
Food	0.0	40.0	57.6	80.0
Paper	24.0	14.4	10.2	4.8
Plastic	22.3	13.4	9.5	4.6
Metal	4.0	2.4	1.7	0.8
Wood	11.2	6.7	4.7	2.2
Glass	6.2	3.7	2.6	1.2
Textile	8.7	5.2	3.7	1.7
Ash	23.7	14.2	10.0	4.7

Table 5-2. Size and moisture content (MC) of each waste component for SSDST and LSDST

Component	SSDST			LSDST		
	Size limit	Size reduction method	MC (%)	Size limit	Size reduction method	MC (%)
Food	Pulp [a]	Food grinder	61.6	No size reduction		63.0
Paper	47 mm × 7 mm	Paper shredder	7.5	140 mm × 220 mm	Scissors	8.8
Plastic	10 mm × 10 mm	Scissors	0.7	< 150 mm	Scissors	1.5
Metal	10 mm × 10 mm	Scissors	0.4	< 150 mm	Scissors	0.2
Wood	< 10 mm	-	8.3	< 150 mm	-	17.3
Glass	< 4.75 mm	Hammer	0.0	< 150 mm	Hammer	0.1
Textile	10 mm × 10 mm	Scissors	5.0	< 150 mm	Scissors	8.2
Ash	No size reduction		0.7	No size reduction		15.3

[a] Food waste for SSDSTs was pulped by grinding.

Table 5-3. Average moisture contents and dry densities (kg/m^3) of the specimens

Food waste content	Moisture content (%)				Dry density (kg/m^3)[c] (LSDST)		
	SSDST		LSDST		Normal stress		
	Initial[a]	Final[b]	Initial	Final	96 kPa	192 kPa	287 kPa
0%	3.5	4.5	8.9	10.4	358.5	462.3	508.5
40%	26.7	20.7	30.0	27.4	425.8	465.6	701.2
58%	37.0	30.0	39.1	42.8	467.6	456.6	651.6
80%	50.0	47.0	51.7	53.4	492.1	522.3	579.7

[a] Measured before consolidation.
[b] Measured after testing shear strength.
[c] Measured after consolidation and before shearing. Density was not monitored for SSDST.

Table 5-4. Mobilized internal friction angle and cohesion values

Displacement[a]	Parameter	SSDST Food Waste				LSDST Food Waste			
		0%	40%	58%	80%	0%	40%	58%	80%
5%	Angle (^{0})	30	27	20	6	25	24	23	13
	Cohesion (kPa)	5	6	17	6	0	12	6	5
10%	Angle (^{0})	36	30	21	7	33	26	24	12
	Cohesion (kPa)	1	10	23	7	0	21	13	9
15%	Angle (^{0})	39	31	20	7	37	24	25	13
	Cohesion (kPa)	2	12	27	7	0	34	18	7
18% - 20%[c]	Angle (^{0})	39	30	18	7	38	25	24	15
	Cohesion (kPa)	3	13	31	8	2	36	24	3
25%	Angle (^{0})	-	-	-	-	37	25	21	15
	Cohesion (kPa)	-	-	-	-	9	38	31	1
30%	Angle (^{0})	-	-	-	-	36	24	21	19
	Cohesion (kPa)	-	-	-	-	15	37	26	2
Peak[b]	Angle (^{0})	39	31	21	7	36	26	24	15
	Cohesion (kPa)	4	13	28	8	17	37	24	4

[a] Displacement represents the relative horizontal displacement of a specimen.
[b] The shear-strength parameters estimated using the fully mobilized shear-strength values of each shear test.
[c] 18% for SSDSTs and 20% for LSDSTs

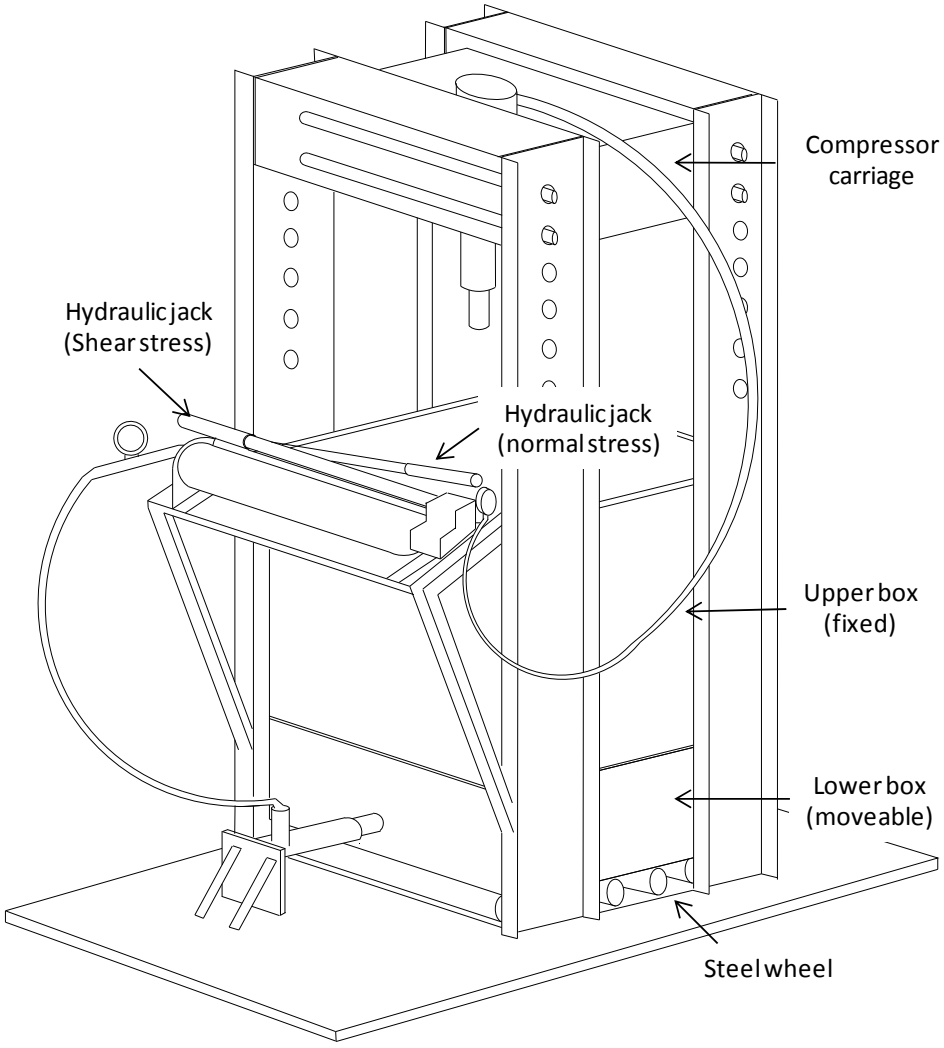

Figure 5-1. Large-scale direct shear test device

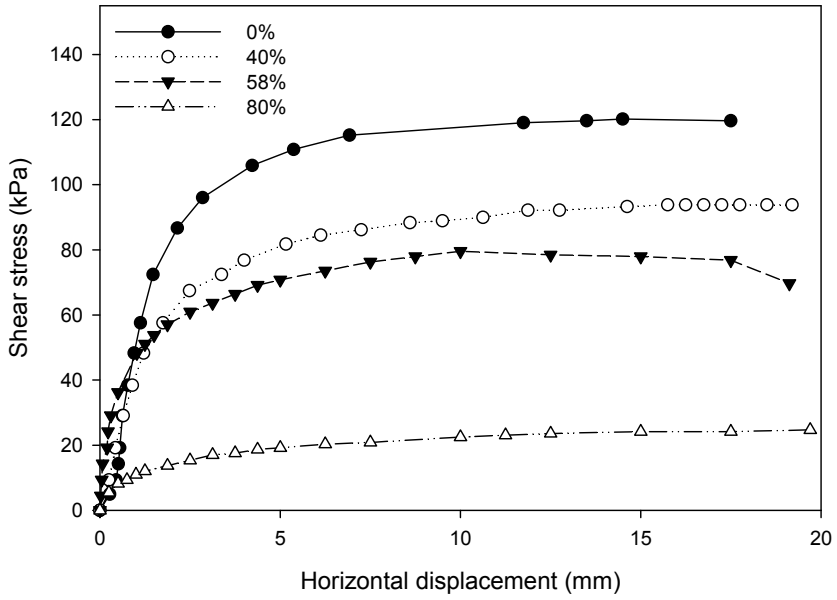

Figure 5-2. Stress-displacement response curves of SSDSTs with 0, 40, 58, and 80% food waste specimens under 145 kPa of effective normal stress

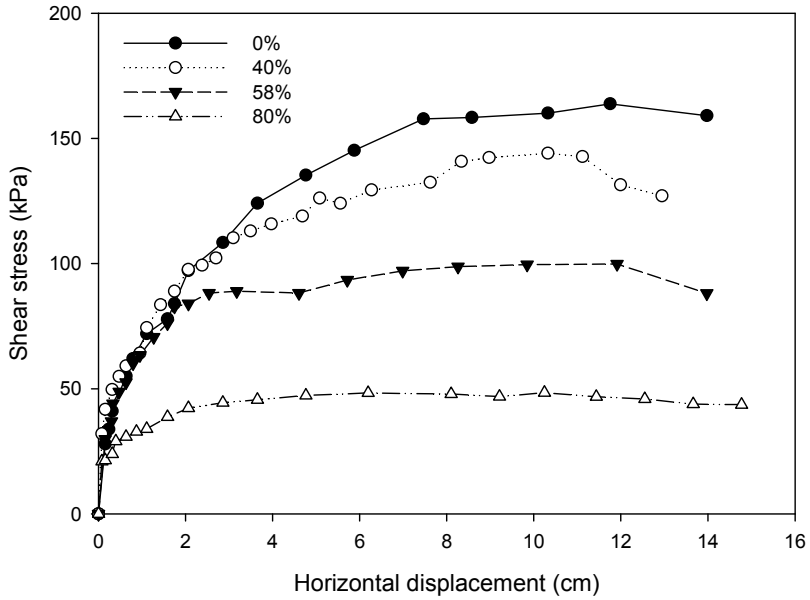

Figure 5-3. Stress-displacement response curves of LSDSTs with 0, 40, 58, and 80% of food waste specimens under 191 kPa of effective normal stress

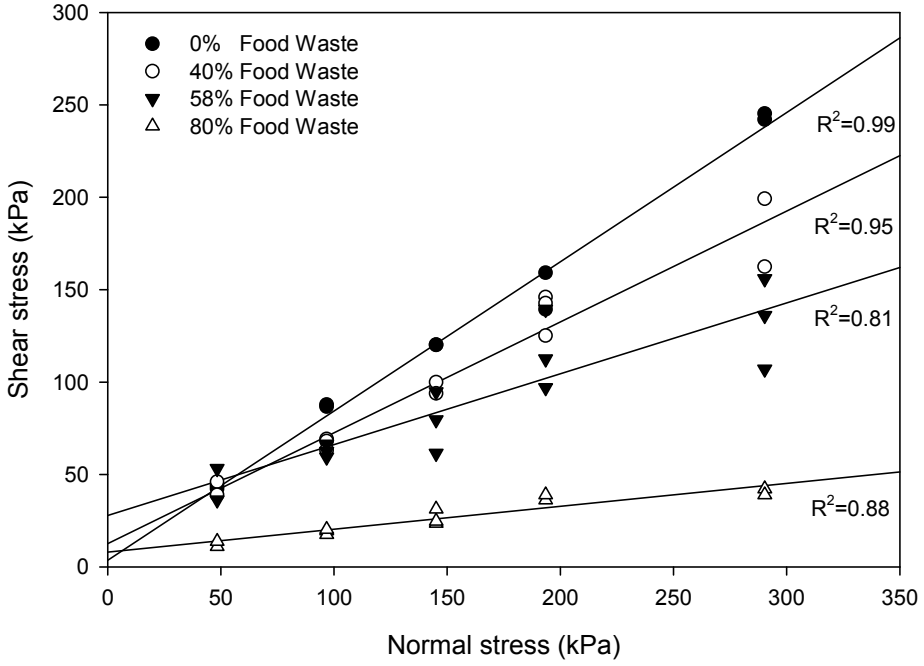

A

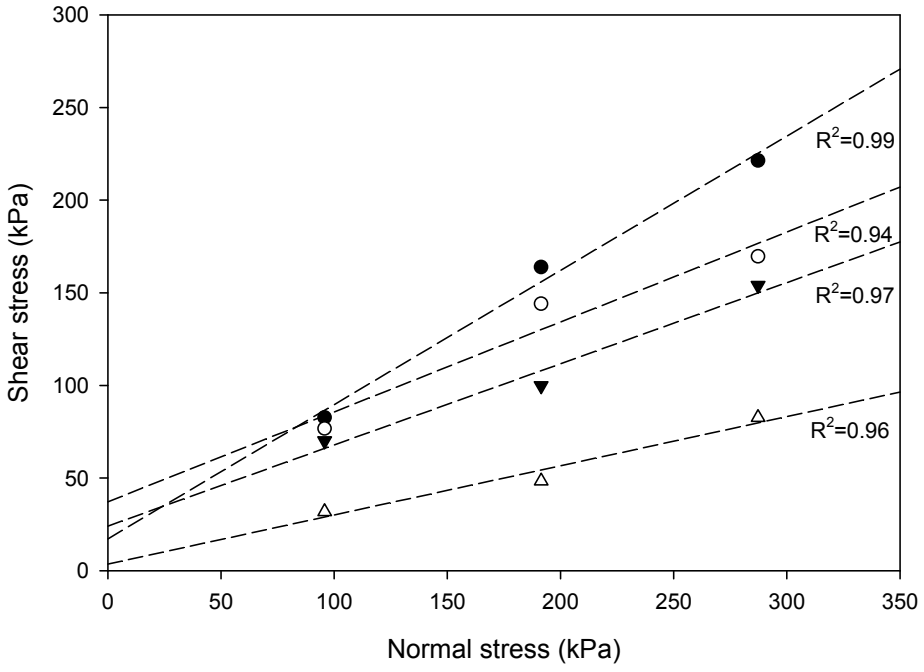

B

Figure 5-4. Mohr-Coulomb failure envelopes of A) SSDSTs and B) LSDSTs. Data points correspond to peak shear strengths under each effective normal stress and at each waste composition; each line was derived by a best-fit linear regression.

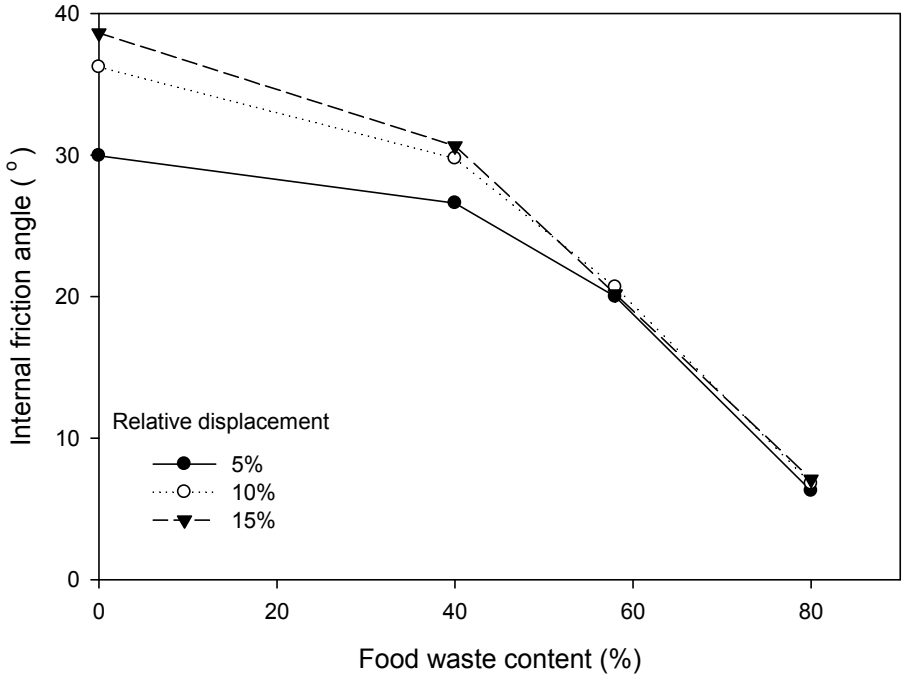

A

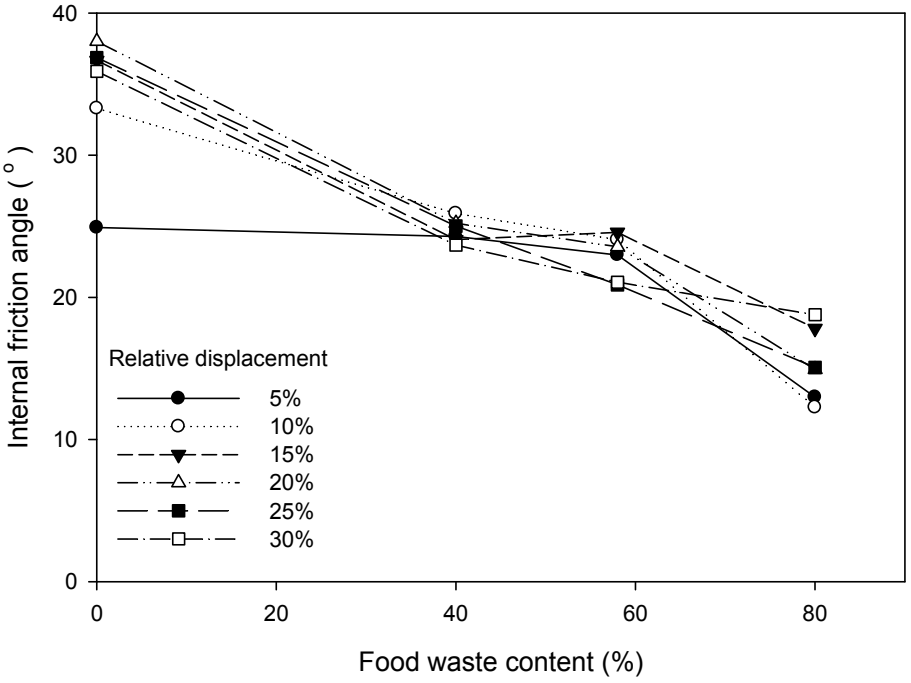

B

Figure 5-5. Impact of food waste contents in synthetic fresh MSW on friction angles at different displacement levels: A) SSDSTs and B) LSDSTs

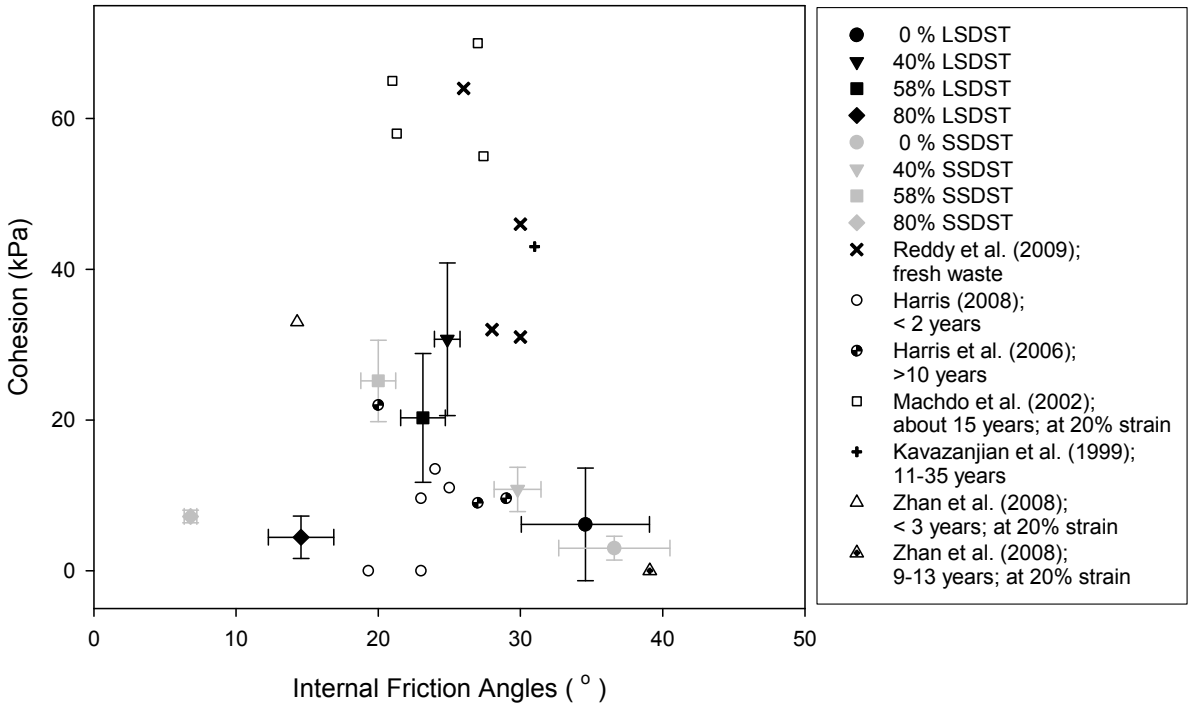

Figure 5-6. Comparison of values of internal friction angle and cohesion values in this study to those of in previous studies; each error bar indicates positive or negative standard deviation

CHAPTER 6
SUMMARY AND CONCLUSIONS

Pore pressure variation resulting from liquids addition was monitored in a bioreactor landfill equipped with horizontal liquid distribution trenches. To measure pore pressure in the landfill, piezometers were installed in liquids-introducing bedding media trenches and in the surrounding waste. This study consisted of two experiments. In Experiment 1, liquids were added at constant flow rates of 0.057 m^3/min (conducted by Kumar (2009) in 2007). In Experiment 2, liquids were added at a rate of 0.076 m^3/min (conducted by the author in 2010). Added liquids were successfully transmitted to the ends of the crushed glass and the shredded tire trenches without considerable head loss. While the added liquids spread out from the trenches, pressure dropped sharply near the trenches and then gradually with increasing horizontal distance; this would suggest that for a slope stability analysis for a landfill with a horizontal liquid addition trenches the rapid pore pressure drop near the bedding media trenches needs to be considered.

Using analytical models presented by Townsend (1995) and the aforementioned pore pressure measurements, K_x and K_y values of the landfilled waste surrounding the horizontal trenches were estimate to be in the ranges of 7.0×10^{-4} to 3.0×10^{-3} cm/sec and 1.0×10^{-6} to 1.9×10^{-5} cm/sec, respectively. These estimated K_x and K_y values fell within a range reported in literature. Thus, it is concluded that the analytical models can be used as useful tools to roughly estimate hydraulic conductivities of waste in a bioreactor landfill equipped with horizontal liquids addition lines. The values of anisotropy were estimated to be in the range of 37 to 277.

Surcharge-induced settlement of landfilled waste with high moisture content (approximately 40%) was investigated using a settlement profiling sensor. Settlement profiling was conducted by inserting the sensor into 10-cm diameter HDPE pipes placed over the top surface of the study landfill prior to additional waste placement. It was hypothesized that the settlement of the landfilled waste with high moisture content might be similar to consolidation settlement. As a result of consolidation, average monthly leachate generation increased from approximately 200 to 1100 m^3 after additional waste placement. Based on the hypothesis, relatively wide ranges of compression parameters (C_c', m_v, and c_v) were estimated and found typically within ranges reported in the literature: C_c' (0.1 – 1.7), m_v (3.0×10^{-4} – 7.3×10^{-3} m^2/kN), and c_v (0.89×10^{-2} to 1.44×10^{-2} cm^2/sec). K_y values of the landfilled waste were estimated in the range of 4.6×10^{-7} to 9.8×10^{-6} cm/sec; these values were calculated using the estimated m_v and c_v values. During the settlement profiling period, the average settlement rate of 3.76% per year was approximately 1.4 times greater than the settlement rate prior to waste placement (2.66% per year).

Settlement behavior of a landfill foundation was investigated in situ, using instrumentation consisting of eight pairs of TPCs and eight pairs of SSs installed under the bottom liner of a municipal solid waste landfill. Settlement was monitored for 39 months from March 2007 to June 2010. During the study period, all sixteen TPCs and twelve out of the sixteen SSs worked properly. The readings of the TPCs near the landfill side slope toe were, on average, 3 times greater than predicted values [(predicted overburden pressure) = (thickness of waste and cover soil) × (bulk unit weight)] and1.3 times greater than those estimated using the Boussinesq influence

factor charts. Settlement readings measured under the toe of the side slope showed no relationship between overburden pressure and settlement while those under the interior area were found to generally increase with increasing overburden pressure. Settlement predictions were made using one-dimensional elastic theory and Terzaghi's consolidation model. Constrained moduli for elastic settlement predictions were estimated using SPT(N), CPT(N), and various stress-strain (Young's) modulus equations from Bowles (1996). The one-dimensional settlement models did not provide reasonable settlement estimates of the area beneath the landfill side slope. Settlement predictions of the landfill central body area were over predicted up to 2.6 cm. It should be noted that at one monitoring point settlement was under predicted by approximately 2.7 cm.

The impacts of food waste content on the mobilized internal friction angle of MSW were investigated by conducting direct shear tests. Generally, mobilized peak shear strength increased with a decrease in food waste content under a given normal stress. Additionally, as food waste content decreased, internal friction angles increased. A greater decrease in the internal friction angle with increasing food waste content was observed in SSDSTs compared to the LSDSTs, which might be due to the bulkier waste components in the LSDSTs; large fibrous material is generally considered to cause additional shear resistance (reinforcement effect). As food waste content increased from 0 to 80%, the mobilized internal friction angles decreased from 39 to 7° in SSDSTs and from 36 to 15° in LSDSTs. The majority of friction angle measurements produced in this study fell within the range of those previously reported for MSW.

APPENDIX A
SUPPLEMENTAL TABLES

Table A-1. Hydraulic conductivities and compression properties of waste in previous studies

C_c'	m_v (m^2/kN)	c_v (m^2/sec)	K_x (cm/sec)	K_y (cm/sec)	Reference
—	2.9×10^{-4} - 5×10^{-3}	—	—	3.7×10^{-6} - 1.5×10^{-2}	Powrie and Beaven (1999)
0.17 - 0.24	4×10^{-4} - 1.25×10^{-3}	—	—		Landva (2000)
0.128 - 0.260	4.48×10^{-4} - 2.5×10^{-4}	5.62×10^{-6} - 5.12×10^{-4}	—	4.7×10^{-6} - 1.24×10^{-4}	Durmusoglu et al. (2006)
0.1 - 0.41	—	—	—	—	Sowers (1973)
0.21	—	—	—	—	Machado et al. (2002)
0.17 - 0.23	—	—	—	—	Anderson et al. (2004)
—	—	—	—	3.0×10^{-6} - 4.0×10^{-6}	Townsend (1995)
—	—	—	5.4×10^{-6} - 6.1×10^{-5} combined K		Jain et al. (2006)
—	—	—	—	1.9×10^{-4} - 7.8×10^{-4}	Larson (2007)

— represents no data.
C_c' represents modified primary compressibility index.
m_v represents coefficient of volume change.
c_v represents coefficient of consolidation.
K_x represents horizontal hydraulic conductivity.
K_y represents vertical hydraulic conductivity.

Table A-2. Summary of literature review and studies on landfill settlement behavior

Site		Study Period (yrs)	Study Area (ha)	Initial Ave. Depth (ft)	Settlement (%)	Settlement Rate (%/yr)	Reference
Crow Wing County, MN	Bioreactor	5.0	5.7	NA	20.0	4.00	Bioreactor Performance, US EPA (2007)
Victoria, Australia	Dry	1.7	0.8	59.1	2.3	1.35	Yuen et al. (1997)
	Bioreactor	1.7	0.8	59.1	3.9	2.29	
Mountain View, CA	Dry	4.0	0.9	47.3	11.7	2.93	M. El-Fadel et al. (1999)
	Bioreactor-A	4.0	0.9	49.7	13.5	3.38	
	Bioreactor-B	4.0	0.9	47.1	13.7	3.43	
	Bioreactor-C	4.0	0.9	52.2	12.5	3.13	
	Bioreactor-D	4.0	0.9	47.7	7.8	1.95	
	Bioreactor-E	4.0	0.9	49.5	15.3	3.83	
Meruelo, Spain	Dry	3.0	—	—	3.0	1.00	Sanchez-Aliciturri et al (1995)
A landfill, WI	Dry	1.5	—	—	1.7	1.13	Edil et al. (1990)
Site C	Bioreactor	1.5	—	—	10.5	7.00	C.H. Benson et al. (2000)
Site S	Dry	2.7	—	—	4.1	1.50	C.H. Benson et al. (2000)
	Bioreactor	2.7	—	—	27.0	10.00	

— represents no data.

Table A-3. Settlement (%) measurements of the profiling pipe 1

Distance from the pipe entry (m)	Waste below Pipe 1 (m)	Waste above Pipe 1 (m)	5/9/2009	6/1/2009	8/31/2009	12/23/2009	3/3/2010
0	14.4	0.00	1.50	2.22	2.39	2.61	2.94
5	14.8	0.44	1.80	2.44	3.32	2.91	3.25
7	15.3	0.61	4.14	4.77	5.22	5.07	5.39
10	15.9	0.80	5.84	6.80	6.80	6.91	7.28
13	16.4	1.02	4.61	5.21	5.58	5.67	6.15
16	16.7	1.33	4.03	4.63	5.33	5.24	5.69
19	16.8	1.92	1.87	2.50	3.07	3.15	3.63
22	16.9	2.37	1.30	1.87	2.46	2.68	3.09
25	17.1	3.24	2.01	2.54	3.08	3.22	3.59
28	17.32	3.77	2.20	2.76	3.23	3.56	3.81
31	17.55	4.42	2.29	2.89	3.44	3.75	4.06
34	17.65	5.21	1.95	2.51	3.39	3.49	3.90
37	17.75	5.84	2.04	2.38	3.23	3.50	3.87
40	17.9	6.75	2.22	2.61	3.28	3.80	4.12
43	18.1	6.98	2.87	3.36	4.21	4.61	4.69
46	18.2	8.07	2.49	2.87	4.39	4.33	4.39

Table A-4. Settlement (%) measurements of the profiling pipe 2

Distance from the pipe entry (m)	Waste below Pipe 2 (m)	Waste above Pipe 2 (m)	5/9/2009	6/1/2009	8/31/2009	12/23/2009	3/3/2010
0	14.9	0.00	3.97	4.89	5.40	5.26	5.89
3	15.2	0.00	1.36	1.95	2.56	3.00	5.22
6	15.5	0.41	1.57	2.33	2.78	2.78	6.01
9	15.9	0.57	2.21	3.00	3.44	3.35	6.15
12	16.3	1.09	1.61	2.46	2.79	2.82	5.53
15	16.6	1.32	2.08	2.98	3.45	3.58	6.41
17	17.0	1.67	2.98	3.78	4.13	4.08	6.94
20	17.4	2.04	1.93	3.19	3.34	2.91	5.87
23	17.8	2.39	1.61	2.86	3.26	2.97	5.55
27	18.1	2.81	1.77	2.71	3.34	3.28	6.26
30	18.5	3.30	2.53	3.30	4.34	4.00	6.80
33	18.8	3.51	2.64	3.56	4.55	4.29	6.32
36	19.1	4.16	2.43	3.38	4.56	4.31	5.43
39	19.1	5.29	1.58	2.44	3.68	3.54	5.18
42	19.3	5.86	1.96	2.78	4.64	3.95	5.14
45	19.4	6.52	1.76	2.64	4.47	3.75	4.82

Table A-5. Settlement (%) measurements of the profiling pipe 3

Distance from the pipe entry (m)	Waste below Pipe 3 (m)	Waste above Pipe 3 (m)	5/9/2009	6/1/2009	8/31/2009	12/23/2009	3/3/2010
0	13.2	0.00	3.28	4.17	3.97	4.00	4.12
3	13.6	0.00	3.43	4.17	4.80	4.31	5.46
6	13.8	0.61	0.28	0.88	1.24	1.05	3.78
9	14.0	1.01	2.12	2.71	3.21	—	6.14
12	14.4	1.32	4.14	4.16	4.35	4.07	7.31
15	14.7	1.64	2.97	3.49	3.81	3.64	6.46
18	15.0	2.02	3.09	3.78	4.21	3.94	6.74
21	15.3	2.27	3.26	3.94	4.45	4.25	7.10
23	15.6	2.06	3.19	4.03	4.50	4.51	6.85
26	15.8	2.52	3.06	3.84	4.44	4.50	7.49
29	16.1	2.89	3.96	4.62	5.38	5.51	8.57
32	16.5	3.39	4.99	5.85	6.68	6.72	9.33
35	16.7	3.96	3.94	4.68	5.68	5.85	7.33
38	16.9	4.38	3.31	4.18	5.03	5.17	7.61
41	17.2	4.64	3.32	3.98	4.90	—	7.04
44	17.4	5.24	3.60	4.16	6.65	8.72	5.16

— represents no data.

Table A-6. Settlement (%) measurements of the profiling pipe 4

Distance from the pipe entry (m)	Waste below Pipe 4 (m)	Waste above Pipe 4 (m)	5/9/2009	6/1/2009	8/31/2009	12/23/2009	3/3/2010
0	13.2	0.00	0.53	0.66	1.01	1.84	2.30
4	13.6	0.56	2.39	2.28	2.76	3.77	4.38
8	13.9	0.97	4.00	4.02	4.50	5.51	5.94
10	14.2	1.27	7.24	4.67	4.99	6.10	6.54
13	14.5	1.53	3.79	3.85	4.26	5.35	5.92
16	14.9	1.80	3.80	3.77	4.26	5.49	5.74
19	15.3	2.11	4.25	4.31	4.91	5.93	6.43
22	15.4	2.68	3.12	3.18	3.97	4.98	5.39
25	15.4	3.40	3.50	3.71	4.33	5.16	5.64
29	15.6	4.02	3.74	3.87	4.65	5.44	5.60
31	15.9	4.55	4.16	3.92	4.74	6.09	6.25
34	16.2	4.91	4.18	3.92	5.17	6.14	6.38
37	16.5	5.38	3.69	3.63	4.74	5.93	6.30
40	16.6	5.18	3.57	3.60	4.64	7.13	6.21
42	16.7	5.19	3.46	3.31	4.54	—	6.03
45	16.9	5.14	2.98	2.79	4.06	—	5.61

— represents no data.

Table A-7. Settlement (%) measurements of the profiling pipe 5

Distance from the pipe entry (m)	Waste below Pipe 5 (m)	Waste above Pipe 5 (m)	5/9/2009	6/1/2009	8/31/2009	12/23/2009	3/3/2010
0	13.6	0.00	2.86	3.11	3.50	3.59	4.31
3	14.0	0.00	2.46	2.62	3.48	3.63	6.43
6	14.3	0.40	2.77	3.09	3.34	3.88	6.09
9	14.4	0.68	3.68	3.98	4.32	4.96	6.77
11	14.5	0.80	4.67	4.99	5.29	6.14	6.94
14	14.6	1.02	3.87	4.26	4.56	4.96	8.97
17	15.0	0.66	2.98	3.37	3.84	8.27	5.96
20	15.1	0.59	4.85	5.23	5.73	6.31	5.06
23	14.9	1.13	3.43	3.99	4.34	4.92	3.87
26	14.7	1.50	3.08	3.53	3.60	4.29	4.99
30	14.7	1.65	3.44	3.81	3.80	4.32	5.08
35	14.7	1.85	3.72	4.08	4.22	4.60	5.62
38	14.7	2.03	4.50	4.91	5.02	5.65	5.74
41	14.7	2.01	3.31	3.84	4.01	4.43	5.99
44	14.8	1.97	2.28	2.64	2.99	3.08	4.58
47	14.9	1.96	3.68	4.07	—	4.64	4.96

— represents no data.

Table A-8. Compressibility properties and hydraulic conductivities estimated using the data obtained from Pipe 1

Distance from the pipe entry (m)	C_c'	c_v (cm^2/sec)	m_v (m^2/kN)	K_y (cm/sec)
0	—	—	0.0046	—
5	0.97	—	0.0065	—
7	1.43	—	0.0071	—
10	1.64	0.012	0.0042	5.62×10^{-6}
13	1.02	0.014	0.0029	9.12×10^{-6}
16	0.72	0.014	0.0011	9.84×10^{-6}
19	0.28	0.011	0.0007	4.60×10^{-6}
22	0.17	0.011	0.0007	3.08×10^{-6}
25	0.18	0.012	0.0006	1.32×10^{-6}
28	0.18	—	0.0005	—
31	0.16	0.012	0.0004	6.29×10^{-7}
34	0.12	0.012	0.0003	4.88×10^{-7}
37	0.11	0.014	0.0003	4.59×10^{-7}
40	0.11	—	0.0004	—
43	0.13	—	0.0003	—
46	0.10	—	0.0046	—

— represents no data.

Table A-9. Compressibility properties and hydraulic conductivities estimated using the data obtained from Pipe 2

Distance from the pipe entry (m)	C_c'	c_v (cm^2/sec)	m_v (m^2/kN)	K_y (cm/sec)
0	—	—	—	—
3	—	—	—	—
6	1.03	0.009	0.0047	4.08×10^{-6}
9	1.00	0.010	0.0044	4.18×10^{-6}
12	0.45	0.010	0.0019	1.81×10^{-6}
15	0.47	0.012	0.0019	2.24×10^{-6}
17	0.49	—	0.0019	—
20	0.35	—	0.0013	—
23	0.28	—	0.0010	—
27	0.23	0.012	0.0008	9.56×10^{-7}
30	0.25	—	0.0008	—
33	0.26	—	0.0008	—
36	0.21	—	0.0007	—
39	0.13	—	0.0004	—
42	0.13	—	0.0004	—
45	0.12	—	0.0003	—

— represents no data.

Table A-10. Compressibility properties and hydraulic conductivities estimated using the data obtained from Pipe 3

Distance from the pipe entry (m)	C_c'	c_v (cm^2/sec)	m_v (m^2/kN)	K_y (cm/sec)
0	—	—	—	—
3	—	—	—	—
6	0.24	—	0.0012	—
9	0.47	—	0.0022	—
12	0.57	—	0.0026	—
15	0.40	—	0.0018	—
18	0.37	—	0.0016	—
21	0.35	—	0.0014	—
23	0.40	—	0.0016	—
26	0.32	—	0.0013	—
29	0.35	—	0.0013	—
32	0.39	—	0.0014	—
35	0.28	—	0.0010	—
38	0.23	—	0.0008	—
41	0.21	—	0.0007	—
44	0.20	—	0.0007	—

— represents no data.

Table A-11. Compressibility properties and hydraulic conductivities estimated using the data obtained from Pipe 4

Distance from the pipe entry (m)	C_c'	c_v (cm^2/sec)	m_v (m^2/kN)	K_y (cm/sec)
0	—	—	—	—
4	0.67	—	0.0034	—
8	0.71	—	0.0035	—
10	0.65	—	0.0031	—
13	0.46	—	0.0021	—
16	0.40	—	0.0017	—
19	0.41	—	0.0017	—
22	0.25	—	0.0010	—
25	0.23	—	0.0009	—
29	0.21	—	0.0008	—
31	0.20	—	0.0007	—
34	0.19	—	0.0007	—
37	0.17	—	0.0006	—
40	0.17	—	0.0006	—
42	0.16	—	0.0005	—
45	0.13	—	0.0005	—

— represents no data.

Table A-12. Compressibility properties and hydraulic conductivities estimated using the data obtained from Pipe 5

Distance from the pipe entry (m)	C_c'	c_v (cm^2/sec)	m_v (m^2/kN)	K_y (cm/sec)
0	—	—	—	—
3	—	—	—	—
6	1.29	—	0.0064	—
9	1.01	—	0.0049	—
11	1.09	—	0.0052	—
14	0.75	0.013	0.0035	4.52×10^{-6}
17	0.91	—	0.0042	—
20	1.59	—	0.0073	—
23	0.65	0.012	0.0029	3.45×10^{-6}
26	0.44	—	0.0020	—
30	0.43	—	0.0019	—
35	0.42	0.013	0.0018	2.40×10^{-6}
38	0.46	—	0.0020	—
41	0.37	—	0.0016	—
44	0.26	—	0.0011	—
47	0.40	—	0.0017	—

— represents no data.

Table A-13. Profiles of the subsurface soils of the study site; the locations correspond to those in Figure 4-1.

Depth m	Location							
	A&A'	B&B'	C&C'	D&D'	E&E'	F&F'	G&G'	H&H'
	SILTY SAND TO SANDY SILT		LOOSE SAND				SILTY SAND TO SANDY SILT	
							SAND	
			MEDIUM STIFF CLAYEY SAND				SAND TO SILTY SAND	
							SILTY SAND TO SANDY SILT	
							SAND TO SILTY SAND	
	SAND TO SILTY SAND						SAND	
	SAND							
2.5	GRAVELLY SAND TO SAND						GRAVELLY SAND TO SAND	
	SAND							
▽ G.T.*							SAND	
	SAND TO SILTY SAND						SAND TO SILTY SAND	
	SILTY SAND TO SANDY SILT						SAND	
	SAND TO SILTY SAND							
	SAND		HARD SILTY SAND				SANDY SILT TO CLAYEY SILT	
5.0	GRAVELLY SAND TO SAND						SILTY SAND TO SANDY SILT	
	SAND						SAND	
	SAND TO SILTY SAND							
	SAND						SAND TO SILTY SAND	
							SILTY SAND TO SANDY SILT	
							SAND	
7.5							GRAVELLY SAND TO SAND	
	GRAVELLY SAND TO SAND						SAND	
	SAND						SILTY CLAY to CLAY	
							CLAYEY SILT TO SILTY CLAY	
			CLAYEY SAND W/ PHOSPHATE					
10.0							SILTY CLAY to CLAY	
							VERY STIFF FINE GRAINED CLAYS	
	GRAVELLY SAND TO SAND						SAND TO SILTY SAND	
			SILTY SAND W/ LIMESTONE				GRAVELLY SAND TO SAND	
12.5								
			HARD CLAY					
	SAND						SAND	
15.0								
	SAND TO SILTY SAND							

* G.T. represents ground water table.

Table A-14. Summary of constrained moduli M of locations A and B

Depth (feet)	Layer Thickness (feet)	σ_o (TSF)	Soil Behavior	CPT (N) (#)	average N-value (#)	Constrained modulus (TSF) Various eq.s	OC sand	saturated sand
1			SILTY SAND TO SANDY SILT	7				
2			SILTY SAND TO SANDY SILT	9				
3			SILTY SAND TO SANDY SILT	10				
4			SILTY SAND TO SANDY SILT	12				
5			SILTY SAND TO SANDY SILT	11				
6	6	0.24	SAND TO SILTY SAND	11	10.00	168.25	679.73	84.13
7			SAND	31				
8			GRAVELLY SAND TO SAND	43				
9			SAND	54				
10			SAND	42				
11			SAND	36				
12			SAND TO SILTY SAND	29				
13			SILTY SAND TO SANDY SILT	26				
14			SAND TO SILTY SAND	27				
15	9	0.71	SAND	39	36.33	345.47	1051.90	172.74
16			GRAVELLY SAND TO SAND	50				
17			GRAVELLY SAND TO SAND	52				
18			SAND	53				
19			SAND	39				
20			SAND TO SILTY SAND	32				
21			SAND	37				
22			SAND	53				
23			SAND	54				
24			SAND	59				
25			SAND	63				
26			GRAVELLY SAND TO SAND	57				
27			SAND	56				
28			SAND	53				
29			SAND	46				
30	15	1.31	SAND	56	50.67	441.94	1254.47	220.97
31			GRAVELLY SAND TO SAND	60				
32			GRAVELLY SAND TO SAND	58				
33			GRAVELLY SAND TO SAND	52				
34			GRAVELLY SAND TO SAND	59				
35			GRAVELLY SAND TO SAND	59				
36			GRAVELLY SAND TO SAND	60				
37			GRAVELLY SAND TO SAND	58				
38			GRAVELLY SAND TO SAND	53				
39			GRAVELLY SAND TO SAND	52				
40			GRAVELLY SAND TO SAND	58				
41			GRAVELLY SAND TO SAND	62				
42			GRAVELLY SAND TO SAND	57				
43			GRAVELLY SAND TO SAND	57				
44	14	2.03	GRAVELLY SAND TO SAND	60	57.50	539.75	1351.05	243.96
45			SAND	56				
46			SAND	52				
47			SAND	44				
48			SAND	35				
49			SAND	28				
50	6	2.53	SAND TO SILTY SAND	22	39.5	366.8	1096.7	183.4

CPT(N) represents a SPT(N) value estimated from CPT using a ratio of tip resistance (q_c) to SPT(N) suggested by Robertson and Campanella (1983).

Table A-15. Summary of constrained moduli M of locations C, D, E, and F

Depth (feet)	Layer Thickness (feet)	σ_o (TSF)	Soil Behavior	SPT (N) (#)	Constrained modulus (TSF) Various eq.s	OC sand	saturated sand
1	2		LOOSE SAND	3	121.1	580.8	60.6
2		0.08	LOOSE SAND				
3	2		MEDIUM STIFF CLAYEY SAND	4	81.8	594.9	63.9
4			MEDIUM STIFF CLAYEY SAND				
5	2		MEDIUM STIFF CLAYEY SAND	8	99.1	651.5	77.4
6			MEDIUM STIFF CLAYEY SAND				
7	2		MEDIUM STIFF CLAYEY SAND	11	112.0	693.9	87.5
8			MEDIUM STIFF CLAYEY SAND				
9	3		MEDIUM STIFF CLAYEY SAND	10	107.7	679.7	84.1
10			MEDIUM STIFF CLAYEY SAND				
11	3		MEDIUM STIFF CLAYEY SAND	10	107.7	679.7	84.1
12			MEDIUM STIFF CLAYEY SAND				
13	11	0.44	MEDIUM STIFF CLAYEY SAND	36	219.7	1047.2	171.6
14			HARD SILTY SAND				
15			HARD SILTY SAND				
16			HARD SILTY SAND				
17	5		HARD SILTY SAND	70	538.4	1527.7	286.0
18			HARD SILTY SAND				
19			HARD SILTY SAND				
20			HARD SILTY SAND				
21			HARD SILTY SAND				
22	5		HARD SILTY SAND	27	538.4	920.0	141.3
23			HARD SILTY SAND				
24			HARD SILTY SAND				
25			HARD SILTY SAND				
26			HARD SILTY SAND				
27	15	1.09	HARD SILTY SAND	18	792.8	792.8	111.0
28			HARD SILTY SAND				
29			CLAYEY SAND W/ PHOSPHATE				
30			CLAYEY SAND W/ PHOSPHATE				
31			CLAYEY SAND W/ PHOSPHATE				
32	5		CLAYEY SAND W/ PHOSPHATE	7	94.8	637.3	74.0
33			CLAYEY SAND W/ PHOSPHATE				
34			CLAYEY SAND W/ PHOSPHATE				
35			CLAYEY SAND W/ PHOSPHATE				
36			CLAYEY SAND W/ PHOSPHATE				
37	9	1.68	CLAYEY SAND W/ PHOSPHATE	13	120.6	722.1	94.2
38			SILTY SAND W/ LIMESTONE				
39			SILTY SAND W/ LIMESTONE				
40			SILTY SAND W/ LIMESTONE				
41			SILTY SAND W/ LIMESTONE				
42			SILTY SAND W/ LIMESTONE				
43	6	2.06	SILTY SAND W/ LIMESTONE	21	835.2	835.2	121.1
44			HARD CLAY				
45			HARD CLAY				
46			HARD CLAY				
47	5		HARD CLAY	27			
48			HARD CLAY				
49			HARD CLAY				
50	7	2.38	HARD CLAY	62			

Table A-16. Summary of constrained moduli M of locations G and H

Depth (feet)	Layer Thickness (feet)	σ_o (TSF)	Soil Behavior	CPT (N) (#)	average N-value (#)	Constrained modulus (TSF) Various eq.s	OC sand	saturated sand
1			SILTY SAND TO SANDY SILT	10				
2			SAND	17				
3			SAND TO SILTY SAND	18				
4			SILTY SAND TO SANDY SILT	8				
5	5	0.20	SAND TO SILTY SAND	14	13.4	191.1	727.8	95.6
6			SAND	34				
7	2	0.46	SAND	35	34.5	333.1	1026.0	166.6
8			GRAVELLY SAND TO SAND	47				
9			GRAVELLY SAND TO SAND	47				
10	3	0.58	GRAVELLY SAND TO SAND	50	48.0	463.0	1216.8	212.0
11			SAND	33				
12			SAND TO SILTY SAND	32				
13			SAND	49				
14			SAND	42				
15			SANDY SILT TO CLAYEY SILT	25				
16			SILTY SAND TO SANDY SILT	37				
17			SILTY SAND TO SANDY SILT	42				
18			SAND	46				
19			SAND	54				
20			SAND	52				
21			SAND TO SILTY SAND	47				
22			SILTY SAND TO SANDY SILT	41				
23			SILTY SAND TO SANDY SILT	34				
24	14	0.85	SAND	57	42.2	385.1	1135.0	192.5
25	1	1.22	GRAVELLY SAND TO SAND	69	69.0	632.6	1513.6	282.7
26	1	1.27	SAND	47	47.0	417.3	1202.7	208.6
27			SILTY CLAY to CLAY	20				
28			CLAYEY SILT TO SILTY CLAY	22				
29			CLAYEY SILT TO SILTY CLAY	22				
30			CLAYEY SILT TO SILTY CLAY	20				
31			CLAYEY SILT TO SILTY CLAY	29				
32			CLAYEY SILT TO SILTY CLAY	33				
33			SILTY CLAY to CLAY	42				
34			VERY STIFF FINE GRAINED	59				
35	9	1.52	CLAYS	41				
36	1	1.77	SAND TO SILTY SAND	33	33.0	323.0	1004.8	161.5
37			GRAVELLY SAND TO SAND	58				
38			GRAVELLY SAND TO SAND	67				
39			GRAVELLY SAND TO SAND	63				
40			GRAVELLY SAND TO SAND	65				
41			GRAVELLY SAND TO SAND	65				
42			GRAVELLY SAND TO SAND	54				
43			GRAVELLY SAND TO SAND	54				
44			GRAVELLY SAND TO SAND	58				
45	9	2.02	GRAVELLY SAND TO SAND	45	58.8	550.1	1369.1	248.3
46			SAND	35				
47			SAND	24				
48			SAND	34				
49			SAND	44				
50	5	2.37	SAND	49	37.2	351.3	1064.1	175.7

CPT(N) represents a SPT(N) value estimated from CPT using a ratio of tip resistance (q_c) to SPT(N) suggested by Robertson and Campanella (1983).

APPENDIX B
SUPPLEMENTARY FIGURES

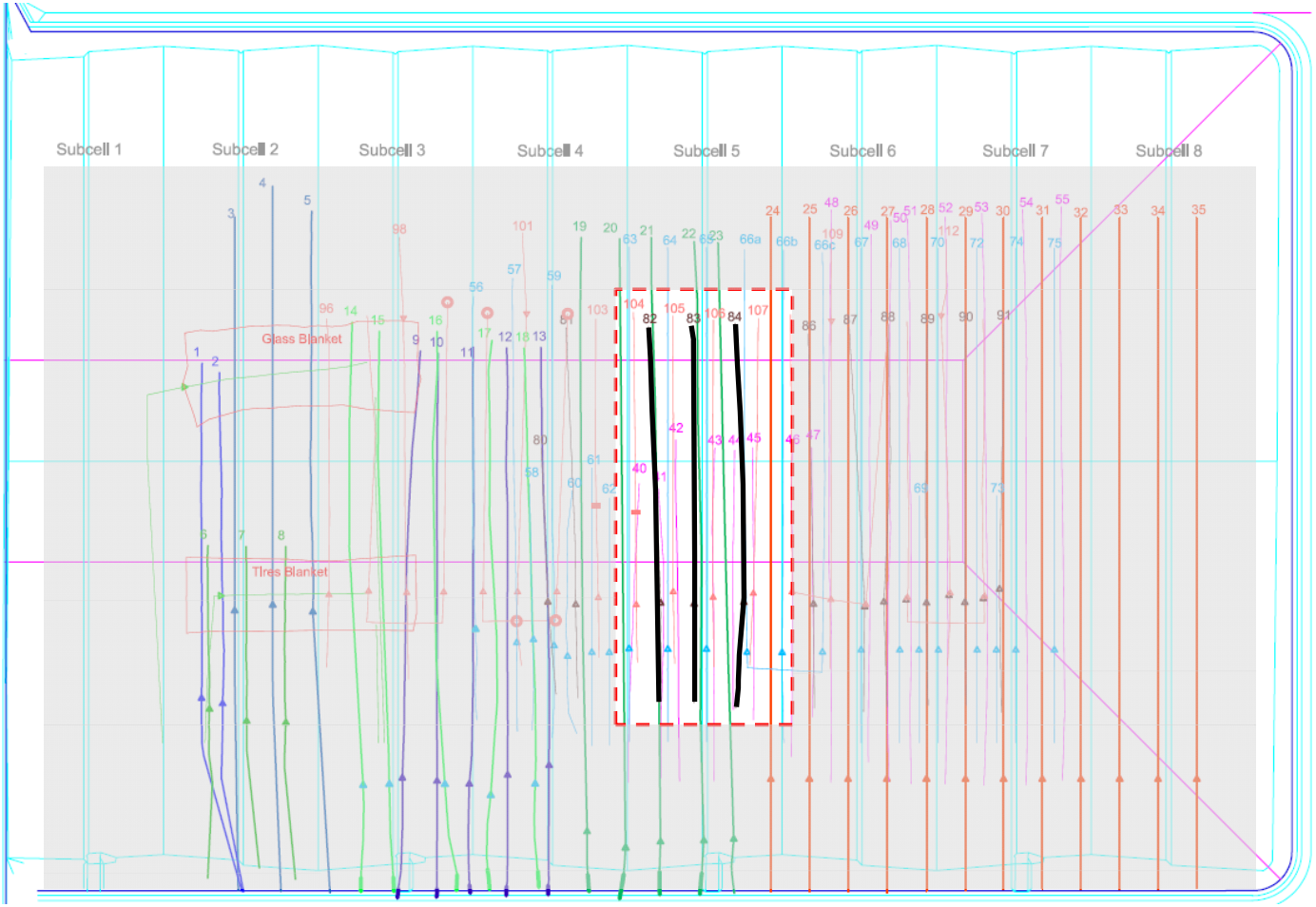

Figure B-1. Plan view of the study area of Chapter 2: the Phase II unit of the Polk County NCLF; Lines 82, 83, and 84 are the horizontal liquids addition lines with shredded-tire, excavated waste, and crushed-glass bedding media, respectively. The drawing was made by Jones Edmonds and Associates, Inc., FL.

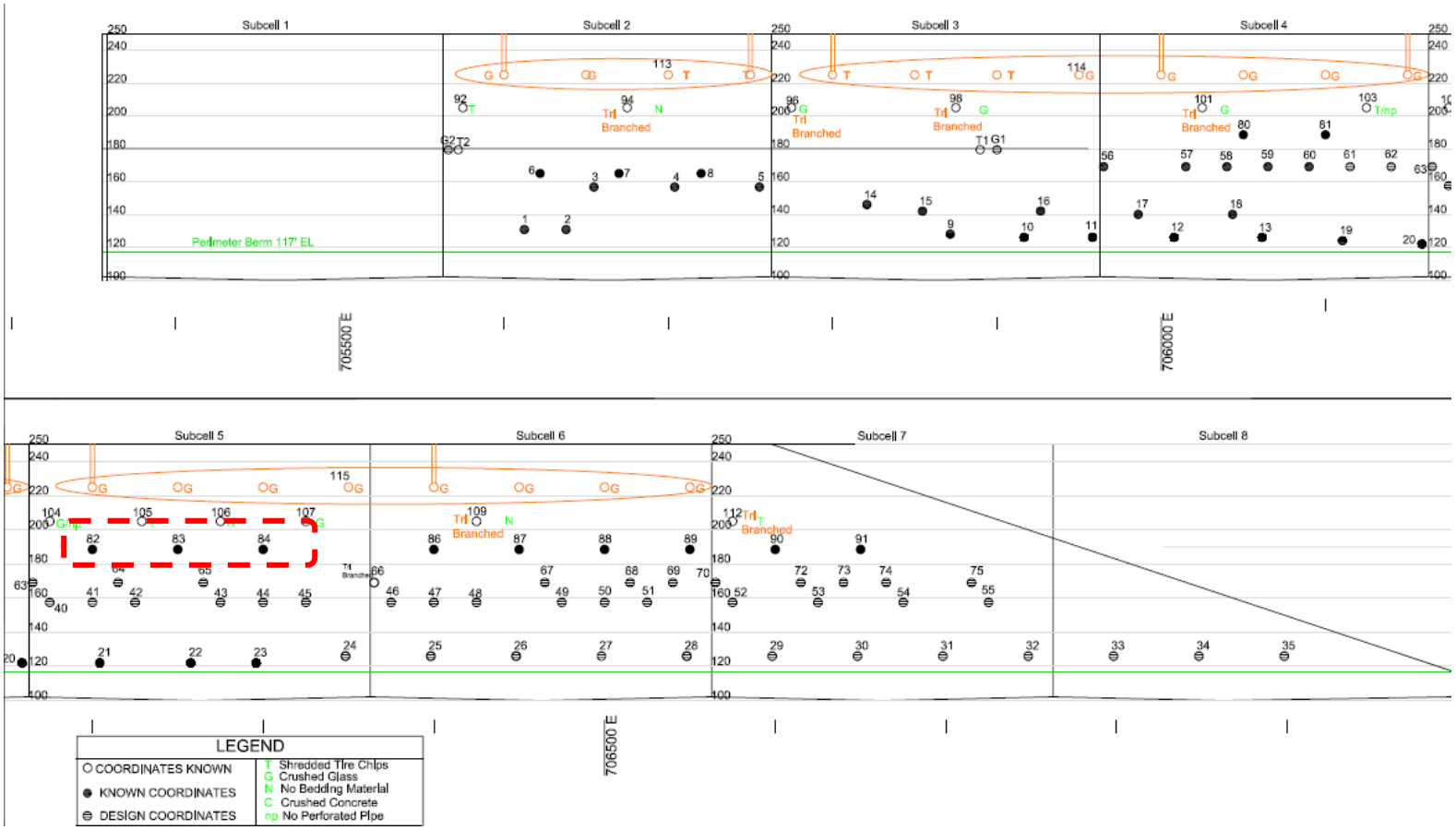

Figure B-2. Cross-sectional view of the study area of Chapter 2: the Phase II unit of the Polk County NCLF; Lines 82, 83, and 84 are the horizontal liquids addition lines with shredded-tire, excavated waste, and crushed-glass bedding media, respectively. The drawing was made by Jones Edmonds and Associates, Inc., FL.

Figure B-3. Data-logger and pore pressure data downloading

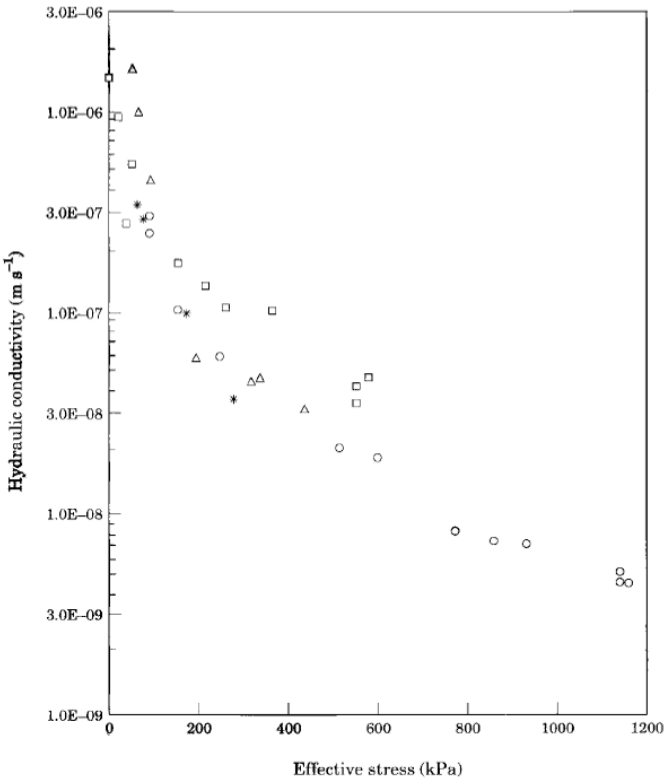

Figure B-4. Hydraulic conductivity versus effective stress. Samples from the Keele Valley Landfill, Material from 4" auger flights, *, sample 105B 105' depth; ○, sample 105 C 105' depth, □, sample 120 A 120' depth; Δ, sample 120B 120' depth (adapted from Bleiker et al., 1995)

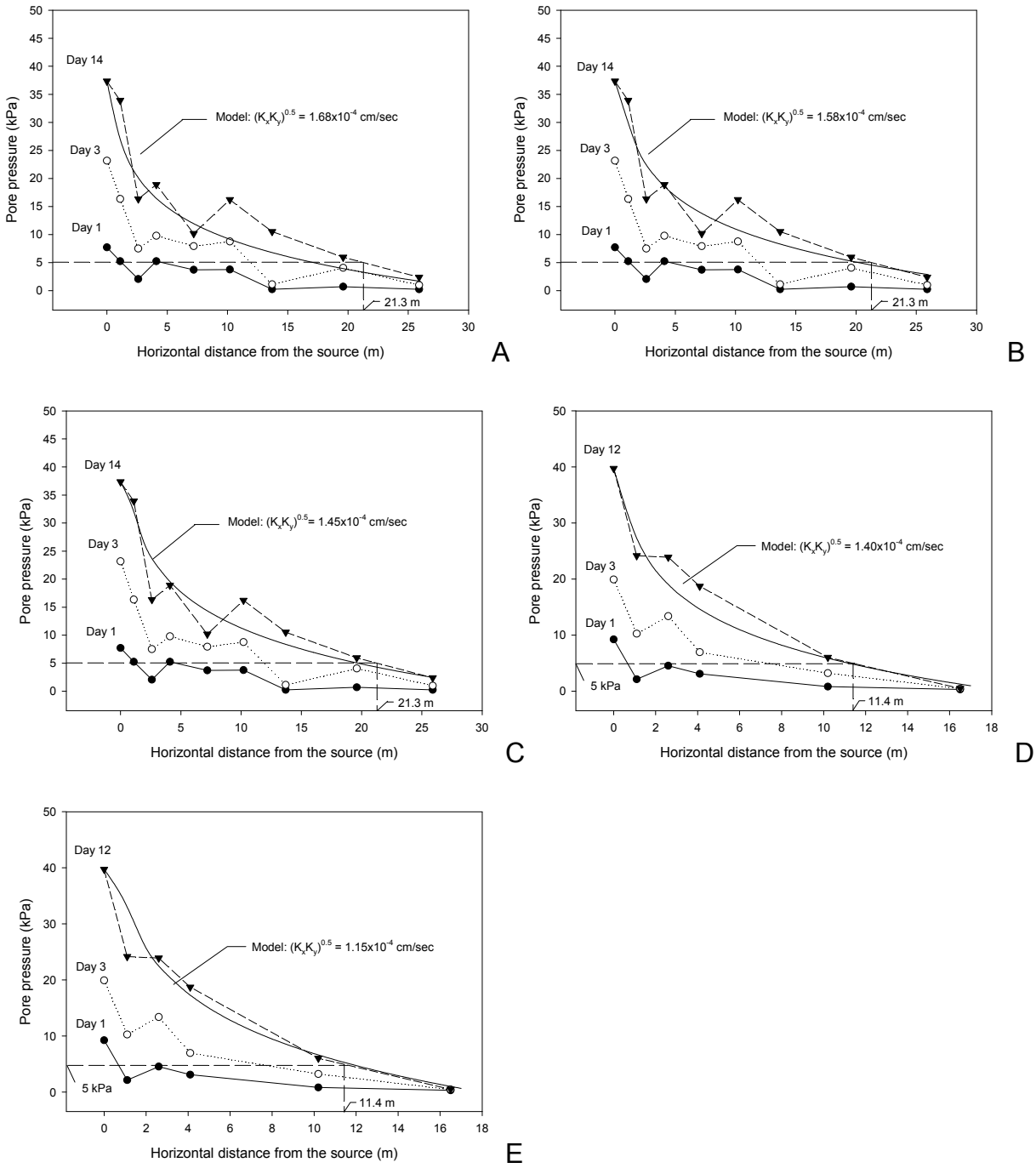

Figure B-5. Comparisons of pore pressure change as a function of a horizontal distance from the line source between the field data and theoretical estimates for Experiment 1: A) shredded tire trench (r_w = 0.3 m), B) shredded tire trench (r_w = 0.45 m), C) shredded tire trench (r_w = 0.6 m), D) crushed glass trench (r_w = 0.3 m), and E) crushed glass trench (r_w = 0.6 m).

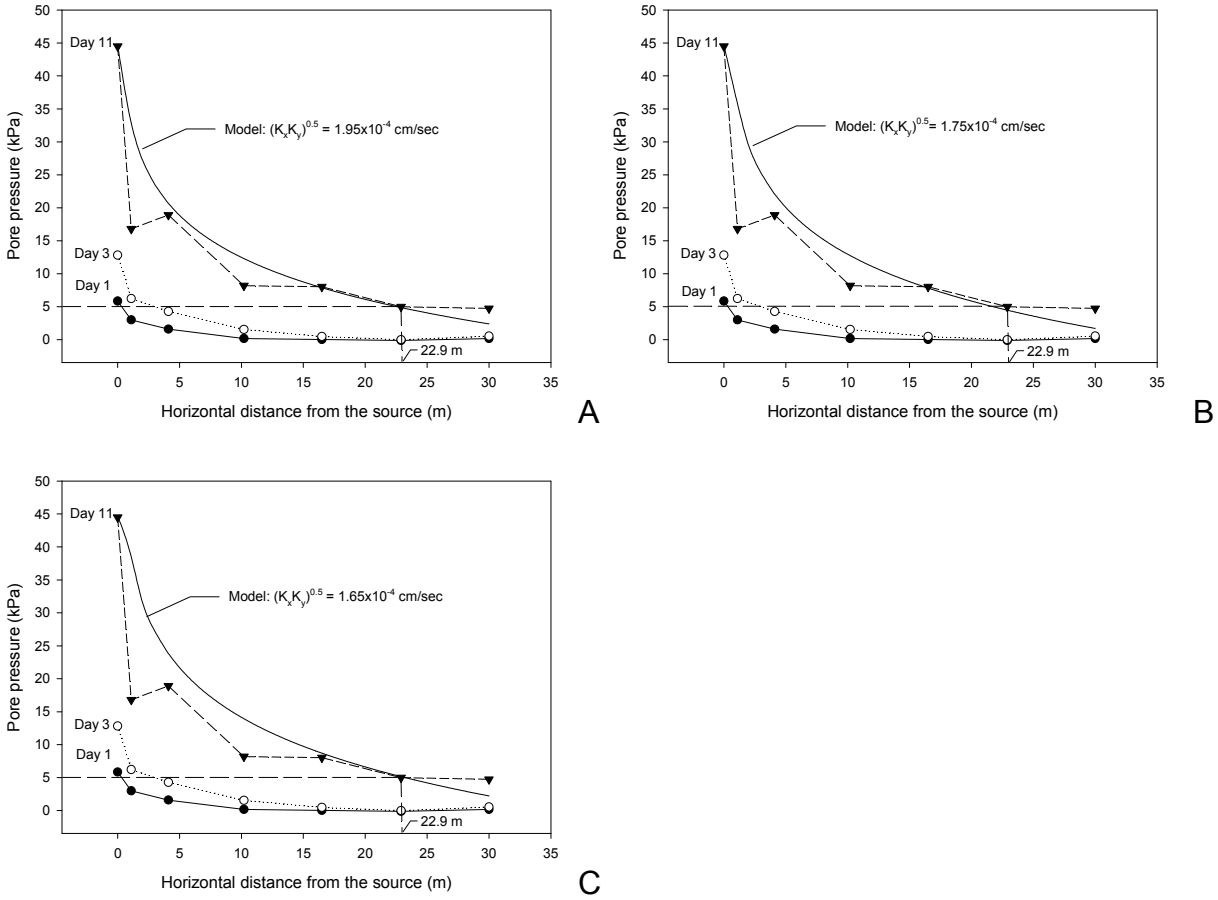

Figure B-6. Comparisons of pore pressure change as a function of a horizontal distance from the line source between the field data and theoretical estimates for Experiment 2: A) crushed glass trench (r_w = 0.3 m), B) crushed glass trench (r_w = 0.45 m), and C) crushed glass trench (r_w = 0.6 m).

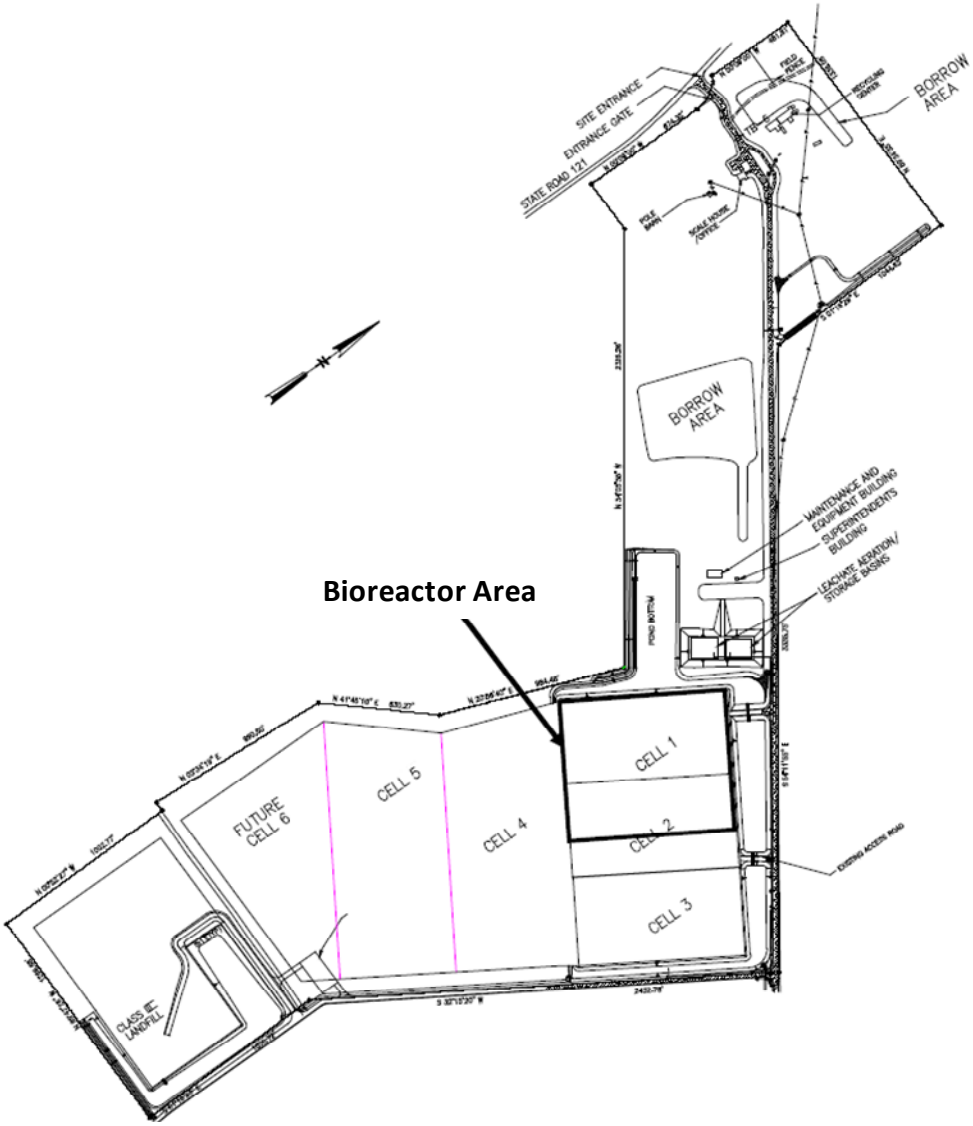

Figure B-7. Plan view of the study landfill of Chapter 3: the New River Regional (adapted from as-built drawings provided by Jones Edmunds and Associates at Gainesville, Florida)

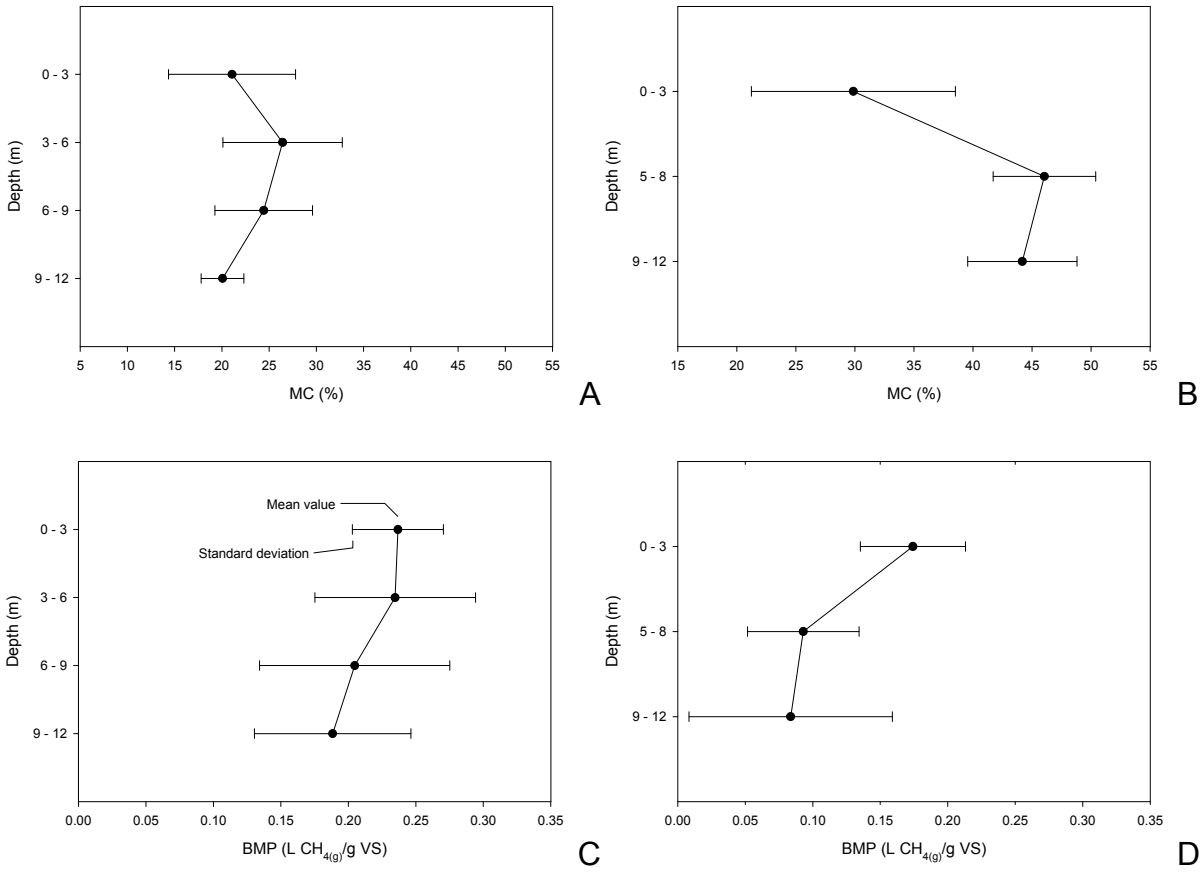

Figure B-8. Changes in waste properties with depth: A) moisture content (MC), 2002, B) MC, 2007, C) biochemical methane potential (BMP), 2002, and D) BMP, 2007.

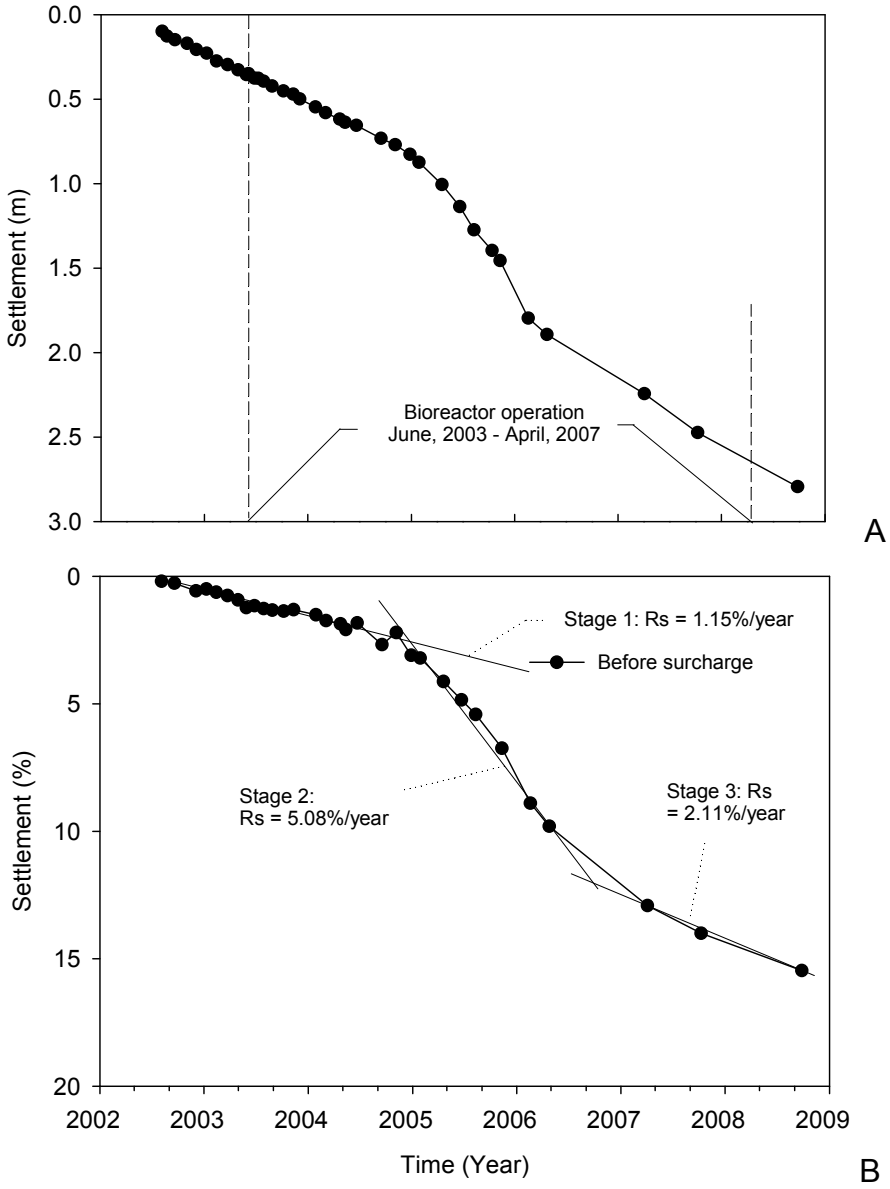

Figure B-9. Historic settlement records of the study landfill site of Chapter 3: A) settlement (m) – time and B) settlement (%) – time; the settlement (m) data was adapted from Kadambala (2009) and re-plotted.

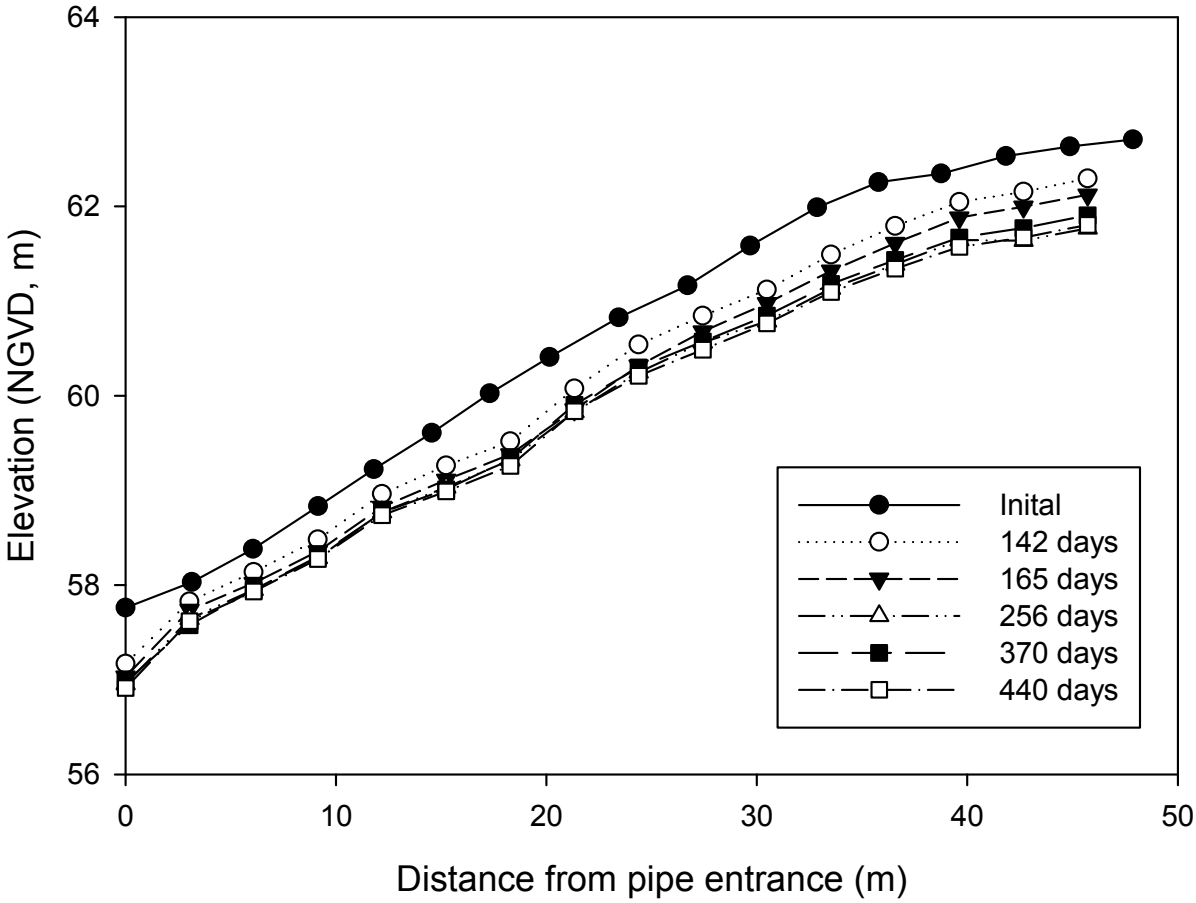

Figure B-10. Elevation change over time at each settlement measurement location in settlement profiling pipe 2; NGVD represents U.S. National Geodetic Vertical Datum

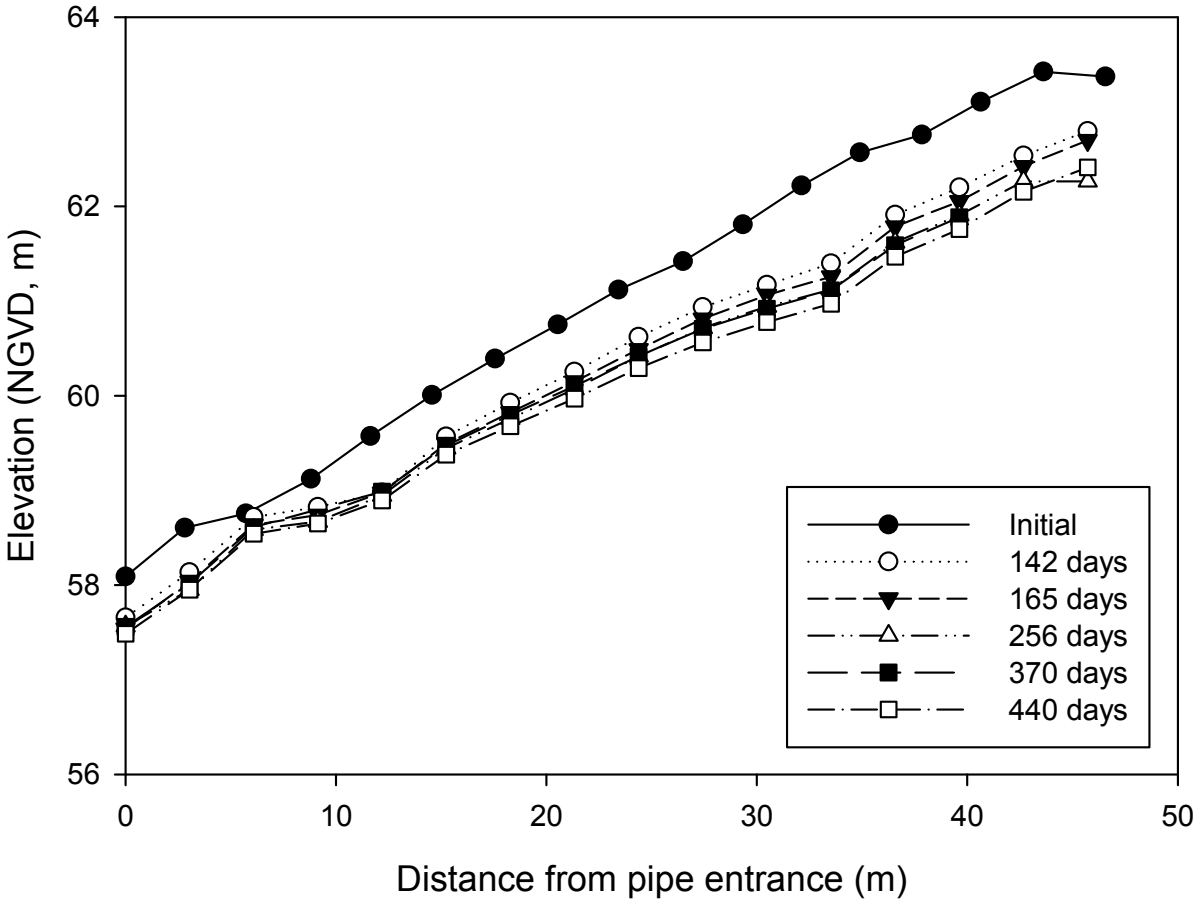

Figure B-11. Elevation change over time at each settlement measurement location in settlement profiling pipe 3; NGVD represents U.S. National Geodetic Vertical Datum

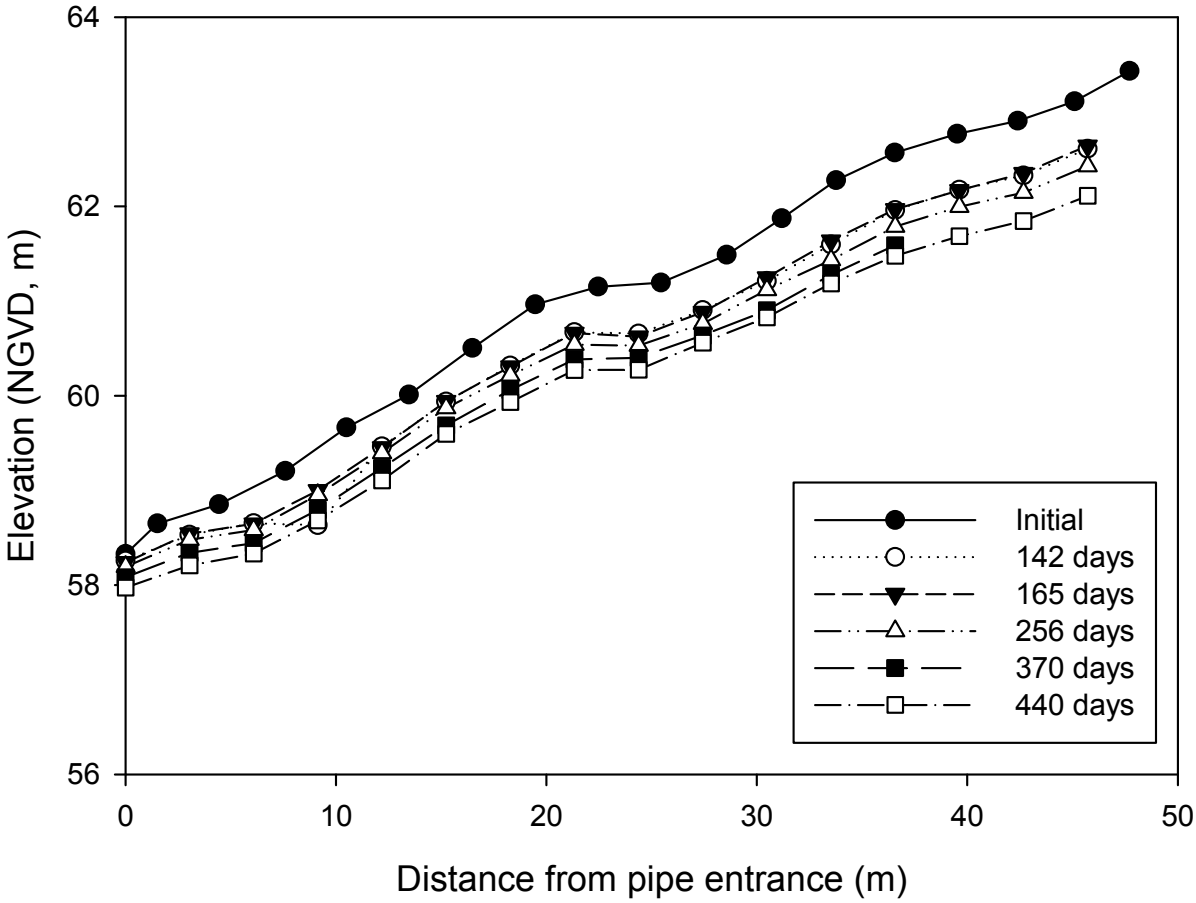

Figure B-12. Elevation change over time at each settlement measurement location in settlement profiling pipe 4; NGVD represents U.S. National Geodetic Vertical Datum

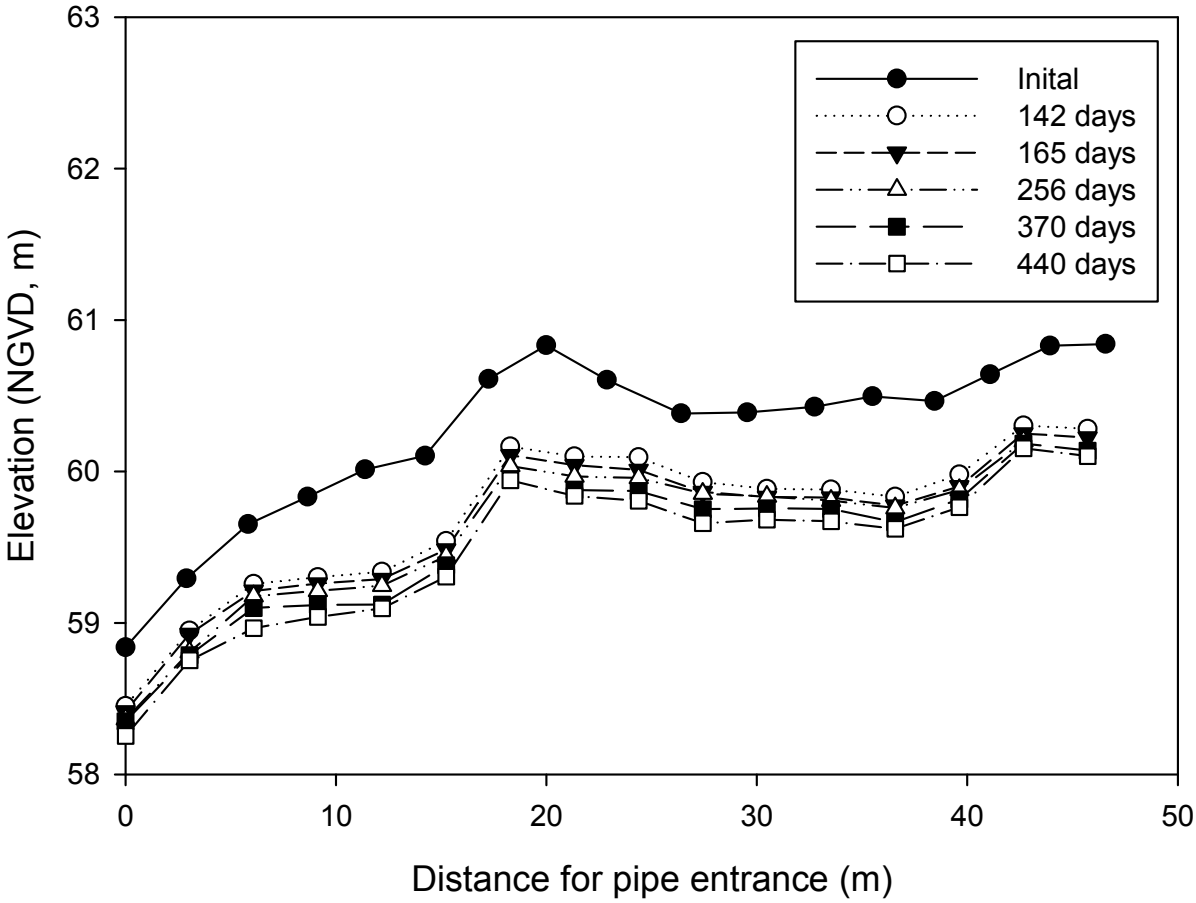

Figure B-13. Elevation change over time at each settlement measurement location in settlement profiling pipe 5; NGVD represents U.S. National Geodetic Vertical Datum

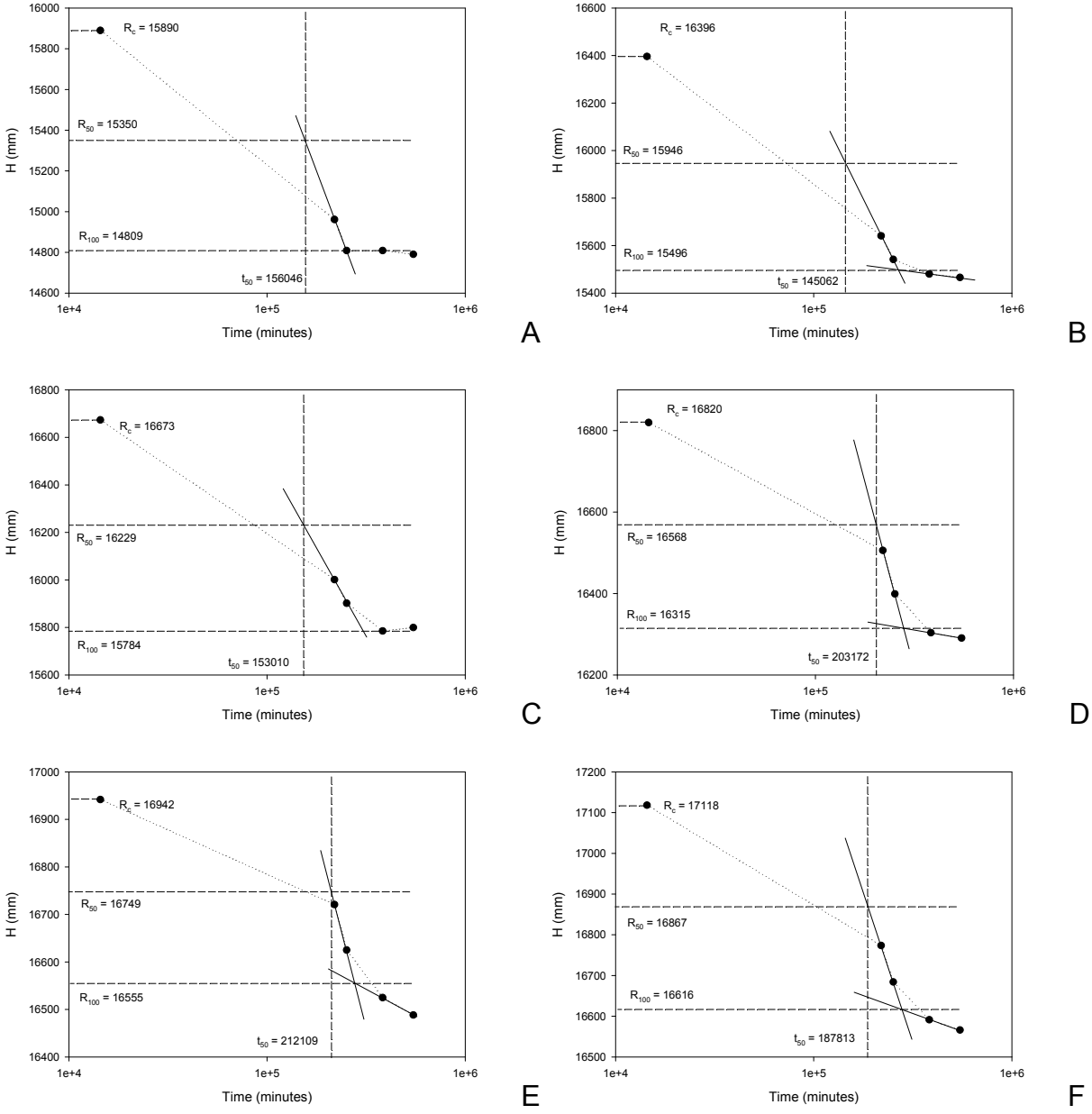

Figure B-14. Logarithm of time fitting model to estimate t_{50} (Pipe 1): data used was collected at A)10 m, B) 13 m, C) 16 m, D) 19 m, E) 22 m, and F) 25 m inside from the entry of Pipe 1.

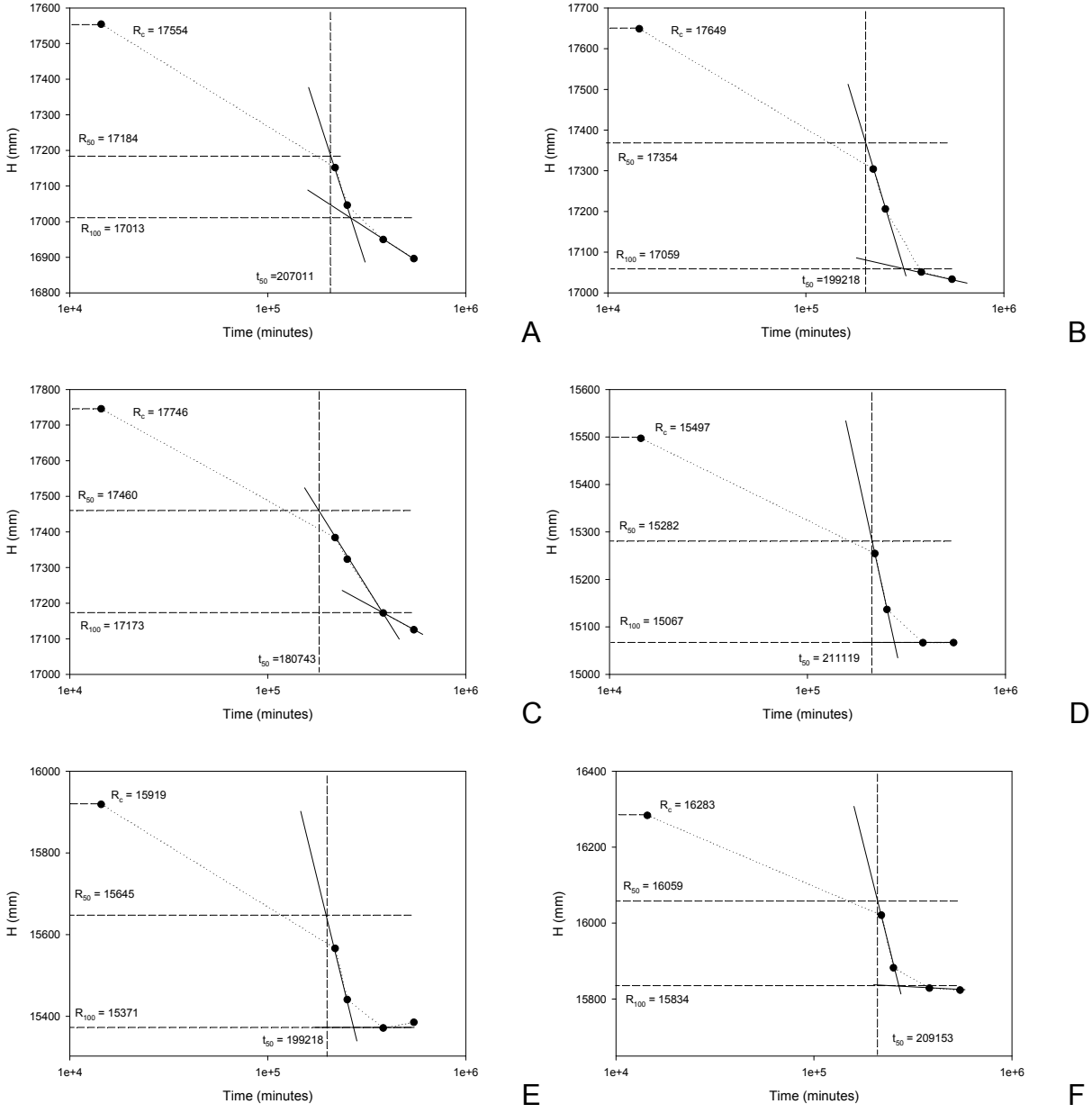

Figure B-15. Logarithm of time fitting model to estimate t_{50} (Pipes 1 and 2): data used was collected at A) 31 m, B) 34 m, and C) 37 m inside from the entry of Pipe 1 and D) 6 m, E) 9 m, and F) 12 m inside from the entry of Pipe 2.

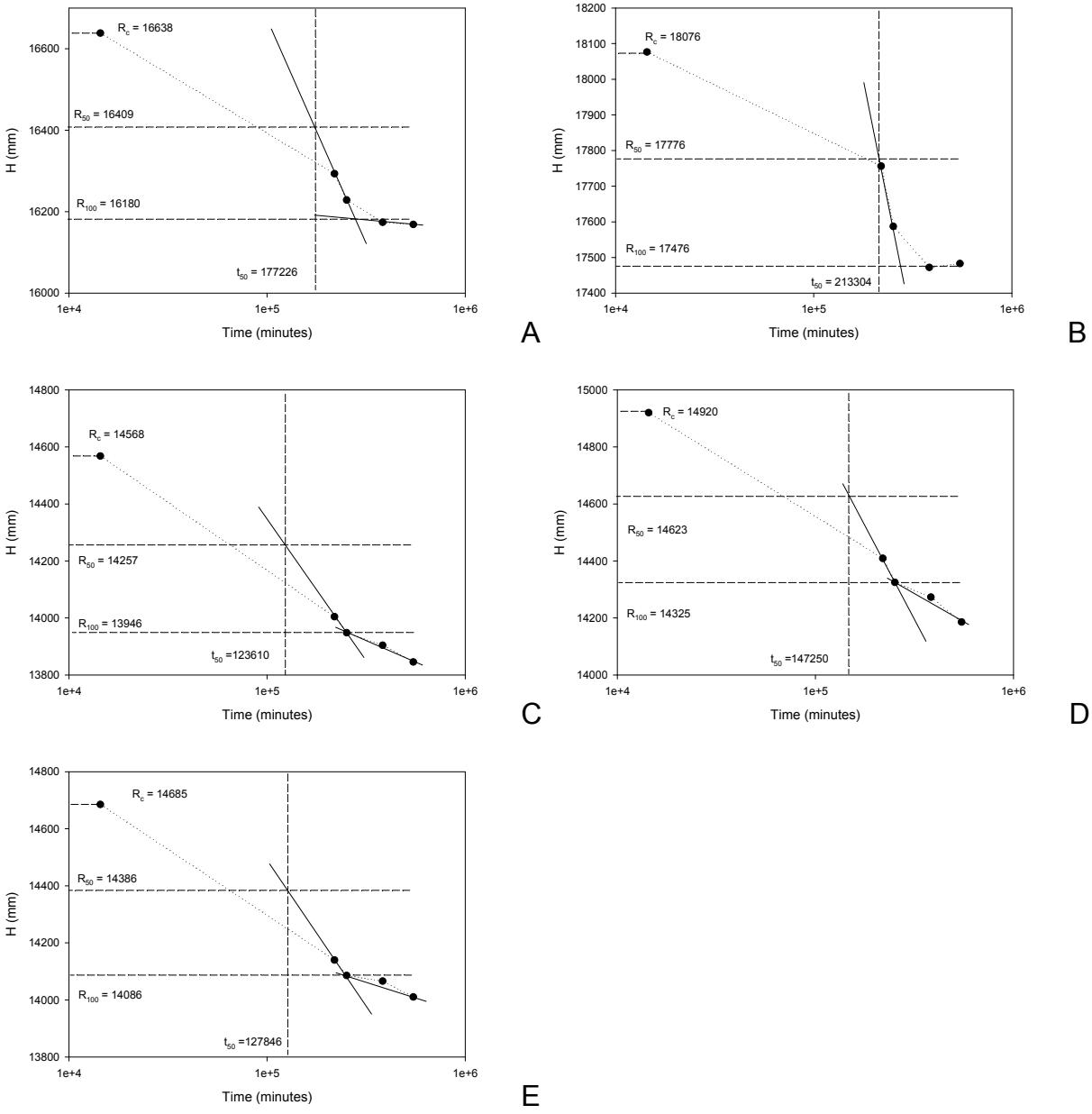

Figure B-16. Logarithm of time fitting model to estimate t_{50} (Pipes 2 and 5): data used was collected at A) 15 m and B) 27 m inside from the entry of Pipe 2 and C) 14 m, D) 23 m, and E) 35 m inside from the entry of Pipe 5

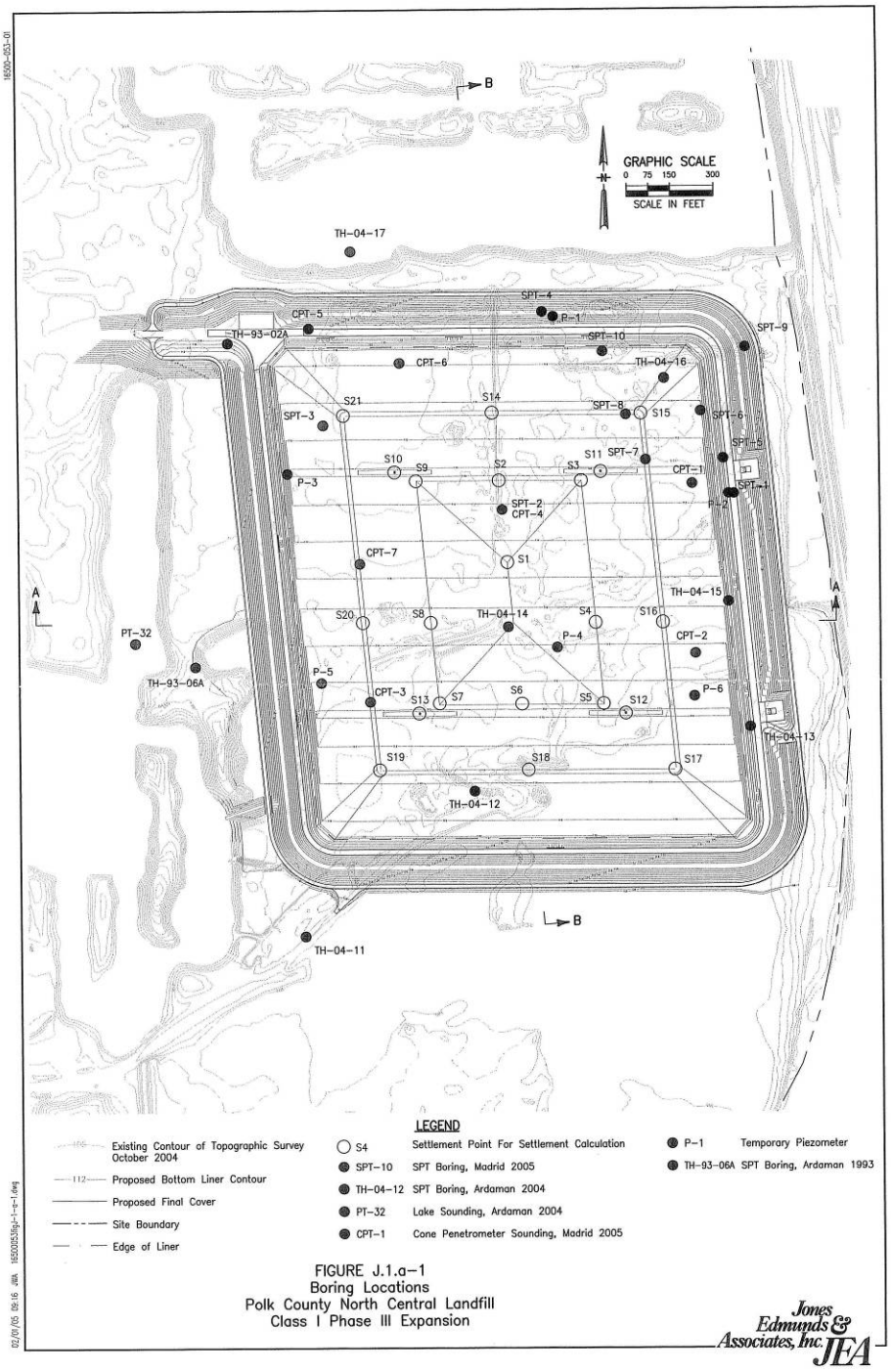

Figure B-17. Plan view of the identification of SPTs and CPTs locations at the study landfill of Chapter 4: the Phase III unit area of the Polk County NCLF (adapted from JEA, Inc.)

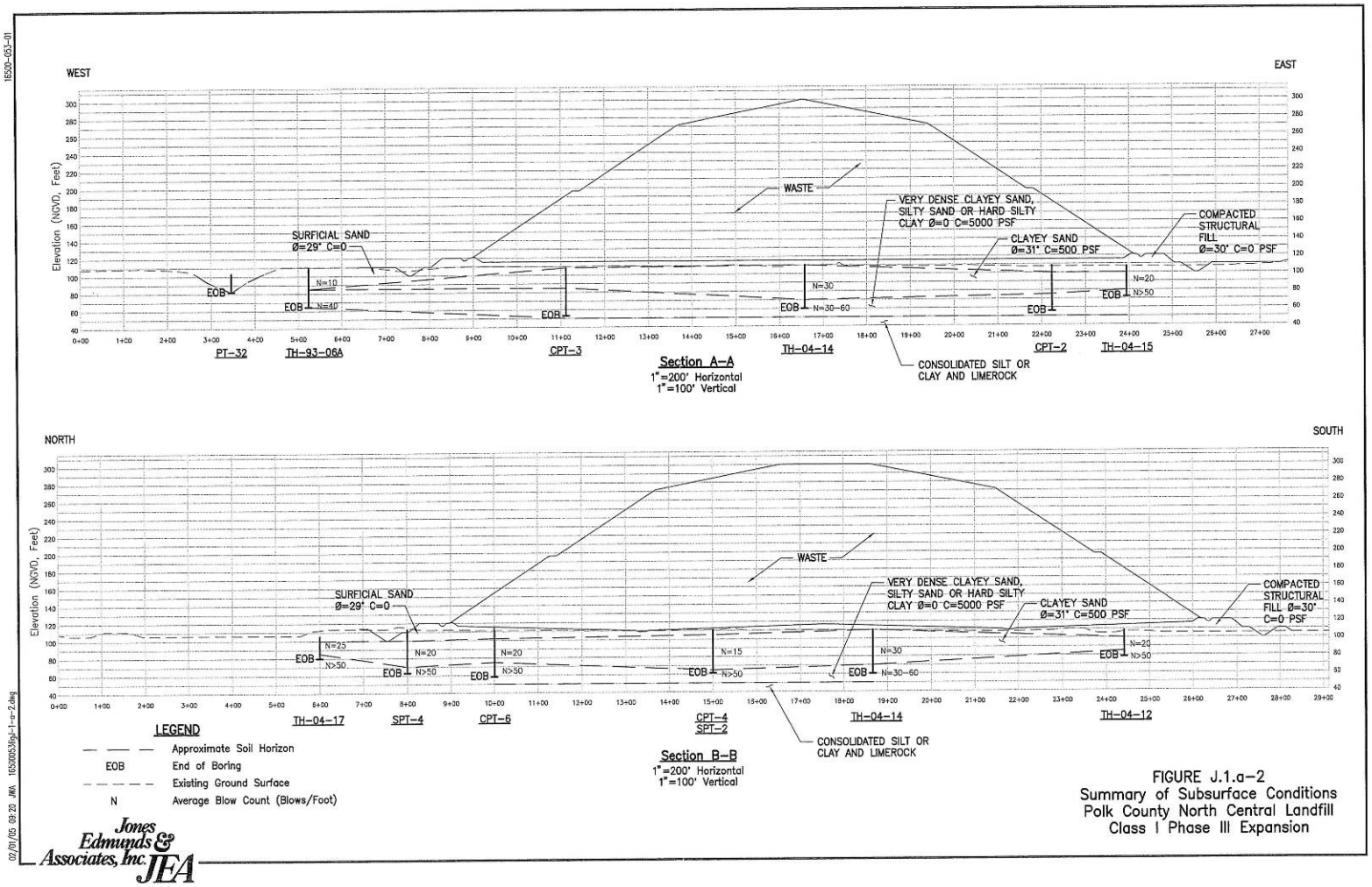

Figure B-18. Cross-sectional view of the identification of SPTs and CPTs locations at the study landfill of Chapter 4: the Phase III unit area of the Polk County NCLF (adapted from JEA, Inc.)

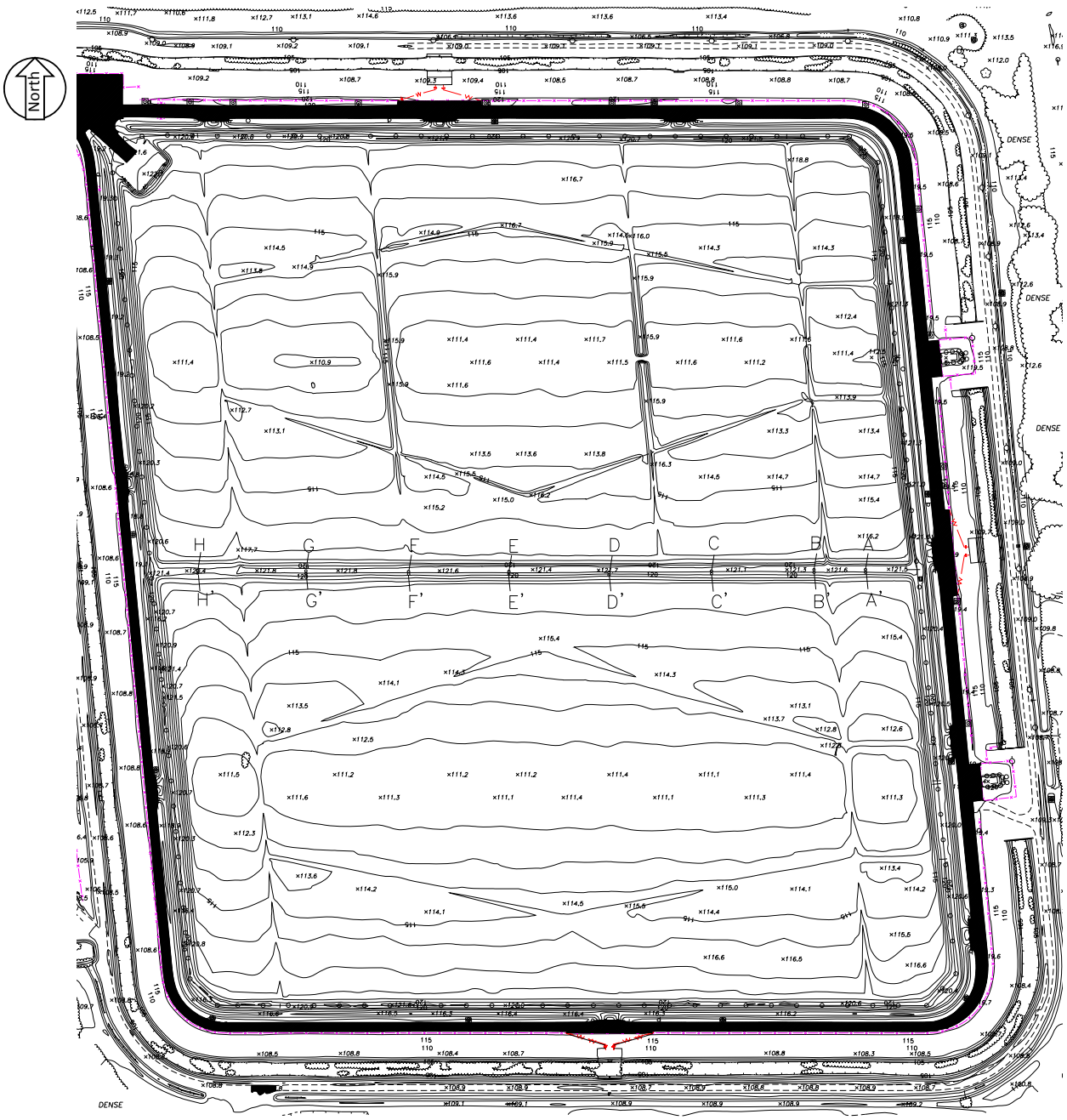

Figure B-19. The topographic surveying of the study landfill of Chapter 4(October 09, 2007): the Phase III unit of the Polk County NCLF

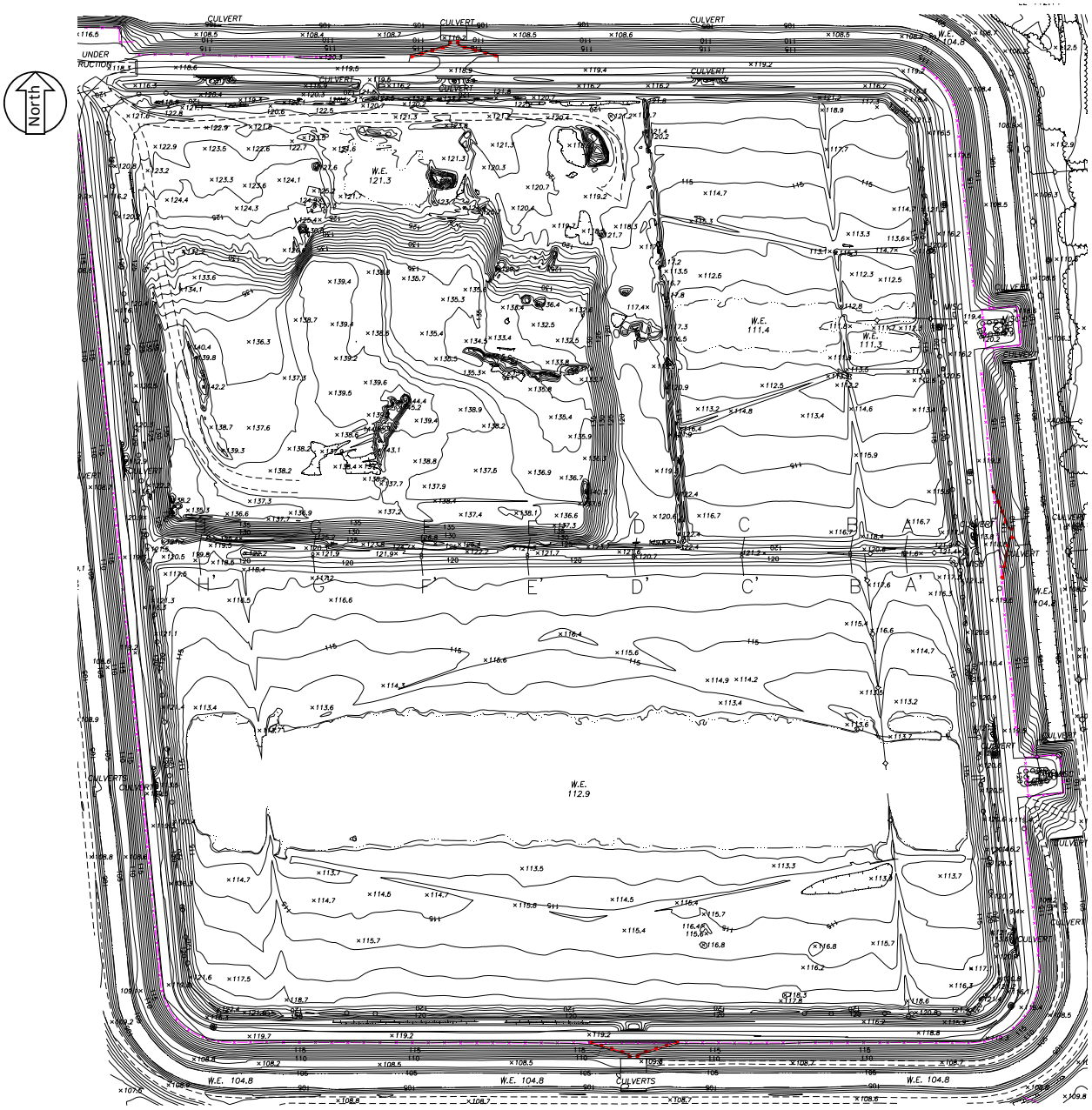

Figure B-20. The topographic surveying of the study landfill of Chapter 4 (April 11, 2008): the Phase III unit of the Polk County NCLF

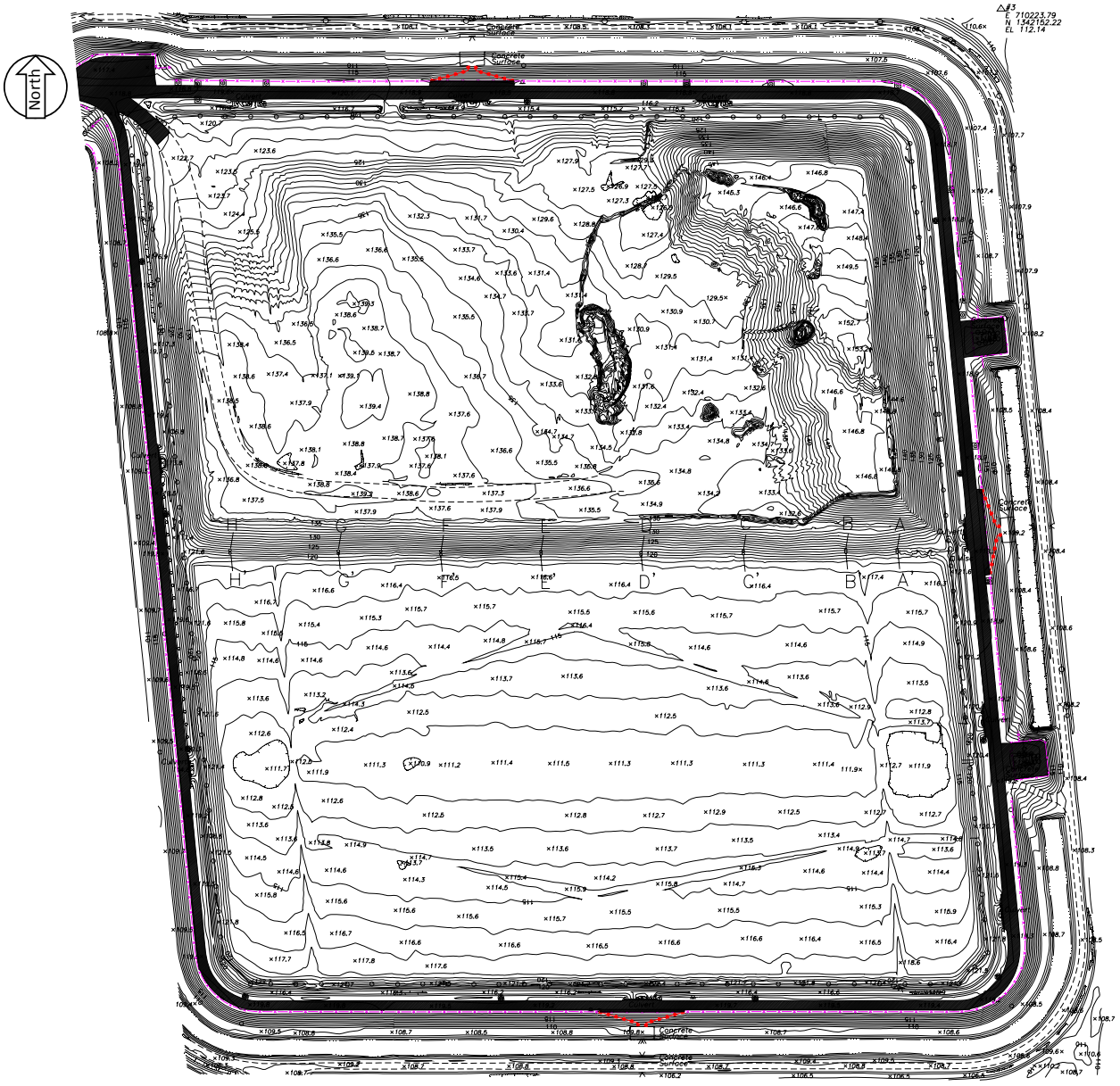

Figure B-21. The topographic surveying of the study landfill of Chapter 4 (September 25, 2008): the Phase III unit of the Polk County NCLF

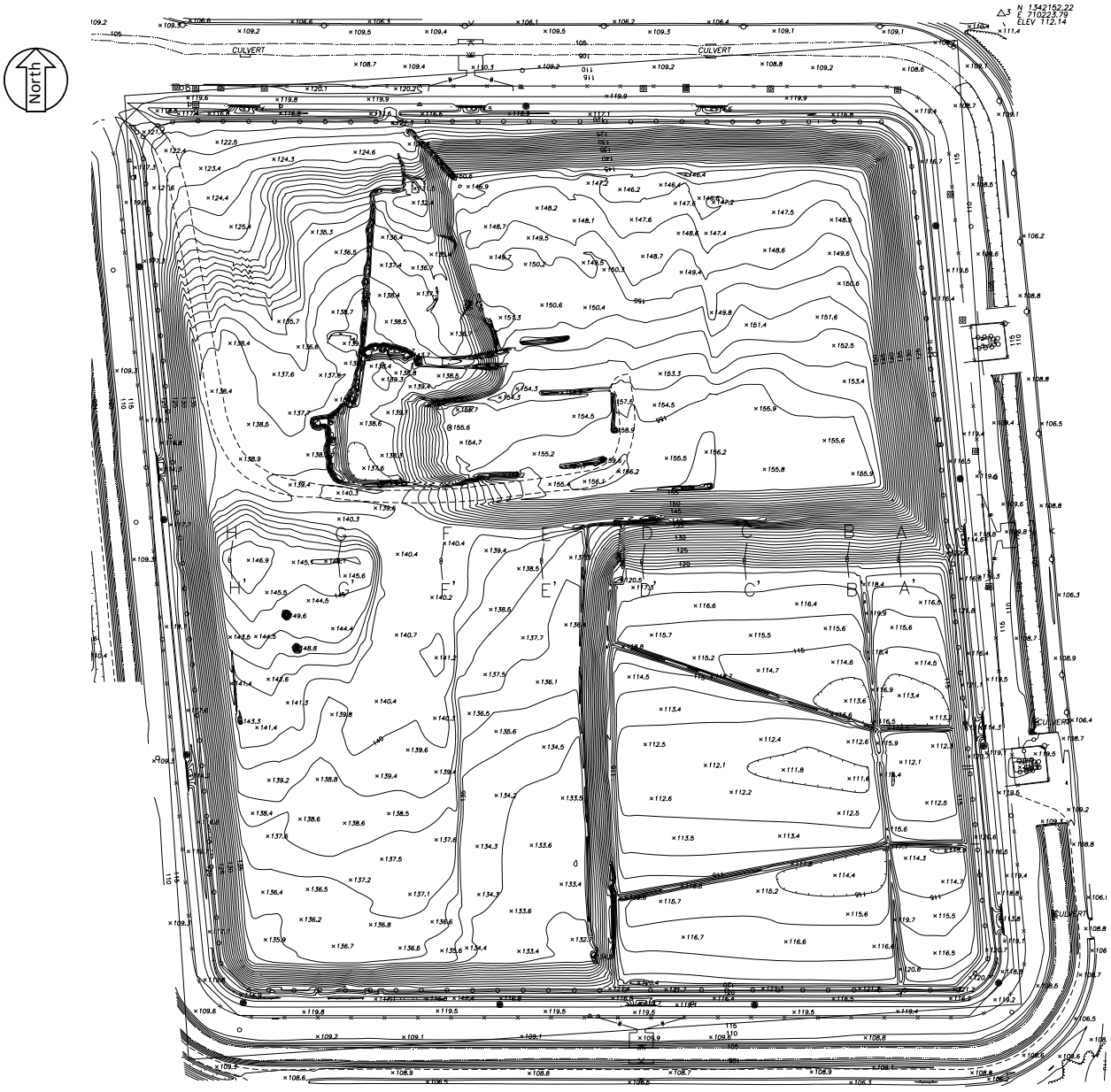

Figure B-22. The topographic surveying of the study landfill of Chapter 4 (September 29, 2009): the Phase III unit of the Polk County NCLF

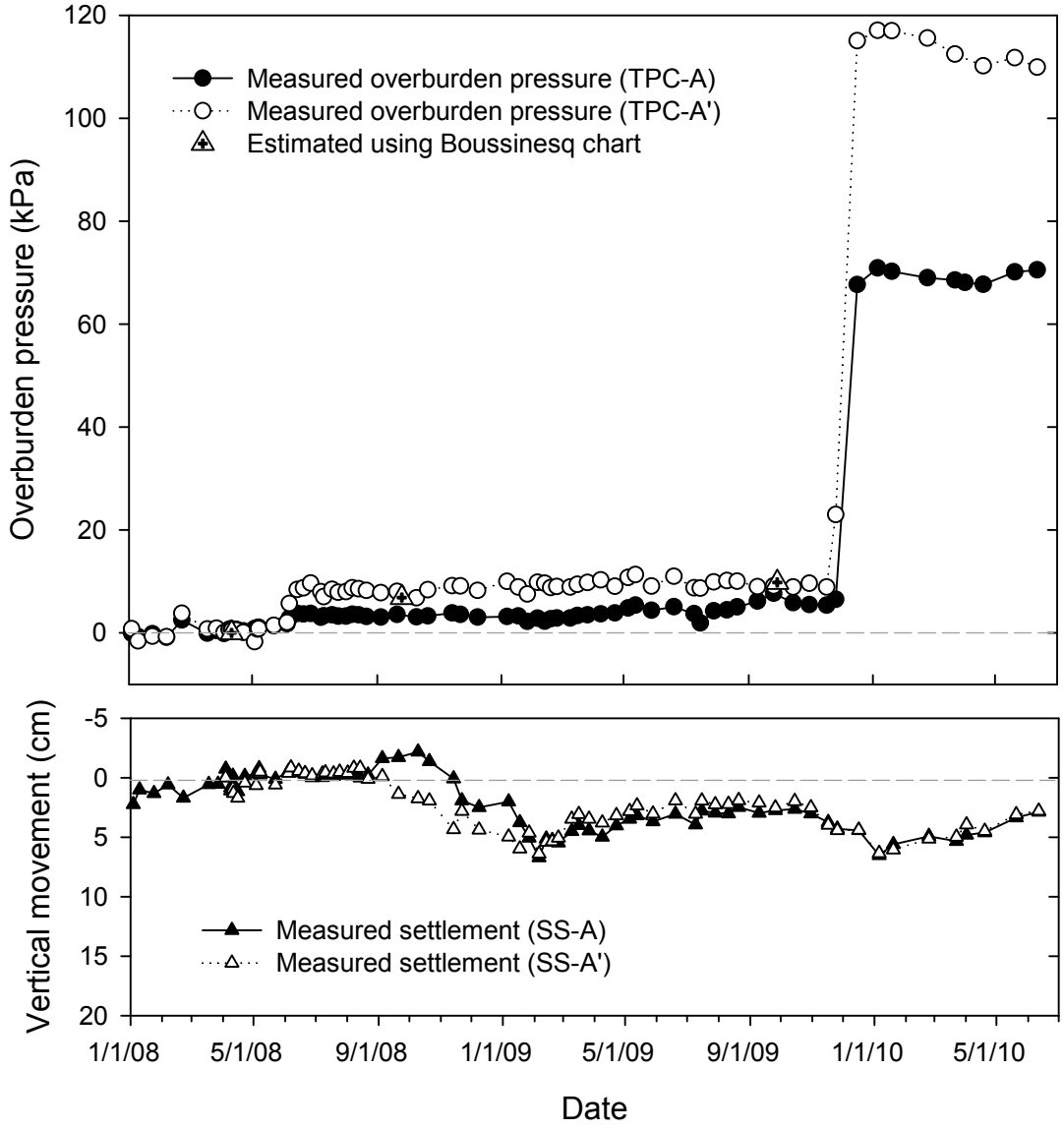

Figure B-23. Variation of overburden pressure and settlement over time due to waste placement at location A: location A in Figure 4-1.

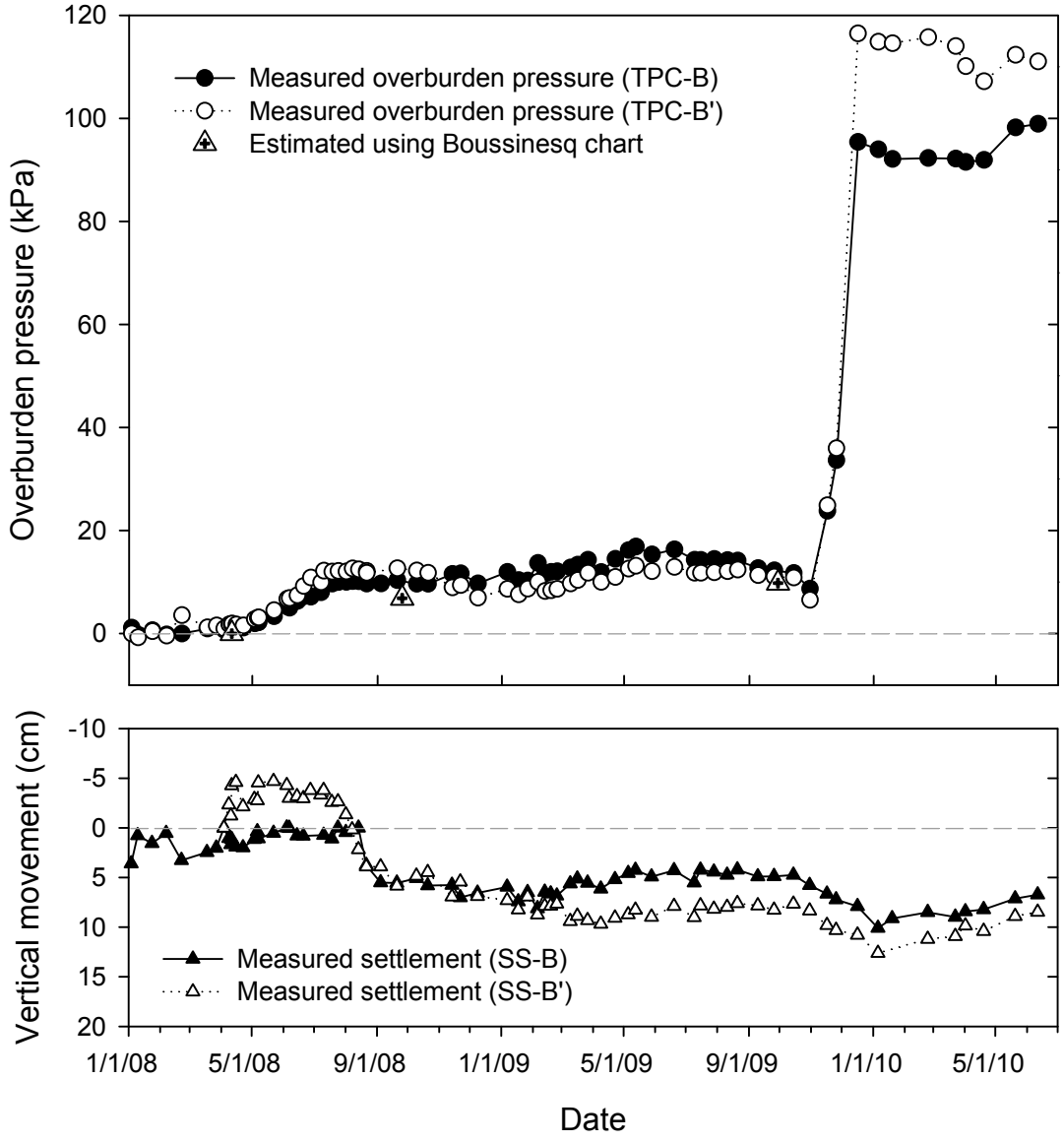

Figure B-24. Variation of overburden pressure and settlement over time due to waste placement at location B: location B in Figure 4-1.

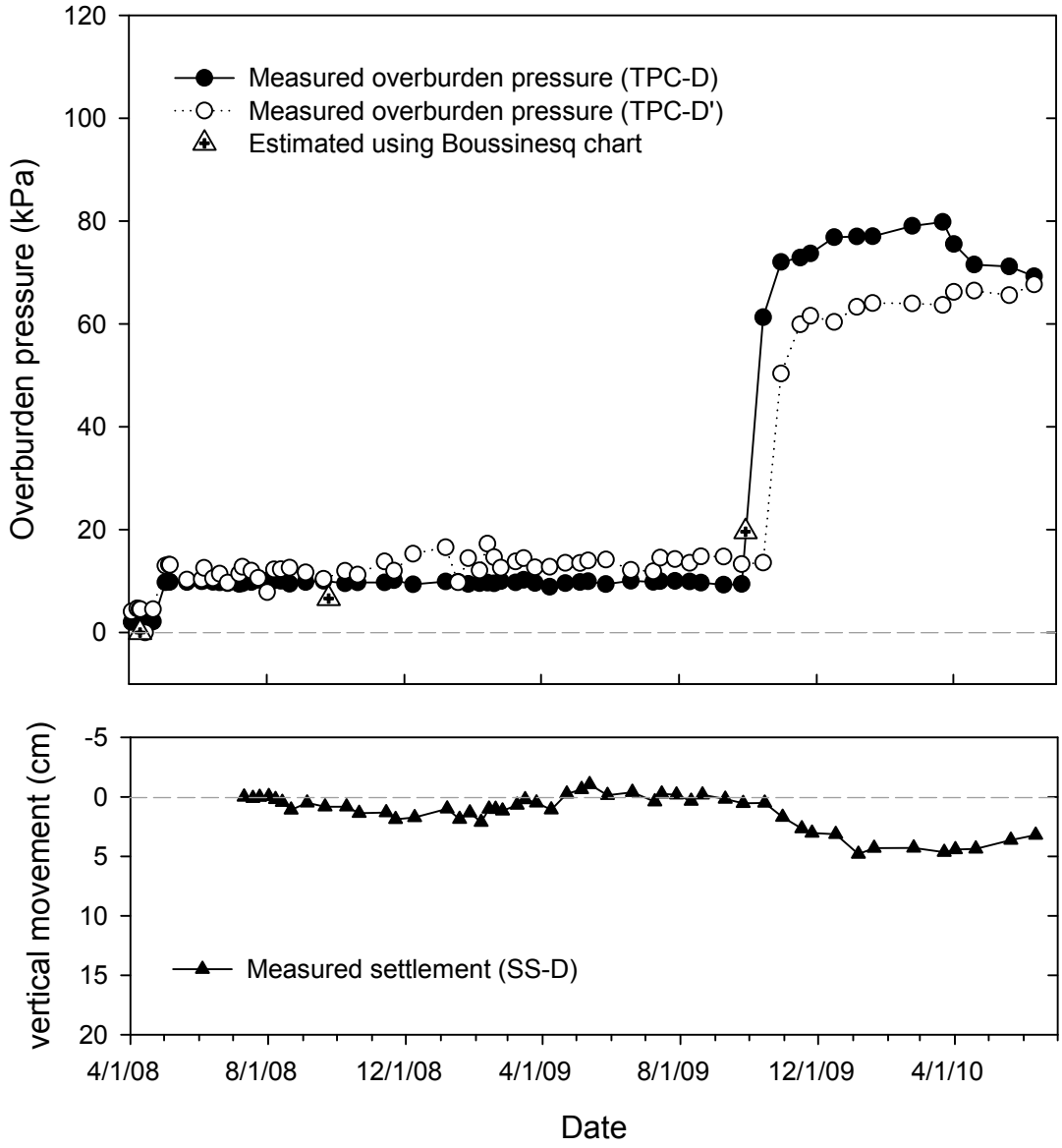

Figure B-25. Variation of overburden pressure and settlement over time due to waste placement at location D; duplicate measurements of settlement by D' was malfunctioned and thus the data was not included: location D in Figure 4-1.

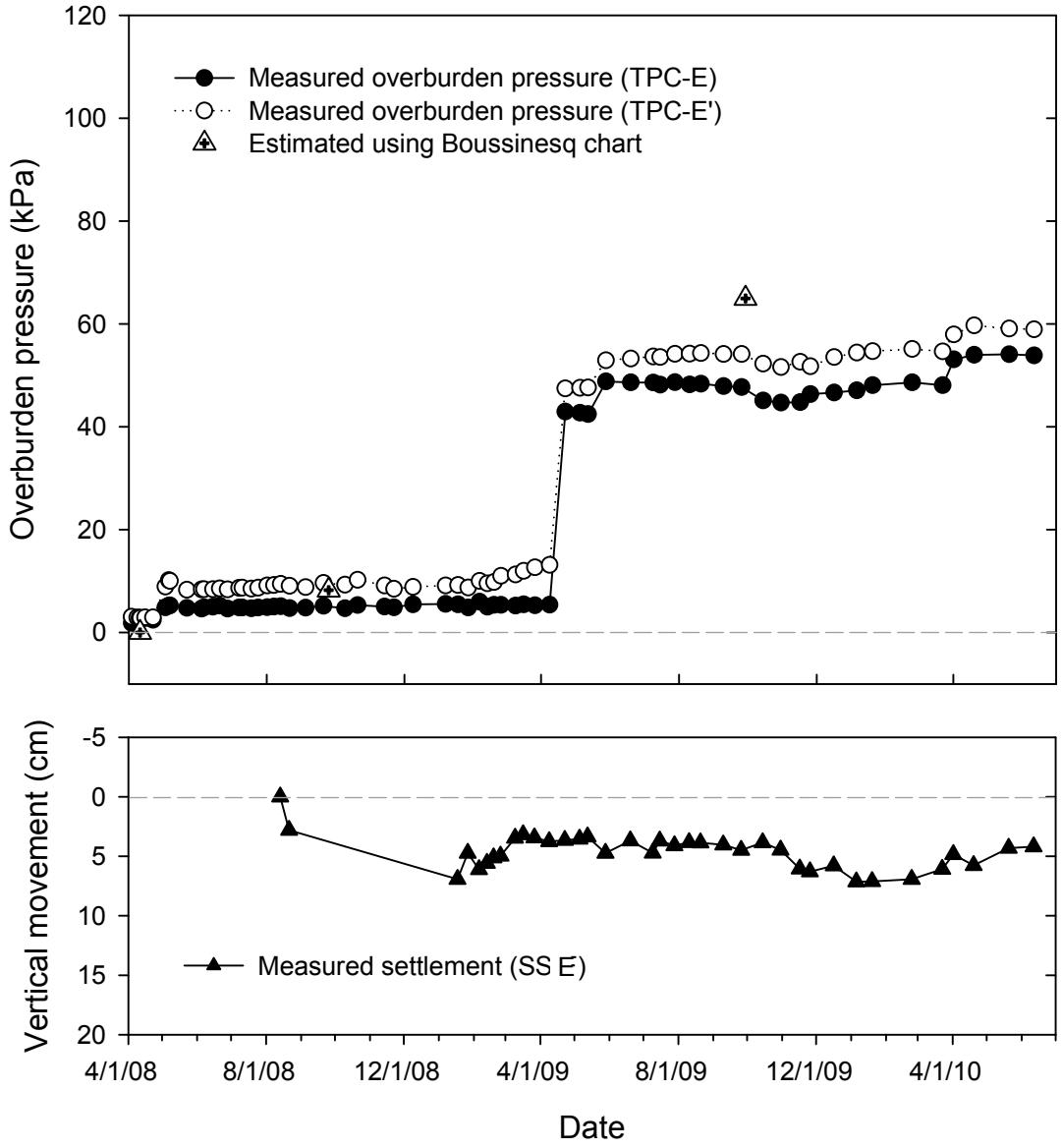

Figure B-26. Variation of overburden pressure and settlement over time due to waste placement at location E; duplicate measurements of settlement by E' was malfunctioned and thus the data was not included: location E in Figure 4-1.

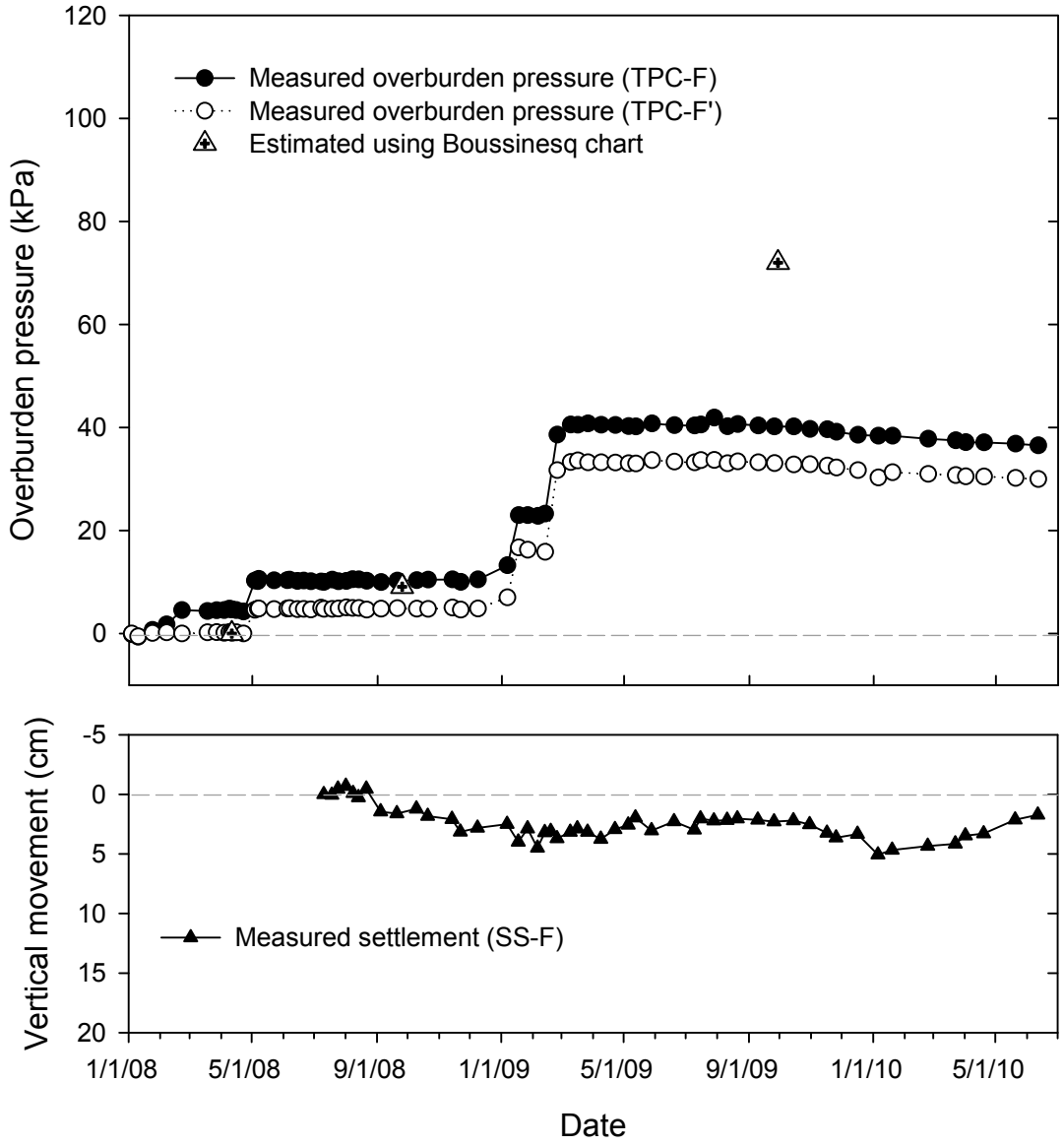

Figure B-27. Variation of overburden pressure and settlement over time due to waste placement at location F; duplicate measurements of settlement by F' was malfunctioned and thus the data was not included: location F in Figure 4-1.

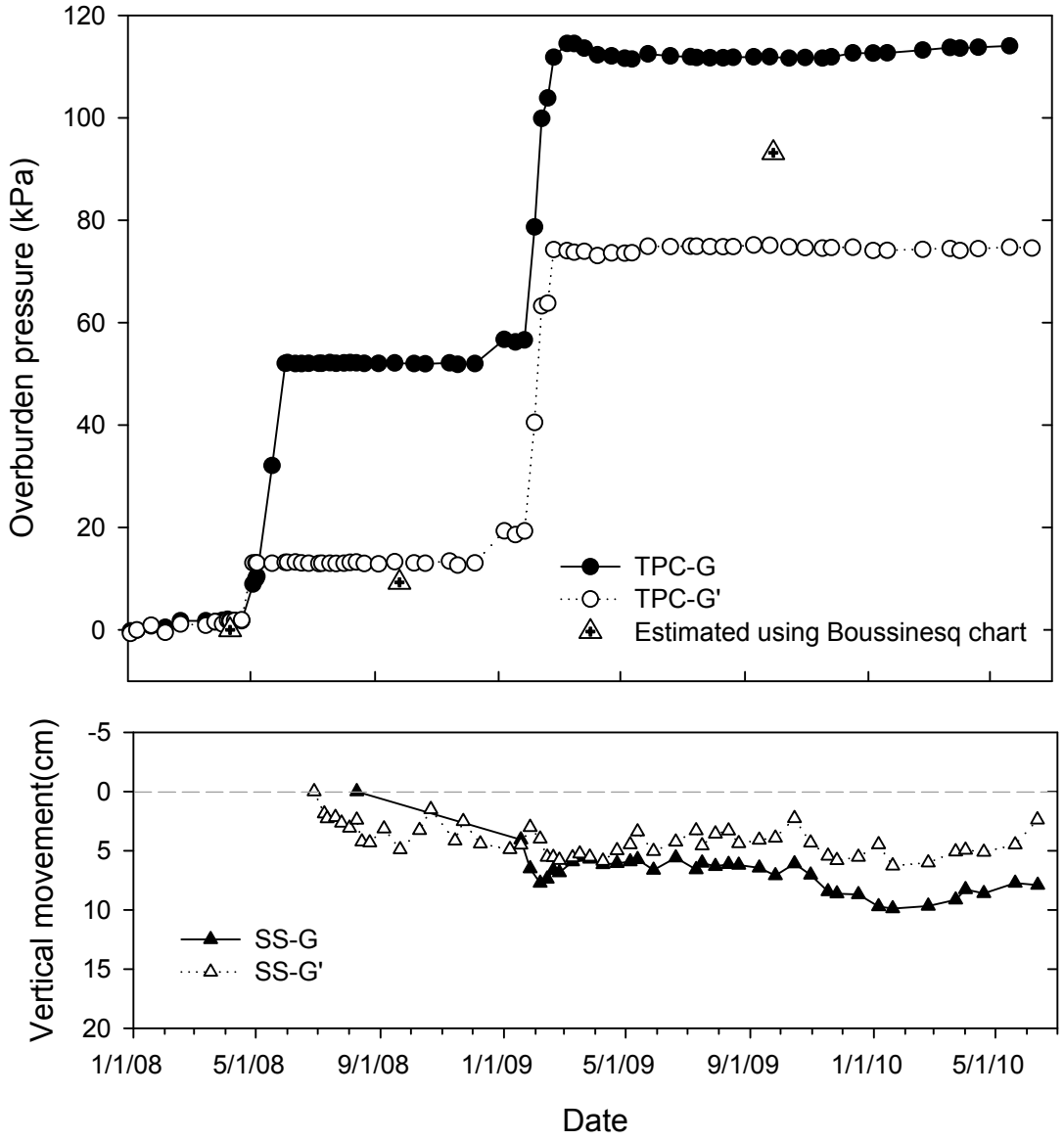

Figure B-28. Variation of overburden pressure and settlement over time due to waste placement at location G: location G in Figure 4-1.

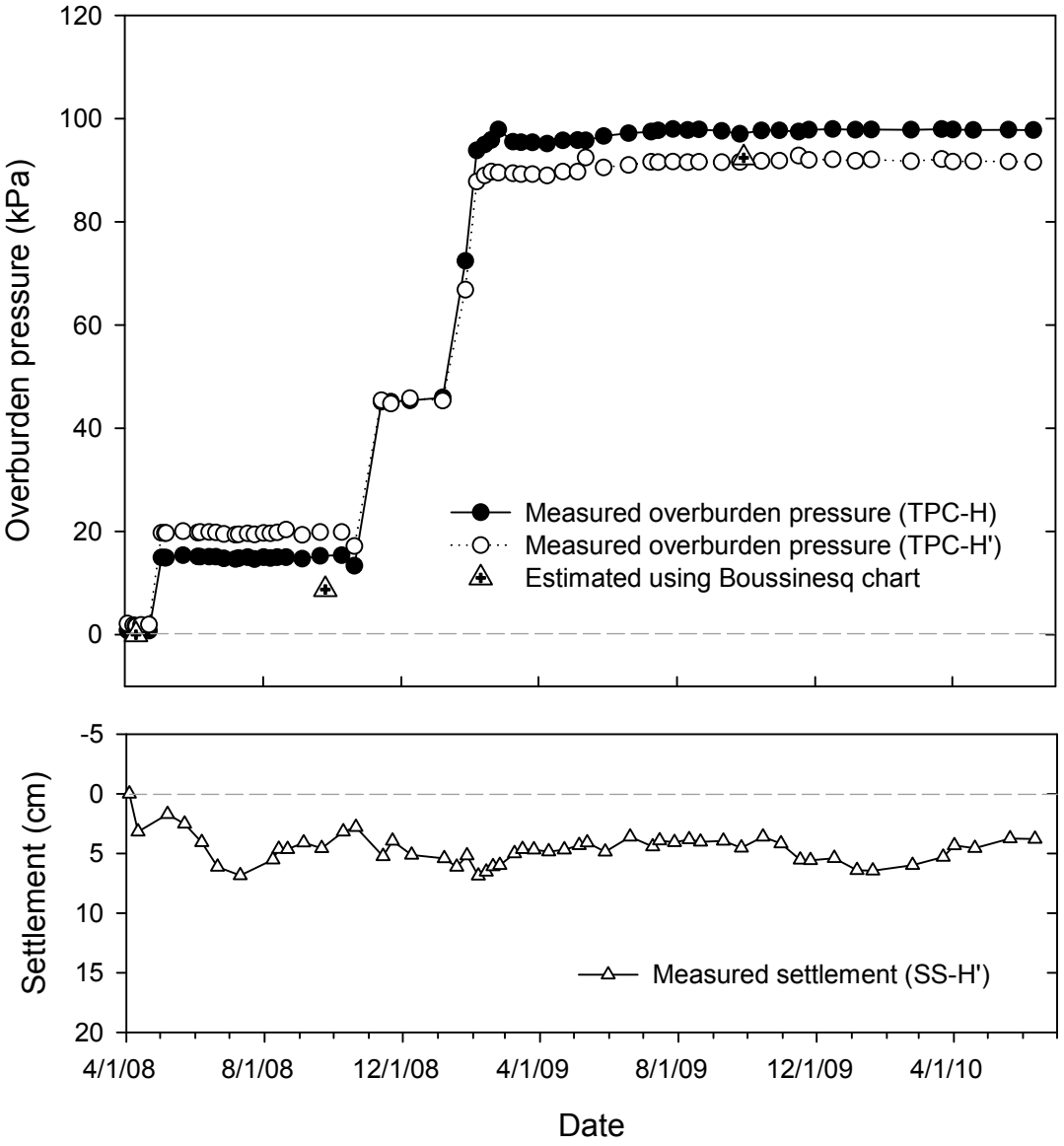

Figure B-29. Variation of overburden pressure and settlement over time due to waste placement at location H; duplicate measurements of settlement by H was malfunctioned and thus the data was not included: location H in Figure 4-1.

Figure B-30. Large-scale direct shear test device

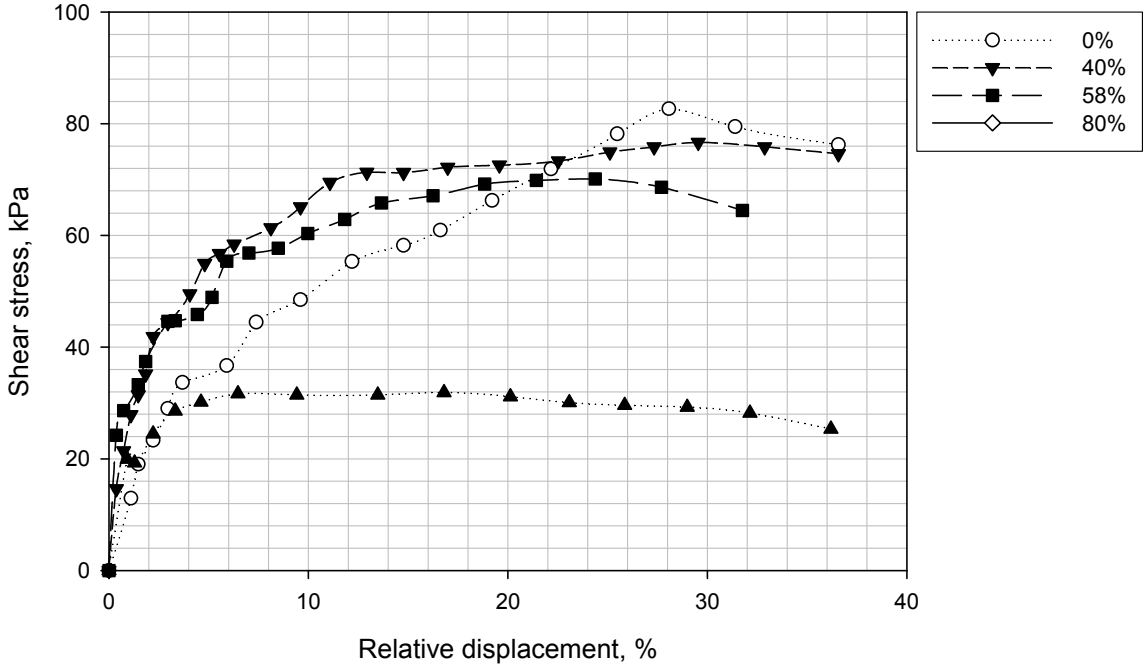

Figure B-31. Large-scale shear tests results under 96 kPa of normal stress

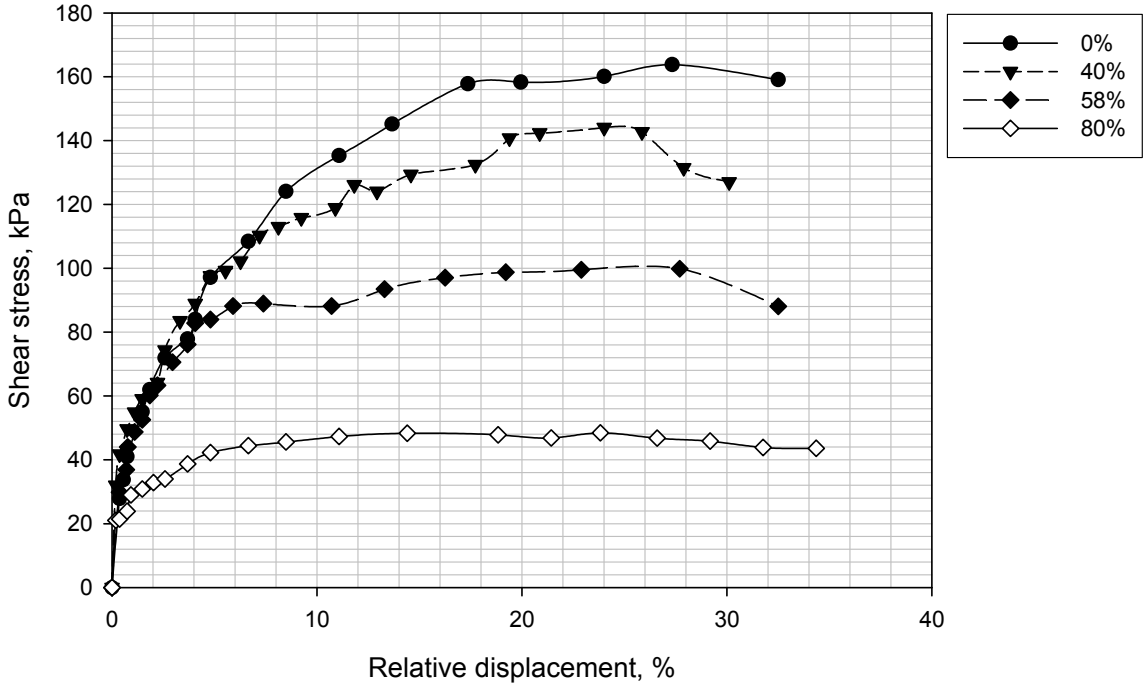

Figure B-32. Large-scale shear tests results under 192 kPa of normal stress

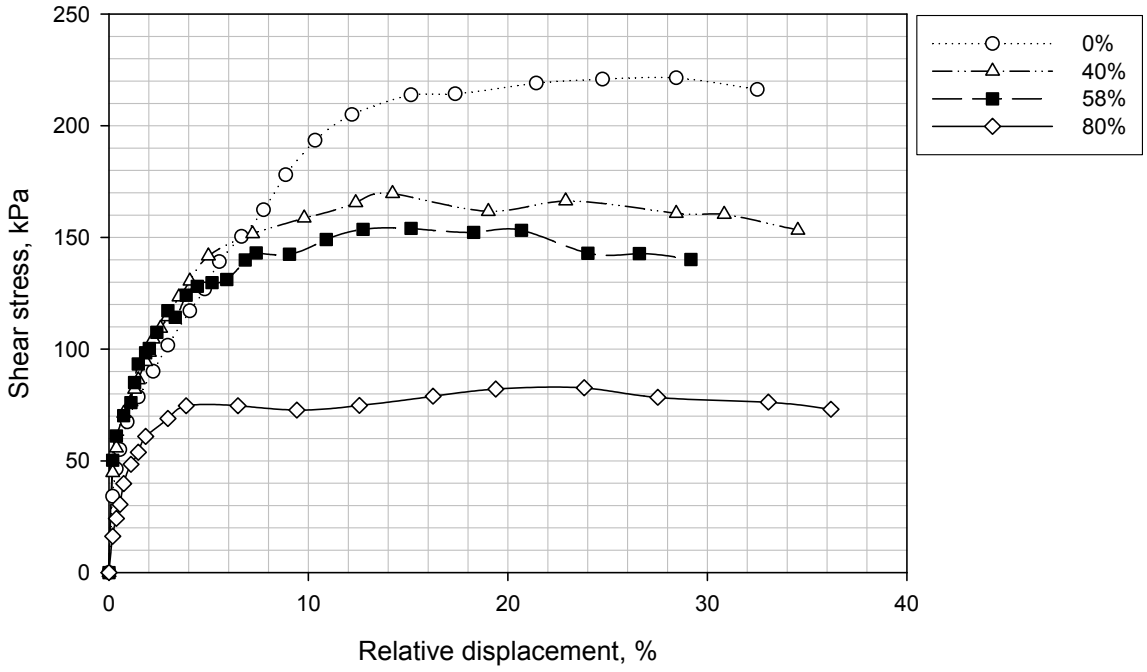

Figure B-33. Large-scale shear tests results under 287 kPa of normal stress

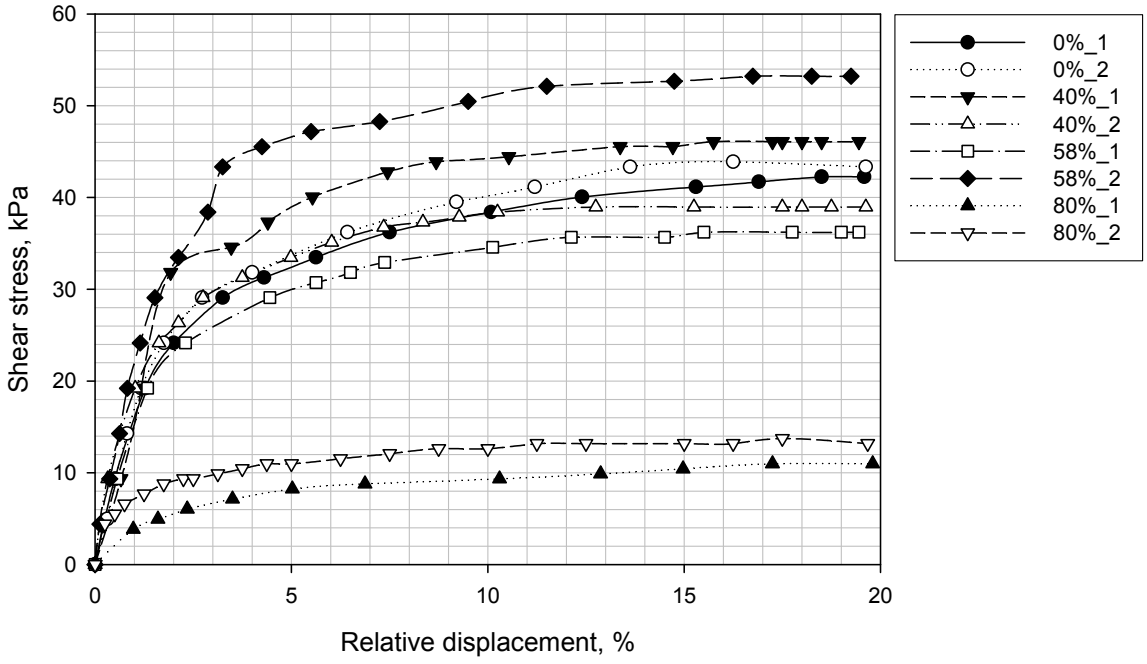

Figure B-34. Small-scale shear tests results under 48 kPa of normal stress

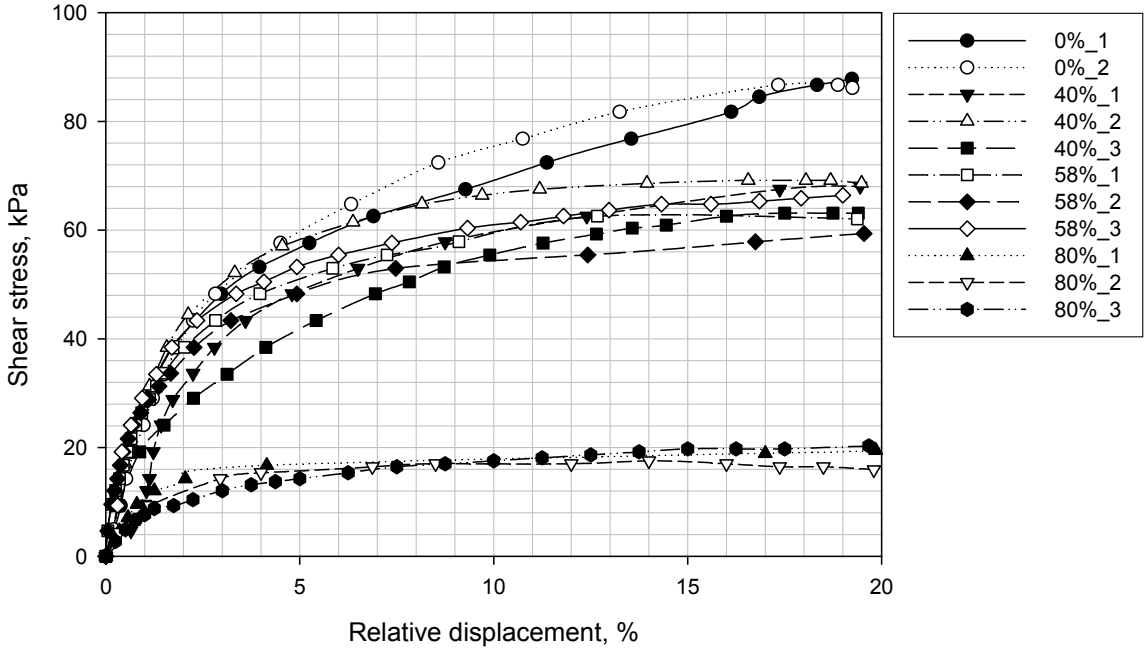

Figure B-35. Small-scale shear tests results under 97 kPa of normal stress

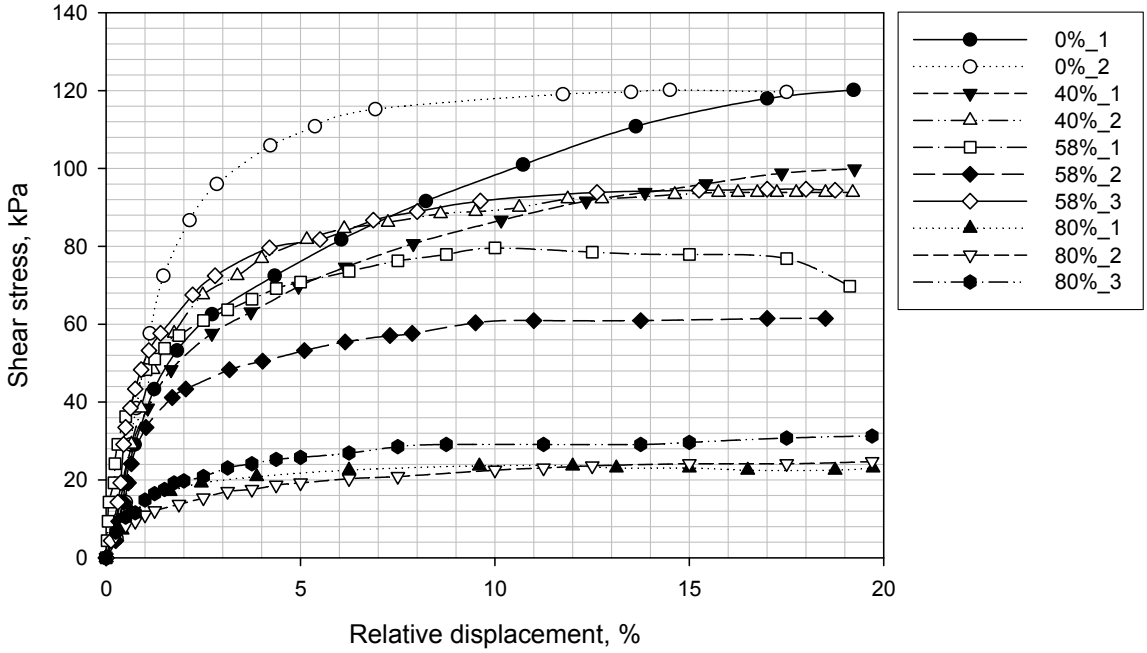

Figure B-36. Small-scale shear tests results under 145 kPa of normal stress

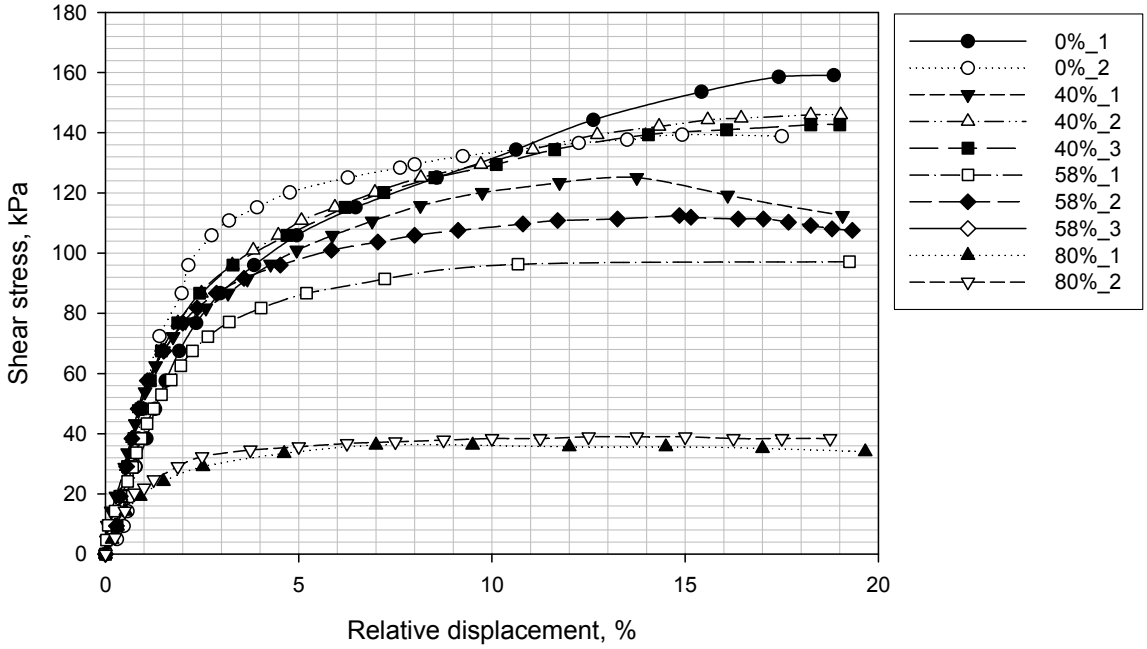

Figure B-37. Small-scale shear tests results under 194 kPa of normal stress

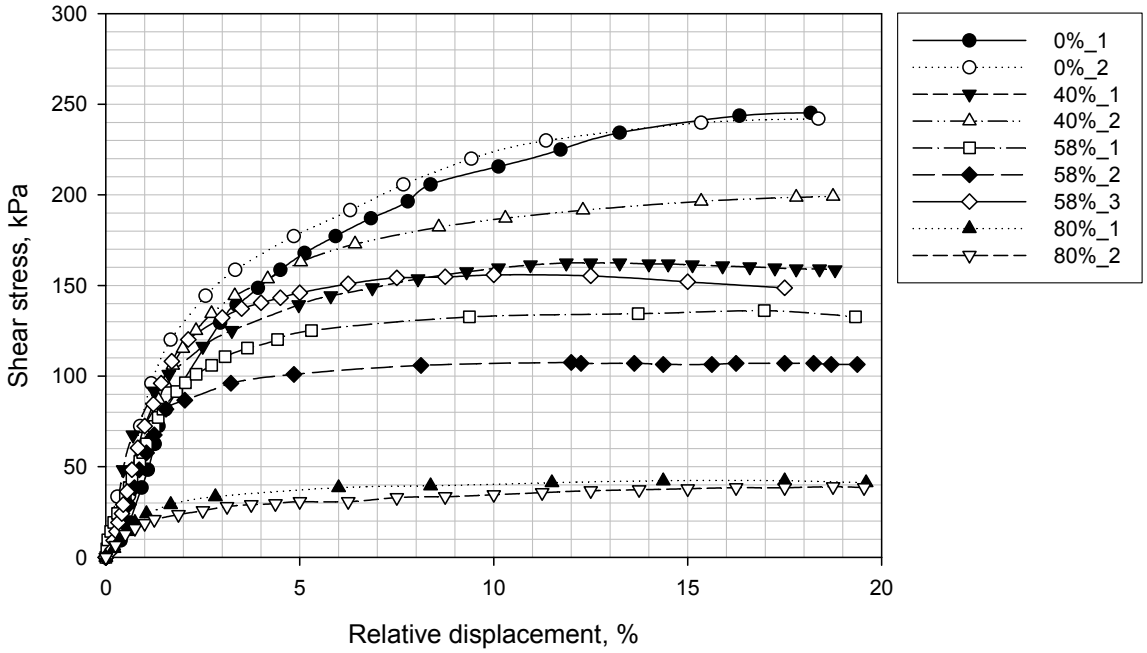

Figure B-38. Small-scale shear tests results under 290 kPa of normal stress

APPENDIX C
LANDFILL BULK DENSITY ESTIMATE METHODOLOGY

1. Estimate the mass of waste (M_W) accepted in a certain period
2. Estimate the volume increment of the landfill (V_T) in the same period.
3. Assume the volume of cover soil (V_C) (e.g. $V_C = 0.18V_T$)
4. Assume a density of cover soil (ρ_C)
5. Calculate a bulk density and a unit weight:

$$\rho_B = \frac{0.15V_T \times \rho_c + M_W}{V_T}$$

APPENDIX D
UNIT CONVERSION OF PORE PRESSURE TRANSDUCER RAW DATA AND THERMAL IMPACT CORRECTION

The raw data (Hz) of each pressure transducer was converted to pressure (kPa) using calibration factors provided by the manufacturer (Geokon, Inc.). The calibration equation for the pressure transducers was provided as follow:

$$R = \frac{(Hz)^2}{1000} \tag{2-1}$$

$$P = G(R_0 - R_i) + K(T_i - T_0) \tag{2-2}$$

where R = reading (digits); (Hz) = raw data of a pressure transducer; P = pressure (kPa); G = calibration factor (kPa/digits); R_0 = initial reading (digits); R_i = reading at time i (digits); K = temperature correction factor (kPa/^{0}C); T_i = temperature at time i (^{0}C); T_0 = initial temperature (^{0}C).

For example, where the frequencies (Hz) at times 0 and i are Hz_0 = 2930.2 (Hz) and Hz_i = 2901.3 (Hz),

$$R_0 = \frac{(Hz)^2}{1000} = \frac{(2930.2)^2}{1000} = 8586.3(digits)$$
$$R_i = \frac{(2901.3)^2}{1000} = 8417.6(digits) \ .$$

If temperature measurements are T_0 = 62.0 ^{o}C, and T_i = 44.7 ^{o}C, then

P = 0.200 kPa/digits (8586.3 – 8417.6) digits + 0.0298 kPa/^{o}C (44.7 – 62.0)^{o}C

= 33 kPa

where G = 0.200 kPa/digits and K = 0.0298 kPa/^{o}C.

APPENDIX E
DERIVATION OF EQUATION 2-3

In this appendix, a method used to estimate vertical hydraulic conductivity of landfilled waste is explained. Townsend (1995) developed equations based on uniform flow theory for saturated conditions to estimate the zone saturated by a horizontal line source with the following assumptions.

1. Steady state saturated flow.
2. Waste is homogeneous.
3. Anisotropic medium.
4. Axes of anisotropy correspond to the principal axes of the system.
5. The well can be treated as a horizontal line source.
6. The line source is subjected to the effect of gravity in the vertical downward direction.
7. The primary driving forces for liquid movement are the injection pressure and gravity.
8. Capillary force and dispersion effects are negligible.
9. Liquid movement in downward direction is not impeded.

The governing equation for the case of steady plane flow is

$$K_x \frac{\partial^2 \phi}{\partial x^2} + K_y \frac{\partial^2 \phi}{\partial y^2} = 0 \qquad \text{(E-1)}$$

where K_x = horizontal hydraulic conductivity (m/sec); K_y = vertical hydraulic conductivity (m/sec); Φ = potential (m); x = distance in x-direction (m); y = distance in y-direction (m). The potential gradient in the gravity drainage scenario, the potential gradient is 1.

$$\frac{\partial \phi}{\partial y} = 1;\ \frac{\partial \phi}{\partial x} = 0 \tag{E-2}$$

$$\therefore \quad \phi = y \tag{E-3}$$

The potential function of the saturated flow is

$$\phi = -\frac{q}{4\pi\sqrt{K_x K_y}} \ln\left(\frac{x^2}{K_x} + \frac{y^2}{K_y}\right). \tag{E-4}$$

By superposing Equation E-3 and Equation E-4, the potential function for a horizontal line source in an anisotropic medium (landfilled waste) can be derived.

$$\phi = -\frac{q}{4\pi\sqrt{K_x K_y}} \ln\left(\frac{x^2}{K_x} + \frac{y^2}{K_y}\right) + y \tag{E-5}$$

The stream function of the flow can be derived as follow.

$$d\psi = \frac{d\phi}{dy} dx$$

$$d\psi = \frac{d\phi}{dy} dx = -\frac{q}{4\pi\sqrt{K_x K_y}} \cdot \frac{\frac{2y}{K_y}}{\frac{x^2}{K_x} + \frac{y^2}{K_y}} dx + 1 \cdot dx$$

$$\psi = -\frac{q}{4\pi\sqrt{K_x K_y}} \cdot 2\int_0^x \left(\frac{\frac{y}{K_y}}{\frac{x^2}{K_x} + \frac{y^2}{K_y}}\right) dx + x$$

$$\psi = -\frac{q}{2\pi K_y} \int_0^x \frac{1}{\sqrt{K_x K_y}} \left(\frac{y K_x K_y}{K_y x^2 + K_x y^2}\right) dx + x$$

$$\psi = -\frac{q}{2\pi K_y}\int_0^x \frac{\frac{1}{y}\sqrt{\frac{K_y}{K_x}}}{1+\left(\frac{x}{y}\sqrt{\frac{K_y}{K_x}}\right)^2}dx + x$$

$$\psi = -\frac{q}{2\pi K_y}\tan^{-1}\left(\frac{x}{y}\sqrt{\frac{K_y}{K_x}}\right) + x \qquad \text{(E-6)}$$

The boundary for the saturated bulb occurs where $\psi = 0$, and this relationship may therefore be determined as

$$x = \frac{q}{2\pi K_y}\tan^{-1}\left(\frac{x}{y}\sqrt{\frac{K_y}{K_x}}\right) \qquad \text{(E-7)}$$

A schematic of the flow system evaluated is presented in Figure E-1.

The value of Y_{max} may be determined where x = 0 and $d\phi/dy = 0$.

$$Y_{\max} = \frac{q}{2\pi\sqrt{K_x K_y}} \qquad \text{(E-8)}$$

The value of X_{max} may be determined when y approaches - ∞.

$$X_{\max} = \frac{q}{2K_y} \qquad \text{(E-9)}$$

The value of X_{well} may be determined at the boundary where y = 0.

$$X_{well} = \frac{q}{4K_y} \qquad \text{(E-10)}$$

where x_{well} = horizontal maximum extent of saturated zone at the elevation of the horizontal liquids addition line source (m); q= constant linear flow rate (flow rate per unit length of line source, m^2/sec). The distances X_{max} and X_{well} are a function of the hydraulic conductivity in the vertical direction only.

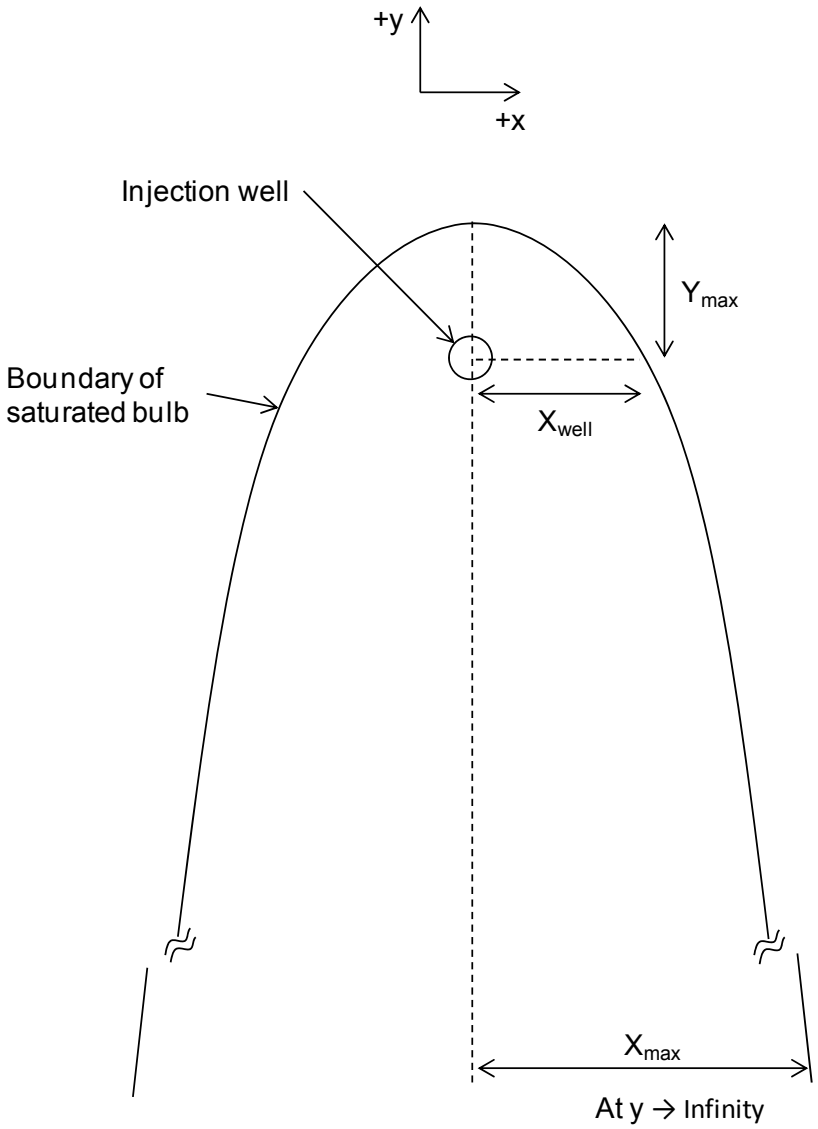

Figure E-1. Saturated flow zone surrounding a horizontal line source under steady state conditions: adapted from Townsend (1995)

APPENDIX F
EXAMPLE CALCULATION OF THE HYDRAULIC CONDUCTIVITY AND ANISOTROPY OF LANDFILLED WASTE USING IN-SITU PORE PRESSURE MEASUREMENTS

1. Determination of X_{well} based on in-situ pore pressure data: In Experiment 1, the increase in pore pressure measured by a pressure transducer at a distance of 11.4 m from the crushed glass trench was only 5 kPa while pore pressure in the trench increased up to 40 kPa. It was assumed that the horizontal extent of the added liquids (saturated zone) was 11.4 m (= X_{well}).

2. Estimation of K_y using Equation 2-3

$$x_{well} = \frac{q}{4K_y} \tag{2-3}$$

where q = constant linear flow rate (flow rate per unit length of line source, m^2/sec); X_{well} = horizontal maximum extent of saturated zone at the elevation of the horizontal liquids addition line source (m)

$$K_x = \frac{8.60\times10^{-6} m^2/\sec}{4(11.4m)} = 1.89\times10^{-5} cm/\sec$$

where Q = 0.057 m^3/min and a length of the line = 110 m, the linear flow rate q = 8.6×10^{-6} m^2/sec.

3. Estimation of $(K_xK_y)^{0.5}$ using Equation 2-4

$$S_{(R)} = \phi_{(R)} - \phi_{(r_w)} = \frac{q}{2\pi\sqrt{K_xK_y}} \ln\left(\frac{R}{r_w}\right) \tag{2-4}$$

where $S_{(R)}$ = head drawdown (m); $\Phi_{(R)}$ = potential at a distance R (m); $\Phi_{(rw)}$ = potential in a horizontal trench (m); R = horizontal distance from a line source (m); r_w = effective well radius (m); K_x = horizontal hydraulic conductivity (m/sec).

A K_x value was determined by finding a theoretical $S_{(R)}$-R curve closest to an actual S(R)-R curve plotted based on the in-situ measurements; by varying $(K_xK_y)^{0.5}$ values while keeping other parameters constant, theoretical $S_{(R)}$-R curves were developed and superimposed on an actual $S_{(R)}$-R curve (Figure F-1).

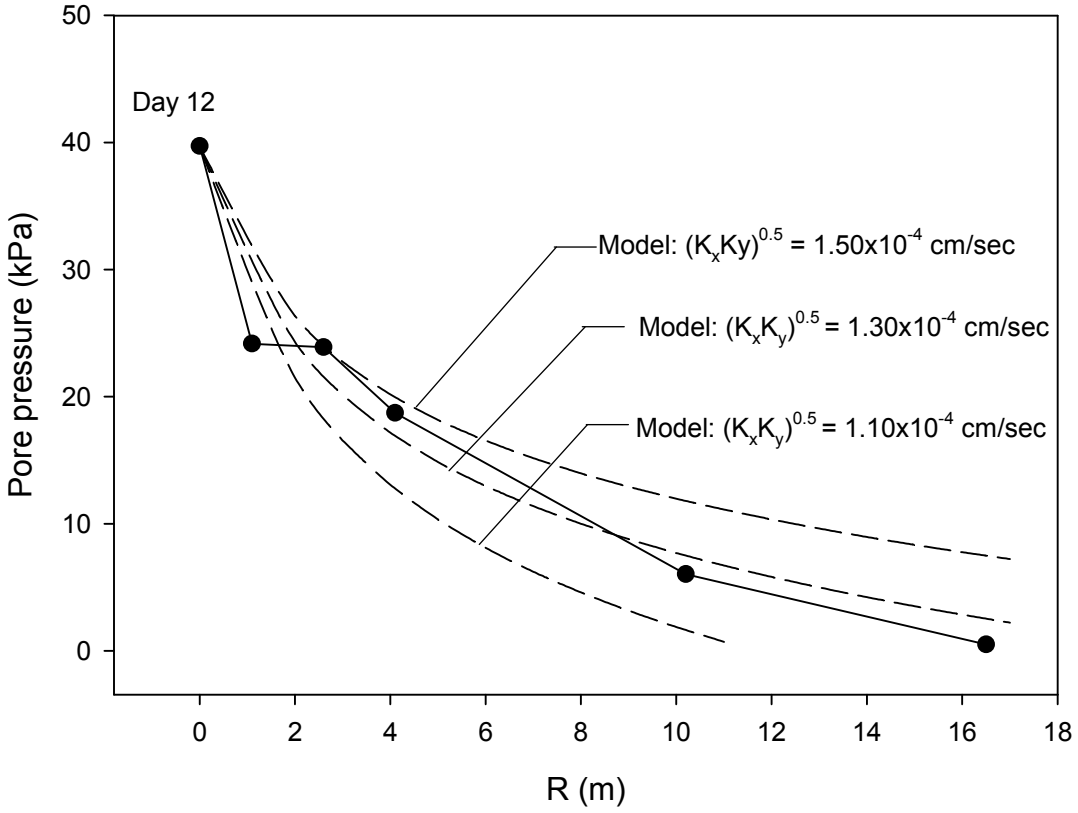

Figure F-1. Example $S_{(R)}$-R curve to determine $(K_xK_y)^{0.5}$

Therefore, $(K_xK_y)^{0.5}$= 1.30×10^{-4} cm/sec and K_x = 8.96×10^{-4} cm/sec

4. Estimation of anisotropy

$$\frac{K_x}{K_y} = \frac{8.96\times10^{-4}}{1.89\times10^{-5}} = 47$$

APPENDIX G
ELEVATION MEASUREMENT USING A THEODOLITE

The elevation (NGVD) of data collection location in each settlement profiling pipe was estimated by measuring the elevation of each settlement profiler reference station using a laser leveling machine (Spectra Precision Gplus, Trimble). Figure G-1 conceptually depicts how to determine the elevation of the reference station of the settlement profiler using the leveling machine.

The elevation of the reference station of the settlement profiler was calculated using the following equation:

$$H_{\mathrm{R}} = H_0 + \sum_{i=1}^{n} \left(H_{2i-1} - H_{2i} \right) \tag{G-1}$$

where H_R = elevation of the reference station (ft, NGVD); H_0 = elevation of the bench mark (ft, NGVD); H_{2i-1} = backward height of the leveling machine at the i th location; H_{2i} = forward height of the leveling machine at the i th location.

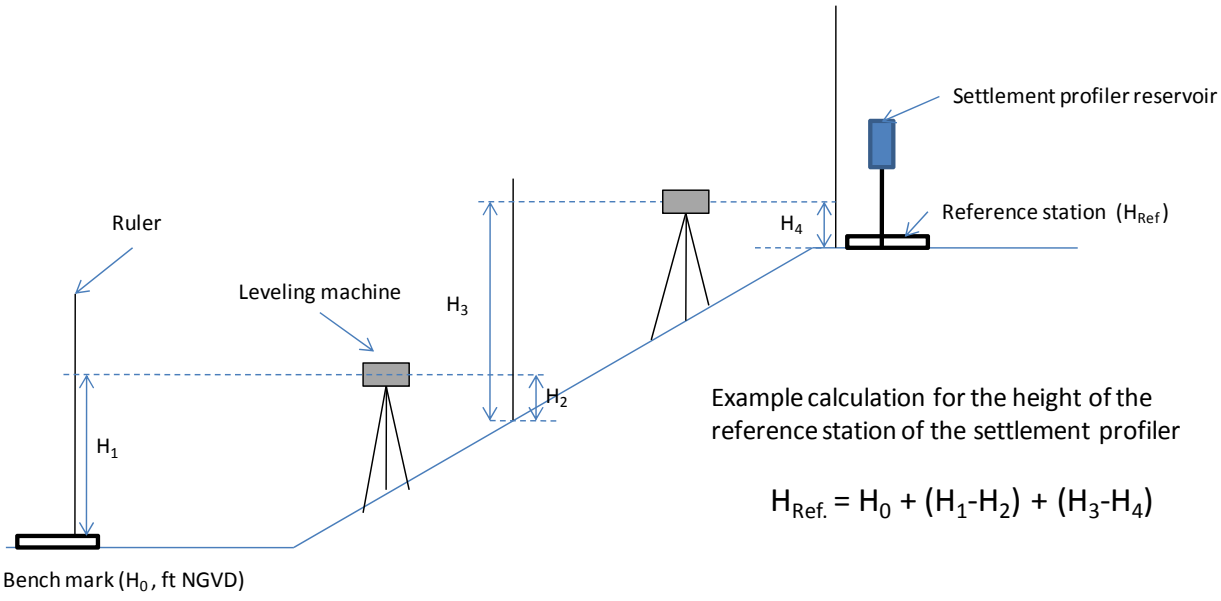

Figure G-1. Elevation determination using a leveling machine

APPENDIX H
UNIT CONVERSION OF SETTLEMENT PROFILER RAW DATA AND SETTLEMENT ESTIMATION

The elevation of a desired location in a settlement profiling pipe was estimated using the following equations provided by the manufacturer.

$$R = \frac{(Hz)^2}{1000} \tag{3-1}$$

$$E = E_{ref} - G(R_o - R_c) \tag{3-2}$$

where R = reading (digits); (Hz) = raw data of a pressure transducer; E = the elevation of the sensor (m); E_{ref} = elevation of the reference station (m); R_o = the reading at the reference station (digits); R_c = reading at a target location (digits); G = the calibration constant (meter per digits).

Assuming the raw data at the reference station and a target location are Hz_0 = 3067.40 (Hz) and Hz_c = 3045.62 (Hz),

$$R_0 = \frac{(Hz)^2}{1000} = \frac{(3067.4)^2}{1000} = 9409.0\,(digits)$$
$$R_c = \frac{(3045.62)^2}{1000} = 9275.8\,(digits)\ .$$

Where the reference station is set-up at an elevation 60.3 m (NGVD) and G = 0.00408 m/digits,

E = 60.3 m – 0.00408 m/digit(9409.0.7-9275.8)digits = 59.7 m .

If the elevation of the target location was measured to be 61.0 m in previous settlement profiling, then 1.3 m of settlement occurred during the period.

APPENDIX I
EXAMPLE CALCUATIONS OF COMPRESSION PROPERTIES AND HYDRAULIC CONDUCTIVITY OF LANDFILLED WASTE

Based on a time-consolidation curve, the primary consolidation period was determined (Figure I-1); data from Pipe 1 (31 m from the entry).

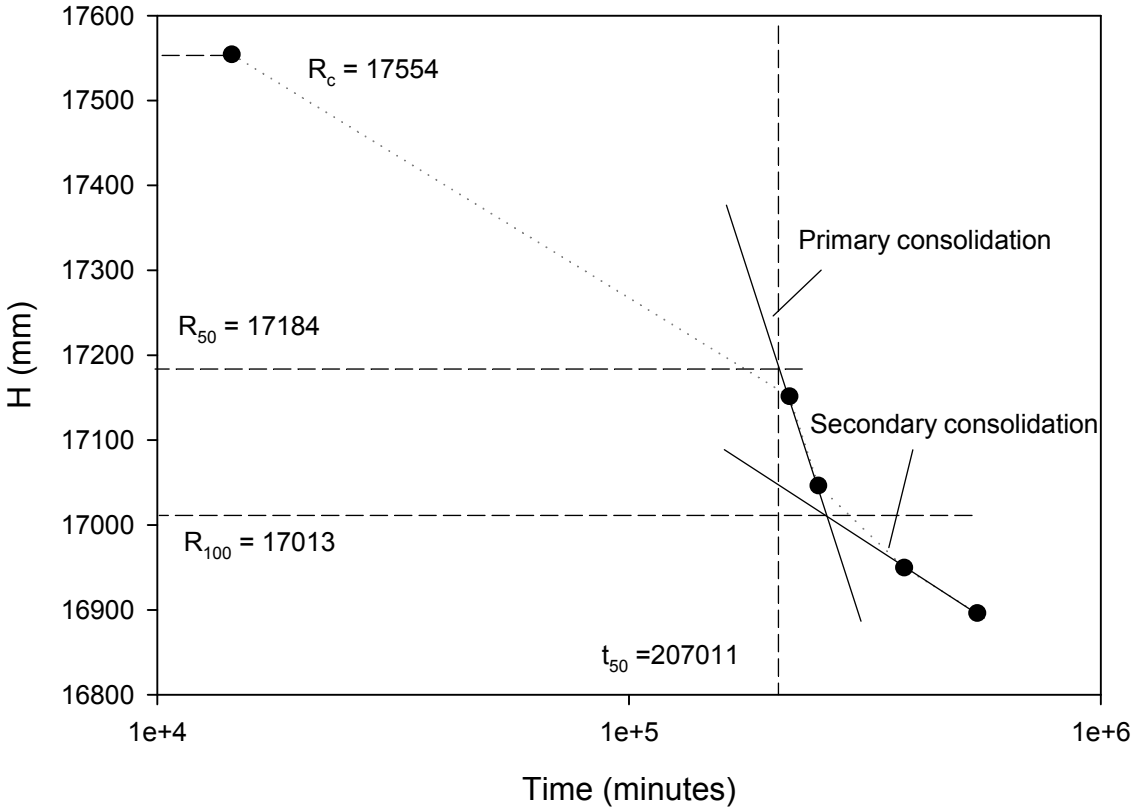

Figure I-1. Example time-consolidation curve: log of time fitting method; R_c = initial thickness of an underlain waste layer; R_{50} = thickness of an underlain waste layer at t_{50}; R_{100} = final thickness of an underlain waste layer after primary consolidation; t_{50} = time required to 50% ultimate primary consolidation.

A modified primary compression index (C_c') of the landfilled waste was estimated using the following expression.

$$C_c' = \frac{\Delta\varepsilon}{\Delta \log \sigma'} \quad \text{(I-1)}$$

where Δε = change in strain during the primary consolidation period (m); σ_i, σ_f = initial and final stress applied to the midpoint of the bioreacted waste layer, 0.5 H_i, (kPa).

During the primary consolidation period, approximately 2.9% of strain occurred due to the increase in vertical stress from 105.3 kPa to 158.3 kPa. Therefore,

$$C_c' = \frac{\Delta\varepsilon}{\Delta \log \sigma'}$$

$$= \frac{2.9\times10^{-2}}{\log(158.3) - \log(105.3)} = 0.16 .$$

Coefficient of volume change (m_v) of the landfilled waste was estimated using the following equation.

$$m_v = -\frac{\Delta V}{V_i}\frac{1}{\Delta\sigma'} \qquad \text{(I-2)}$$

where ΔV = change in volume (m^3); V_i = initial volume prior to pressure increment (m^3); $\Delta\sigma'$ = pressure increment.

By assuming no lateral deformation occurs, Equation I-2 can be rearranged.

$$m_v = -\frac{\Delta H}{H_i}\frac{1}{\Delta\sigma'} \qquad \text{(I-3)}$$

where ΔH = change in height (m); H_i = initial height of a soil layer (m). Therefore,

$$m_v = \frac{\Delta\varepsilon}{\Delta\sigma'} = \frac{2.9\times10^{-2}}{158.3kPa - 105.3kPa} = 0.00055\ {}^{m^2}\!/_{kN} .$$

To estimate coefficient of consolidation (c_v), the logarithm of time fitting method developed by Casagrande (1940) was used (Figure I-1). For example, t_{50} was determined to be 207,011 min from Figure I-1. Where H_i = 17.55 m and H_f = 17.04 m,

$$c_v = \frac{(T_v)_{50}\, d^2}{t_{50}} = \frac{0.197 d^2}{t_{50}} \qquad \text{(I-4)}$$

$$d = \frac{H_i + H_f}{4} \qquad \text{(I-5)}$$

$$d = \frac{17.55 + 17.04}{4} = 8.6$$

Therefore, $c_v = \frac{0.197(8.6)^2}{207,011} = 7.05 \times 10^{-5}\ m^2/\min = 0.012\ cm^2/\sec$.

By rearranging an equation to estimate coefficient of consolidation (c_v), hydraulic conductivity (K) of media can be estimated.

$$c_v = \frac{K_y}{m_v \gamma_w} \tag{I-7}$$

$$K_y = c_v m_v \gamma_w \tag{I-8}$$

Assuming γ_w = unit weight of water (9.8 kN/m^3),

$$K_y = c_v m_v \gamma_w = \left(7.05 \times 10^{-5}\ m^2/\min\right)\left(0.00055\, m^2/kN\right)\left(9.8\, kN/m^3\right)$$

$$= 4.0 \times 10^{-7}\, m/\min = 6.7 \times 10^{-7}\ cm/\sec \quad .$$

APPENDIX J
UNIT CONVERSION OF SETTLEMENT SENSOR RAW DATA AND BAROMETRIC PRESSURE AND THERMAL IMPACT CORRECTION

Readings from each SS have a unit of frequency and thus were converted to proper units such as kPa or cm, respectively. Unit conversion and calibration equations for the SSs are as follows:

$$R = \frac{(Hz)^2}{1000} \tag{4-1}$$

$$E = G\,(R_o - R_i) + \Delta E_{res} + K(T_i - T_0) + \{B_0 - B_i\} \tag{4-2}$$

where R = reading (digits); (Hz) = raw data from settlement sensor; E = elevation of the sensor (cm); ΔE_{res} = any change of the liquid level inside the reservoir sight glass (cm); R_o = initial sensor reading (digits); R_i = reading at time i (digits); G = calibration constant provided by the manufacturer (cm/digits); T_i = temperature at time i (^{0}C); T_0 = initial temperature (^{0}C); K = temperature correction factor (cm/^{0}C) provided by the manufacturer; $\{B_0 - B_i\}$ = barometric pressure correction for non-vented SSs (cm H_2O).

For example, the frequencies (Hz) readings at times 0 and i are Hz_0 = 2573.8 (Hz) and Hz_i = 2557.0 (Hz) can be converted as follow;

$$R_0 = \frac{(Hz)^2}{1000} = \frac{(2573.8)^2}{1000} = 6624.4\,(digits)$$
$$R_i = \frac{(2557.0)^2}{1000} = 6538.2\,(digits)\ .$$

If barometric pressure measurements are B_0 = 29.86 in-Hg and B_i = 30.04 in-Hg, then

P = 0.171 cm/digits(6624.4 – 6538.2) digits + 0.4 cm + 0.425 cm/^{o}C(30.2 – 29.9)^{o}C

= 15.27 cm

where G = 0.171 cm/digits, ΔE_{res} = 0.4 cm, K = 0.425 cm/^{o}C, T_i = 30.2^{o}C, and T_o = 29.9^{o}C.

For non-vented SSs, barometric pressure impact should be corrected. For example, if B_0 = 29.89 in-Hg and B_i = 30.18 in-Hg, then

P = 15.27 cm – (30.18 – 29.89)×34.53 cm /in-Hg = 5.26 cm.

APPENDIX K
UNIT CONVERSION OF TOTAL PRESSURE CELL RAW DATA AND BAROMETRIC PRESSURE AND THERMAL IMPACT CORRECTION

Unit conversion and calibration equations for the TPCs were as follow:

$$R = \frac{(Hz)^2}{1000} \tag{4-3}$$

$$P = G(R_0-R_i) + (B_0-B_i) - K(P) \tag{4-4}$$

where R = reading (digits); (Hz) = raw data from pressure transducer; P = pressure (kPa); G = calibration factor provided by the manufacturer (kPa/digits); R_0 = initial reading (digits); R_i = reading at time i (digits); B_0 = initial barometric pressure (kPa); B_1 = current barometric pressure (kPa); K(P) = thermal impact correction equation derived from a best-fit regression of P versus (T_0-T_i) data; T_i = temperature at time i (^{0}C); T_0 = initial temperature (^{0}C).

For example, the frequencies (Hz) readings at times 0 and i are Hz_0 = 2890.6 (Hz) and Hz_i = 2860.6 (Hz) can be converted as follow;

$$R_0 = \frac{(Hz)^2}{1000} = \frac{(2890.6)^2}{1000} = 8357.4(digits)$$
$$R_i = \frac{(2860.6)^2}{1000} = 8183.3(digits) \ .$$

If G = 0.0927 kPa/digits, B_0 = 29.86 in-Hg and B_i = 30.04 in-Hg, then

P = 0.0927 kPa/digits (8357.4 – 8183.3) digits

+ 6.89 kPa/2.036 in-Hg(29.86 – 30.04)in-Hg = 15.5 kPa

A thermal impact correction equation can be derived using a best-fit regression as shown in Figure K-1.

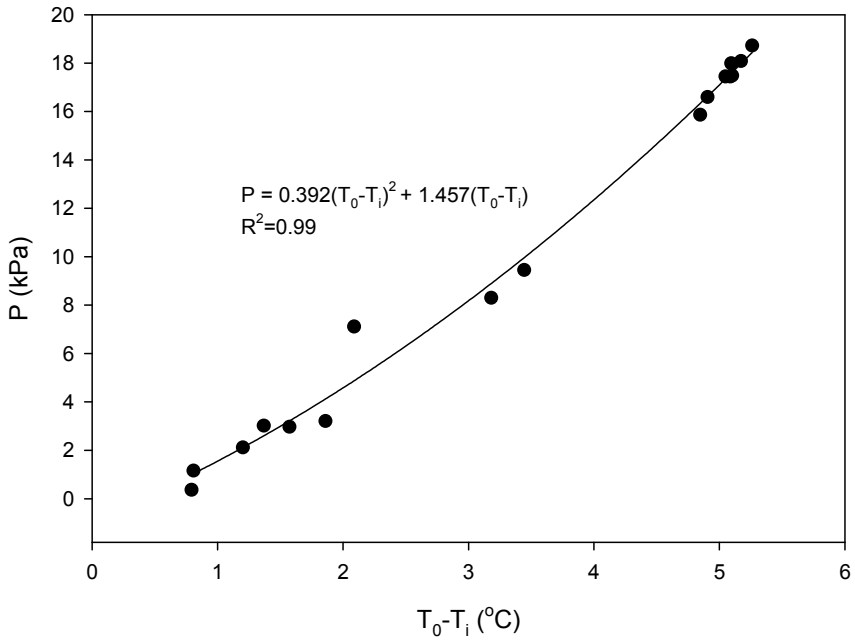

Figure K-1. Example best-fit regression to derive a thermal impact correction equation for TPC

$$P = 15.5 \text{ kPa} - \{0.392(20.5 - 24.5)^2 + 1.457(20.5 - 24.5)\} \text{ kPa} = 15.03 \text{ kPa}$$

where $T_0 = 22.3\ ^oC$ and $T_i = 30.8\ ^oC$.

APPENDIX L
EXAMPLE ESTIMATION OF LANDFILL FOUNDATION SETTLEMENT

In Chapter 4, one-dimensional (vertical) elastic and primary consolidation settlements of the subsurface soil layers under the study landfill foundation were estimated using the following equations:

$$S_t = S_e + S_c \tag{4-7}$$

$$S_e = \sum_i^n H_{0i} \frac{\Delta \bar{\sigma}_{vi}}{M_i} \tag{4-8}$$

$$S_c = \sum_{i=1}^{n} C_{ci} \frac{H_{0i}}{1+e_{0i}} \log \frac{\bar{\sigma}_{v,0i} + \Delta \bar{\sigma}_{vi}}{\bar{\sigma}_{v,0i}} \tag{4-9}$$

where S_t = total settlement (m); S_e = elastic settlement (m); S_c = primary consolidation settlement (m); H_{oi} = thickness of soil layer i (m); $\Delta \bar{\sigma}_{vi}$ = overburden stress increase caused by the waste placement at midpoint of soil layer i; M_i = constrained modulus of soil layer i (MPa); C_{ci} = primary compression index; e_{oi} = initial void ratio of soil layer i; $\bar{\sigma}_{oi}$ = initial overburden stress at the center of soil layer i.

To estimate elastic settlement, constrained modulus of a soil layer should be determined first. Various equations introduced in Bowles (1996) were used to estimate the stress-strain (Young's) modulus E of each soil layer with the CPT(N) and SPT(N) and then a constrained modulus M was determined using the E value. For example, for the gravelly sand to sand layer at depths of 31 to 44 ft in Table L-1, Equation 4-14 was used to estimate a stress-strain modulus.

E(kPa) = 600(N + 6) + 2000 for gravelly sand, N>15 (4-14)

E(kPa) = 600(57.5 + 6) + 2000 = 40,100 kPa = 401 TSF

Then, constrained modulus M was estimated using the following equation.

$$M = \frac{E(1-\nu)}{(1+\nu)(1-2\nu)} \tag{4-15}$$

where ν = Poisson's ratio (effective); Poission's ratio of 0.3 was assumed (Budhu 2000).

$$M = \frac{E(1-\nu)}{(1+\nu)(1-2\nu)} = \frac{401TSF(1-0.3)}{(0.3+1)(1-2\cdot 0.3)} = 539.7\,TSF$$

Assuming 0.91 tsf of vertical stress increase, the elastic settlement of the layer is estimated to be

$$S_e = H_0 \frac{\Delta\bar{\sigma}_v}{M} = 14\ ft \frac{0.91TSF}{539.7\,TSF} = 0.024\ ft\,.$$

Assuming $C_c/(1+e_o)$ = 0.002 for sand or silty sand (Conuto 2004), for example, the consolidation settlement of the sand layer at depths of 45 to 50 ft in Table L-1 was estimated to be

$$S_c = C_c \frac{H_0}{1+e_0} \log \frac{\bar{\sigma}_{v,0} + \Delta\bar{\sigma}_v}{\bar{\sigma}_{v,0}} = 0.002 \times 6\ ft \times \log \frac{2.53TSF + 0.91TSF}{2.53TSF} = 0.016\ ft\ .$$

Table L-1. Example settlement estimates at location A; the data used were collected on May 20, 2010.

Depth (ft)	Soil Behavior	CPT (N) (#)	Layer Thickness (ft)	average N-value (#)	σo (TSF)	Constrained Modulus (TSF)	Settlement	
							Elastic (ft)	Consolidation (ft)
1	SILTY SAND TO SANDY SILT	7						
2	SILTY SAND TO SANDY SILT	9						
3	SILTY SAND TO SANDY SILT	10						
4	SILTY SAND TO SANDY SILT	12						
5	SILTY SAND TO SANDY SILT	11						
6	SAND TO SILTY SAND	11	6	10.0	0.24	168.3	0.032	0.008
7	SAND	31						
8	GRAVELLY SAND TO SAND	43						
9	SAND	54						
10	SAND	42						
11	SAND	36						
12	SAND TO SILTY SAND	29						
13	SILTY SAND TO SANDY SILT	26						
14	SAND TO SILTY SAND	27						
15	SAND	39	9	36.3	0.71	345.5	0.024	0.006
16	GRAVELLY SAND TO SAND	50						
17	GRAVELLY SAND TO SAND	52						
18	SAND	53						
19	SAND	39						
20	SAND TO SILTY SAND	32						
21	SAND	37						
22	SAND	53						
23	SAND	54						
24	SAND	59						
25	SAND	63						
26	GRAVELLY SAND TO SAND	57						
27	SAND	56						
28	SAND	53						
29	SAND	46						
30	SAND	56	15	50.7	1.31	441.9	0.031	0.007
31	GRAVELLY SAND TO SAND	60						
32	GRAVELLY SAND TO SAND	58						
33	GRAVELLY SAND TO SAND	52						
34	GRAVELLY SAND TO SAND	59						
35	GRAVELLY SAND TO SAND	59						
36	GRAVELLY SAND TO SAND	60						
37	GRAVELLY SAND TO SAND	58						
38	GRAVELLY SAND TO SAND	53						
39	GRAVELLY SAND TO SAND	52						
40	GRAVELLY SAND TO SAND	58						
41	GRAVELLY SAND TO SAND	62						
42	GRAVELLY SAND TO SAND	57						
43	GRAVELLY SAND TO SAND	57						
44	GRAVELLY SAND TO SAND	60	14	57.5	2.03	539.7	0.024	0.004
45	SAND	56						
46	SAND	52						
47	SAND	44						
48	SAND	35						
49	SAND	28						
50	SAND TO SILTY SAND	22	6	39.5	2.53	366.8	0.015	0.002
				Total Settlement		(ft)	0.125	0.028
						(cm)	3.82	0.84

LIST OF REFERENCES

Abuel-Naga, H.M., Bergado, D., and Bouazza, A. (2007). “Thermally induced volume change and excess pore water pressure of soft Bankok clay.” *Engineering Geology*, 89, 144–154.

Al-Yousfi, A.B., and Pohland, F.G. (1998). “Strategies for simulation, design, and management of solid wastes disposal sites as landfill bioreactors.” *Practice Periodical of Hazardous, Toxic, and Radioactive Waste Management*, 2(1), 13–21.

American Society of Testing and Material (2004). “Standard test method for direct shear test of soils under consolidated drained conditions.” *D 3080-04*, West Conshohocken, Pennsylvania.

Anderson, E.O., Balanko, L.A.L., Lem, J.M., and Davis, D.H. (2004). “Field monitoring of the compressibility of municipal solid waste and soft alluvium.” *Proceedings of the 5th International Conference on Case Histories in Geotechnical Engineering*, New York, 8.08.

Aschieri, F. and Uliana F.A. (1984). “Seasonal temperature effects on a foundation.” *Journal of Geotechnical Engineering*, 110 (6), 796–806.

Bear, J. (1979). “Hydraulics of groundwater.” *Dover Publications, Inc.*, New York, 60 - 69, 184 - 189, and 377–378.

Beaven, R.P. (2000). "The hydrological and geotechnical properties of household waste in relation to sustainable landfilling." Ph.D. dissertation, Queen Mary and Westfield College, University of London, United Kingdom.

Benson, C.H., Barlaz, M.A., Lane, D.T., and Rawe, J.M. (2007). “Practice review of five bioreactor/recirculation landfills.” *Waste Management*, 27, 13–29.

Bleiker, D.E., Farquhar, G., McBean, E. (1995). “Landfill settlement and the impact on site capacity and refuse hydraulic conductivity.” *Waste Management Research*, 13, 533–554.

Bowles, J.E. (1996). “Foundation analysis and design, 5th Edition.” *McGraw-Hill*, New York.

Budhu, M. (2000). “Soil mechanics and foundations.” *Wiley & Sons, Inc.*, New York.

Burnley, S.J. (2007). “A review of municipal solid waste composition in the United Kingdom.” *Waste Management*, 27, 1274–1285.

Coduto, D.P. (2000). “Foundation design: principles and practices, 2nd Edition.” *Prentice Hall, Inc.*, New Jersey.

Daigle, L., and Zhao, J.Q. (2003). “Assessing temperature effects on earth pressure cells.” *National Research Council Canada, Institute for Research in Construction*, IRC-RR–131.

Das, B.M. (1990). “Principles of Foundation Engineering, 2nd Edition.” *PWS-Kent Pub. Co*., Boston.

Durmusoglu, E., Sanchez, I.M., and Corapcioglu, M.Y., (2006). “Permeability and compression characteristics of municipal solid waste samples.” *Environmental Geology*, 50, 773–786.

Edil, T.B., Ranguette, V.J., and Wellner, W.W. (1990). “Settlement of municipal refuse.” *Geotechnics of Waste Fills - Theory and Practice: ASTM STP 1070*, ASTM, Philadelphia, 225–239.

Elagroudy, S.A., Abdel-Razik, M.H., Warith, M.A., and Ghobrial, F.H. (2007). “Waste settlement in bioreactor landfill models.” *Waste Management*, 28(11), 2366–2374.

El-Fadel, M., Shazbak, S., Saliby, E., and Leckie, J. (1999). “Comparative assessment of settlement models for municipal solid waste landfill applications.” *Waste Management Research*, 17, 347.

El-Fadel, M. and Khoury, R. (2000). “Modeling settlement in MSW landfills: a critical review.” *Critical Reviews in Environmental Science and Technology*, 30(3), 327–361.

Fassett, J.B., Leonards, G.A., and Repetto, P.C. (1994). “Geotechnical properties of municipal solid waste and their use in landfill design.” *Proceedings of the Waste Tech ’94 Solid Waste Association of North America. Silver Springs,* Maryland, 1–31.

Gabr, M.A., Hossain, M.S., and Barlaz, M.A. (2007). “Shear strength parameters of municipal solid waste with leachate recirculation.” *Journal of Geotechnical and Geoenvironmental Engineering*, 133(4), 478–484.

Grubb, D.G., Gallagher, P.M., Wartman, J., Liu, Y., and Carnivale, M. III (2006). “Laboratory evaluation of crushed glass–dredged Material blends.” *Journal of Geotechnical and Geoenvironmental Engineering*, 132 (5), 562–576.

Harris, J.M., Shafer, A.L., DeGroff, W., Hater G.R., Gabr M., and Barlaz, M.A. (2006). “Shear strength of degraded reconstituted municipal solid waste.” *Geotechnical Testing Journal*, 29 (2), 1–8.

Hossain, M.S., Gabr, M.A., and Barlaz, M.A. (2003). “Relationship of compressibility parameters to municipal solid waste decomposition.” *Journal of Geotechnical and Geoenvironmental Engineering*, 129 (12), 1151–1158.

Hudson, A.P., Beaven, R.P., and Powrie, W. (1999). “Measurement of the horizontal hydraulic conductivity of household waste in a large scale compression cell.” *Proceedings of the 7th International Landfill Symposium, Sardinia 99, CISA*, Cagliari, Italy, 4–8.

Jain, P. (2005) “Moisture addition at bioreactor landfills using vertical wells: mathematical modeling and field application.” Ph.D. Dissertation, University of Florida, Gainesville, Florida, United States.

Jain, P., Farfour, W.M., Jonnalagadda, S., Townsend, T.G., and Reinhart, D.R. (2005) “Performance evaluation of vertical wells for landfill leachate recirculation.” *Proceedings of Geo Frontier 2005*, ASCE, Austin, Texas.

Jain, P., Powell, J., Townsend, T.G., and Reinhart, D.R. (2006). “Estimating the hydraulic conductivity of landfilled municipal solid waste using the borehole permeameter test.” *Journal of Environmental Engineering*, 132 (6), 645–652.

Kadambala, R. (2009). “Evaluation of a buried vertical well leachate recirculation system and settlement resulting from moisture addition using vertical wells for municipal solid waste landfills.” Ph.D. dissertation, University of Florida, Gainesville, Florida, United States.

Kavazanjian, E. (2008). “The impact of degradation on MSW shear strength.” *Proceedings of GeoCongress 2008, Geotechnics of Waste Management and Remediation*, ASCE, New Orleans, Louisiana, 224–231.

Kavazanjian, E. Jr., Matasovic, N. and Bachus, R.C. (1999). “Large-diameter static and cyclic laboratory testing of municipal solid waste.” *Proceedings of the 7th International Landfill Symposium, Sardinia 99, CISA*, Cagliari, Italy, 437–445.

Kavazanjian, E., Matasovic, N., Bonaparte, R., and Schmertmann, G. (1995). “Evaluation of MSW properties for seismic analysis.” *Proceedings of Specialty Conference, Geoenvironmental 2000*, ASCE Geotechnical Special Publication, 46(2), 1126–1141.

Kumar, S. (2009). “Study of pore water pressure impact and fluid conductance of a landfill horizontal liquids injection system.” Master’s Thesis, University of Florida, Gainesville, Florida, United States.

Landva, A., and Clark, J.I. (1990). “Geotechnics of waste fill.” *Geotechnics of Waste Fills - Theory and Practice: ASTM STP 1070*, ASTM, Philadelphia, 86–106.

Landva, A.O., Pelkey, S.G., and Valsangkar, A.J. (1998). “Coefficient of permeability of municipal refuse.” *Proceedings of the 3rd International Congress on Environmental Geotechnics*, Balkema, Rotterdam, 163–67.

Landva, A.O., Valsangkar, A.J., and Pelkey, S.G. (1999). “Lateral earth pressure at rest and compressibility of municipal solid waste.” *Canadian Geotechnical Journal*, 37, 1157–1165.

Larson J.A. (2007). “Investigation at a bioreactor landfill to aid in bioreactor operation and design of horizontal injection liquids addition system.” Master’s thesis, University of Florida, Gainesville, Florida, United States.

Ling, H.I., Leshchinsky, D., Mohri, Y., and Kawabata, T. (1998). “Estimation of municipal solid waste landfill settlement.” *Journal of Geotechnical and Geoenvironmental Engineering*, 124 (1), 21–28.

Liu, C.N., Chen , R.H. and Chen , K.S. (2006). “Unsaturated consolidation theory for the prediction of long-term municipal solid waste landfill settlement.” *Waste Management Research*, 24, 80–91.

Landva A.O., Valsangkar, A.J., and Pelkey, S.G. (2000). “Lateral earth pressure at rest and compressibility of municipal solid waste.” *Canadian Geotechnical Journal*, 37, 1157–1165.

McCarthy, D.F. (2007). “Essentials of soil mechanics and foundations: basic Geotechnics, 7th Edition.” *Pearson Education*, New Jersey.

Machado, S.L., Carvalho, F.M., and Vilar, O.M. (2002). “Constitutive Model for municipal solid waste.” *Journal of Geotechnical and Geoenvironmental Engineering*, 128 (11), 940–951.

Mahler, C.F. and Netto, A.D.L. (2003). “Shear resistance of mechanical biological pre-treated domestic urban waste.” *Proceedings of the 9th International Landfill Symposium, Sardinia 99, CISA* (CD-Rom), Cagliari, Italy.

McKnight, T. (2005). “Engineering properties and cone penetration testing of municipal solid waste to predict landfill settlement.” Master’s degree Thesis. University of Florida, Gainesville, Florida, United States.

Ministry of Environment of Republic of Korea (2006). “Food Waste Reduction.” Waste, <http://eng.me.go.kr/main.do> (March 6, 2009).

Morris, D.V. and Woods, C.E. (1990). “Settlement and engineering considerations in landfill and final cover design.” *Geotechnics of Waste Fills - Theory and Practice: ASTM STP 1070*, ASTM, Philadelphia, 9–21.

Oweis, I.S. (2006). “Estimate of landfill settlements due to mechanical and decomposition processes.” *Journal of Geotechnical and Geoenvironmental Engineering*, 152 (5), 644–650.

Oweis, I.S., Smith, D.A., Ellwood, R.B., and Greene, D. (1990). “Hydraulic characteristic of municipal refuse.” *Journal of Geotechnical Engineering*, 116 (4), 539–553.

Pohland, F.G. (1975). “Sanitary landfill stablization with leachate recycle and residual treatment.” *EPA-600/2-75-043*. US EPA, Washington DC, USA.

Powrie, W. and Beaven, R.P. (1999). “Hydraulic properties of household waste and implications for landfills.” *Institution of Civil Engineers Geotechnical Engineering Journal*, 137, 235–247.

Reddy, K.R., Hettiarachchi, H., Parakalla, N.S., Gangathulasi, J., and Bogner J.E. (2009). “Geotechnical properties of fresh municipal solid waste at Orchard Hills landfill, USA.” *Waste Management*, 29, 952–959.

Reinhart, D.R. (1996). “Full scale experiences with leachate recirculation landfills: case studies.” Waste Management and Research, 14(4), 347–365.

Reinhart, D.R., and Townsend, T.G. (1997). “Landfill bioreactor design and operation.” *Lewis Publishers*, New York, New York.

Reinhart, D.R., McCreanor, P.T., and Townsend, T.G., (2002). “The bioreactor landfill: its status and future.” *Waste Management & Research*, 20, 172–186.

Robertson, P.K. and Campanella, R.G. (1983). “Interpretation of cone penetration tests: Parts 1 and 2.” Canadian Geotechnical Journal, 20(20), 718–745.

Sadek, S., Abou-Ibrahim, A., Manasseh, C. and El-Fadel, M. (2001). “Stability of solid waste sea fills: shear strength determination and sensitivity analysis.” *International Journal of Environmental Studies*, 58(2), 217–234.

Sanchez-Alciturri, J.M., Palma, J., Sagaseta, C., and Canizal, J. (1995).‘‘Three years of deformation monitoring at Meruelo landfill.’’ *Waste disposal by landfill—GREEN ’93*, R. W. Sarsby, ed., A. A. Balkema, Rotterdam, The Netherlands, 365–371.

Shan, C., Falta, R.W., and Javandel, I. (1992). “Analytical solution for steady state gas flow to a soil vapor extraction well.” *Water Resources Research*, 28(4), 1105–1120.

Shank, K.L. (1993). “Determination of hydraulic conductivity of the Alachua County Southwest Landfill.” Master's thesis, University of Florida, Gainesville, Florida, United States.

Sowers, G.F. (1973). “Settlement of waste disposal fills.” *Proceedings of the 8th International Conference on Soil Mechanics and Foundation Engineering*, Moscow, 207–210.

Spangler, M.G. and Handy, R.L. (1982). “Soil engineering: 4th Edition.” *The Harper and Row Series*, Harpercollins College Division, New York.

The World Bank (1999). “Urban development sector unit and East Asia and Pacific Region, what a waste: solid waste management in Asia.” *The International Bank for Reconstruction and Development*, 4–24.

Townsend, T.G. (1995). “Leachate recycle at solid waste landfills using horizontal addition.” Ph.D. dissertation, University of Florida, Gainesville, Florida, United States.

Townsend, T.G., Miller, W.L, Lee, H.J., and Earle, J.F.K. (1996). “Acceleration of landfill stabilization using leachate recycle.” *Journal of Environmental Engineering*, 122(4), 263–268.

Townsend, T.G. and Miller, W.L. (1998). “Leachate recycle using horizontal injection.” *Advances in Environmental Research*, 2 (2), 129–138.

US Environmental Protection Agency (EPA) (2007). “Bioreactor performance.” EPA530-R-07-007.

US EPA (2007). “Municipal solid waste in the United States: 2007 facts and figures.” <http://www.epa.gov/epawaste/nonhaz/municipal/pubs/msw07-rpt.pdf> (Jan. 5, 2010).

Wang, H. and Nie, Y. (2001). “Municipal solid waste characteristics and management in China.” *Journal of Air & Waste Management Association,* 51, 250–263.

Whelan, K.R.T., Smith, T.J., Cahoon, D.R., Lynch, J.G., and Anderson, G.H. (2005). “Groundwater control of Mangrove surface elevation: shrink and swell varies with soil depth.” *Estuarine Research Federation*, 28 (6), 833–843.

Yuen, S.T.S., Styles, J.R., Wang. Q.J., and Mcmahon, T.A. (1999). “Findings from a full-Scale landfill bioreactor study in Australia.” *Proceedings of the 7th International Landfill Symposium, Sardinia 99, CISA*, Cagliari, Italy, 403–418.

Zekkos, D., Bray, J.D., Stokoe, K., Kavazanjian, E., Rathje, E., Athanasopoulos, G A., Riemer, M., Matasovic, N., Lee, J.J., and Seos, B. (2008). “Recent findings on the static and dynamic properties of municipal solid waste.” *Proceedings of GeoCongress 2008, Geotechnics of Waste Management and Remediation*, ASCE, New Orleans, Louisiana, 176–183.

Zekkos, D., Bray, J.D., Athanasopoulos, G.A., Riemer, M.F., Kavazanjian, E. Jr., Founta, P.A., and Grizi, A.F. (2007). “Compositional and loading rate effects on the shear strength of municipal solid waste.” *Proceedings of the 4th International Conference on Earthquake Geotechnical Engineering*, Thessaloniki, Greece, Paper No. 1525.

Zhan, T.L.T., Chen, Y.M., and Ling, W.A. (2008). “Shear strength characterization of municipal solid waste at the Suzhou landfill, China.” *Engineering Geology,* 97, 97–111.

BIOGRAPHICAL SKETCH

Youngmin Cho was born in 1976 in South Korea to In-ok Hwang and Myung-hyun Cho. He enrolled in the Chungnam National University, South Korea, in March 1995, and graduated with a Bachelor of Engineering in environmental engineering in February 2003. He had served in the military army of South Korea from January 1997 to March 1999. He also enrolled in the Johns Hopkins University, Baltimore, United States, in August 2006 and graduated with a Master of Science and engineering in geography and environmental engineering in May 2007.